A LABORATORY SIMULATION OF LOW VELOCITY PROJECTILE IMPACT ON THIN PLATES

A thesis submitted to the faculty of Engineering at the University of Cape Town in fulfilment of the requirements for the degree of Masters of Science in Engineering

By
Paul Cartmel
Department of Material Engineering
June 1999

ABSTRACT

This project concerns the development of a test apparatus that will both accurately simulate a projectile impact event and provide an accurate means of analysing a material response to projectile impact events.

A low velocity apparatus, based on the conventional instrumented drop tower apparatus, was designed and constructed. The apparatus is instrumented in order that the penetration resistance force history and impact velocity can be measured by a data acquisition system for further analysis. A software package, developed specifically for the apparatus, manipulates the acquired load-time trace and generates the necessary force and energy-deflection curves.

A series of tests were performed to verify the validity and reproducibility of the results. The plastic deformation that occurs during a rebound impact event is compared to the plastic deformation as measured by the impact testing apparatus. These tests show that the apparatus can accurately measure the plastic deformation that occurs during a rebound impact event. A series of reproducibility tests proved that the apparatus is capable of generating almost identical force-deflection curves for tests conducted with given impact parameters.

A series of tests were performed to analyse the impact response of the ductile material, aluminium alloy grade 1200. The aim of these tests is to illustrate the performance capabilities of the test apparatus and to analyse the influence of individual system variables, such as impact velocity, kinetic energy and projectile shape, on the impact response of a ductile material. The impact apparatus generates force-deflection curves that are in agreement with the observed impact response. The essential features that define a material response to impact loading such as stiffness, yield point and point of maximum load were identified on the force-deflection curves.

A secondary aspect of this study was to investigate the impact behaviour of aluminium and glass laminate plates. The impact response of the laminate plates was

compared to that of singular glass and aluminium plates. The apparatus is capable of generating force-deflection curves for the, short duration, impact response of a singular 6mm thick glass plate and well as the highly sensitive laminate plate tests.

ACKNOWLEDGEMENTS

I would like to express my sincere appreciation and thanks for the assistance I have received during the course of this work, in particular from:

Professor A Ball, my supervisor, for his guidance, advice and encouragement.

Mr. Glen Newins, Mr. Nicholas Dreze and Mr Reginald Hendriks for there expert workmanship in machining the test apparatus, preparing the test specimens and general workshop advice.

Mr. Dave Dean for his electronic expertise and help in the development of the data acquisition system.

Mr. Mattiea De Villiers for his electrical engineering knowledge regarding high-frequency data acquisition and his assistance in the development of the software package.

Mr. Adriaan Loedolff and Mr. James Petersen for their photographic assistance.

Ms. Julie-Ann Henry for her secretarial support.

The staff and students of the Department of Materials Engineering, University of Cape Town, for their advice and assistance during the duration of this project.

I would also like to express my sincere appreciation to the Foundation for Research and Development (FRD) for their financial support.

Dedicated to my parents – Roy and Pauline Cartmel. For their constant encouragement, guidance and love over the years and throughout this project.

TABLE OF CONTENTS

1. INTRODUCTION

1.1 Background to the Research

In recent years there has been an increased emphasis on lighter and safer vehicles and structures. As impact is one of the most common end use stresses to which materials are subjected, a clear understanding of material and structural response to impact loading is required in order to design towards safer and lighter structures.

Previous research into the impact response of materials and structures has been performed from both an experimental and analytical perspective. Due to the complex nature of an impact event analytical solutions can be both limited in scope and accuracy[1]. Hence the bulk of research on impact dynamics has been performed from an experimental perspective[2]. Impact testing provides us with a means of characterising a materials impact response and correlating it to in service product performance.

The concept of a "good impact test" has two aspects: the quality of the test result and the applicability of the test result[3]. Thus, the aim of this project was to develop an apparatus that would both accurately simulate a typical projectile impact event and provide an accurate means of analysing a materials response to typical projectile impact events. In a study by Wu, Sheen, Chen and Chan[4] they conclude that the penetration force history is one of the most important parameters for researchers to understand the penetration process of a projectile impacting on a structure. The apparatus was thus instrumented in such a way that the penetration resistance force history could be measured by a data acquisition system for further analysis.

1.2 Scope and Limitations of the Research

The scope of the project encompasses the design and construction of a low velocity projectile impact simulation apparatus and an investigation into the apparatus's ability to accurately analyse the impact response of selected materials to projectile impact. The focus of this study was on the design and construction of a versatile

instrumented impact simulating rig. A software package manipulates the force history and generates a force-time, force-deflection and energy-deflection curve for the impact event. These curves are then used to analyse the projectile impact response.

A series of tests were performed to verify the validity and reproducibility of the test results. After proving the test results valid, a series of test were performed to analyse the impact response of a ductile material. The ductile material chosen was aluminium grade 1200. The aim of these tests was primarily to demonstrate the effectiveness of the rig at simulating low velocity projectile impact. The secondary aim was to analyse the influence of individual system variables, such as impact velocity, kinetic energy and projectile shape, on the impact response of ductile materials.

An additional aspect of the study was to investigate the impact behaviour of laminated plates made up of a combination of a ductile and brittle material acting together. The Aluminium grade 1200 and conventional untreated float glass was used as the ductile and brittle material respectively. The performance of the laminated plates was compared to individual specimens of glass and aluminium resisting the impact. The emphasis of these tests was on proving the test rigs capability to analyse these highly sensitive tests and in so doing establish an upper bound to the performance capabilities of the test rig.

Analysis of the impact response of the individual materials was performed using the force-time, force-deflection and energy-deflection curves generated by the impact simulating rig. The impacted specimens were also analysed on a macroscopic level to check the correlation between the fracture mode inferences made from the data generated by the test apparatus and the observable fracture characteristics.

instrumented impact simulating rig. A software package manipulates the force history and generates a force-time, force-deflection and energy-deflection curve for the impact event. These curves are then used to analyse the projectile impact response.

A series of tests were performed to verify the validity and reproducibility of the test results. After proving the test results valid, a series of test were performed to analyse the impact response of a ductile material. The ductile material chosen was aluminium grade 1200. The aim of these tests was primarily to demonstrate the effectiveness of the rig at simulating low velocity projectile impact. The secondary aim was to analyse the influence of individual system variables, such as impact velocity, kinetic energy and projectile shape, on the impact response of ductile materials.

An additional aspect of the study was to investigate the impact behaviour of laminated plates made up of a combination of a ductile and brittle material acting together. The Aluminium grade 1200 and conventional untreated float glass was used as the ductile and brittle material respectively. The performance of the laminated plates was compared to individual specimens of glass and aluminium resisting the impact. The emphasis of these tests was on proving the test rigs capability to analyse these highly sensitive tests and in so doing establish an upper bound to the performance capabilities of the test rig.

Analysis of the impact response of the individual materials was performed using the force-time, force-deflection and energy-deflection curves generated by the impact simulating rig. The impacted specimens were also analysed on a macroscopic level to check the correlation between the fracture mode inferences made from the data generated by the test apparatus and the observable fracture characteristics.

2. LITERATURE REVIEW: THE IMPACT PHENOMENON

2.1 Introduction

Although a rich literature on the subject of material response to impact loading exists there is limited literature on the design of low velocity impact testing apparatus. The review thus focuses on defining the critical impact parameters that characterise the various impact regimes, leading to a description of the low velocity impact regime. The relevant structural and material properties that determine a material's response to impact loading and the expected failure modes are reviewed. The methodology for impact testing using an instrumented drop tower and the subsequent data interpretation is discussed.

2.2 Fundamentals for Characterising the Impact Regimes

In order to characterise the impact regimes it is necessary to outline the features that define the various impact regimes. These features include dynamic stress, strain and fracture relationships. These characteristics are outlined in order to define the low velocity impact regime and explain certain trends that occurred during the impact testing.

2.2.1 Dynamic Strain Relationships

Impact imposes sudden stresses and strains on a structure. The intensity of these stresses and strains alone does not uniquely determine the yield behaviour within most metals. The rate at which the strain is applied also plays a part in the yield behaviour. The rate at which this strain is applied to the structure has often been referred to as the normalised measure of loading velocity[5]. It is well established that most metals and many non-metallic materials show significant change in mechanical response under increased loading rates[6]. An understanding of the rate dependence of the mechanical properties of the material involved is required, if problems associated with impact loading are to be properly analysed and impact resistant structures are to be effectively designed.

At high strains and strain rates there can be abrupt changes in deformation mode. These changes in deformation mode can give rise to changes in metallurgical effects: microstructurally related flow stress, ductility, hardness and other related property changes[7].

Although minor variations in material properties are observed with small changes in strain rate it is common to consider only the order of magnitude of the strain rate[5]. This simplification is acceptable due to the extreme range of strain rates over which the various phenomena are observed.

The various strain rate regimes have been categorised according to the different dynamic considerations that must be taken into account during testing. The various impact regimes, impact test method and dynamic consideration are illustrated in Figure 2.1. The range of strain rates from $10^{-1}s^{-1}$ to $10^{2}s^{-1}$ is generally referred to as the intermediate or medium strain rate regime[8]. The low velocity impact regime falls into this regime. Within this regime strain rate effects may become a consideration, although the magnitude of such effects is quite small or non-existent[8]. Thus, the strain rate effect for separate impacts between 2 and 10 $m.s^{-1}$ is expected to be negligible.

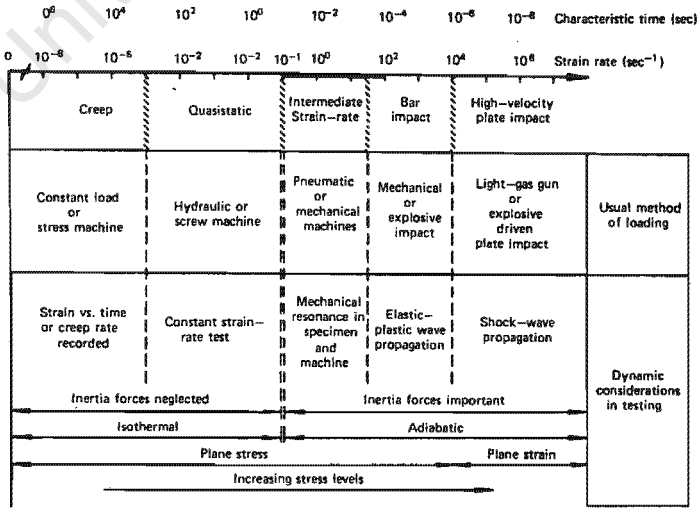

Figure 2.1 Dynamic aspects of mechanical testing [After ref. 9].

2.2.2 Dynamic Stress Wave Propagation

Stress waves are used to describe the time dependent deformation that occurs during an impact event.

According to the elastic theory of isotropic solids there are two fundamental types of waves that propagate during an impact event[10]. Tensile and compressive deformations travel in the form of dilatational waves. Dilatational waves are those in which the particle motion induced by the disturbance is normal to the wave front as shown in Figure 2.2. A second basic wave carries shear deformation and is commonly described as distortional or deviatoric, in which particle motion occurs in planes normal to the wave front propagation direction as shown in Figure 2.3[10].

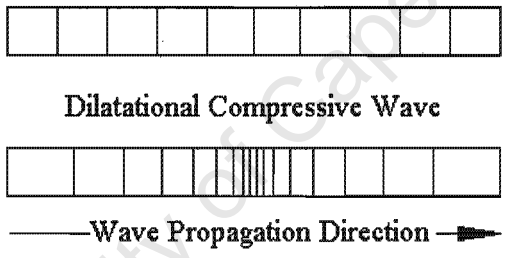

Figure 2.2 Illustration of a dilatational compressive wave.

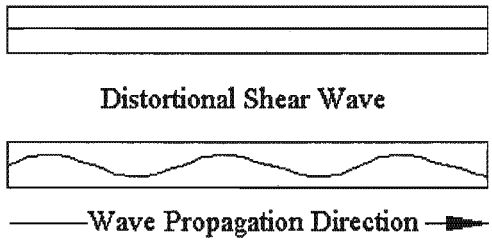

Figure 2.3 Illustration of a distortional shear wave.

In order to determine the characteristic response time for an impacted plate it is necessary to define the various wave speeds. Typical wave speeds for steel, aluminium and glass are given in Table 2.1. According to these wave speeds, taking the standard bounded drop tower test specimen diameter of 76.2mm, dilatational

waves are expected to make in excess of 100 wave traversals in a characteristic 2 to 3 second impact event. Due to the high degree of stress communication the energy absorption of the global structure can not be ignored.

Wave speeds ($m.s^{-1}$)	Steel	Aluminium	Glass
Dilatational	5000	5000	5250
Distortional	3200	3050	3200

Table 2.1 Bounded media wave speeds for common materials.

Elastic waves reflect off the free surface of the material in which it is travelling[10 11]. Because the stress at a free surface boundary must be zero, the reflected stress pulse will be equal in magnitude and opposite in sign. Figure 2.4 shows a compressive stress pulse reflected off a free surface as a tensile wave. For materials strong in compression and weak in tension, the reflected tensile wave is often the main cause of fracture[12]. This form of fracture is known as spalling or scabbing and the fracture occurs at an area remote to the causative impact load[11].

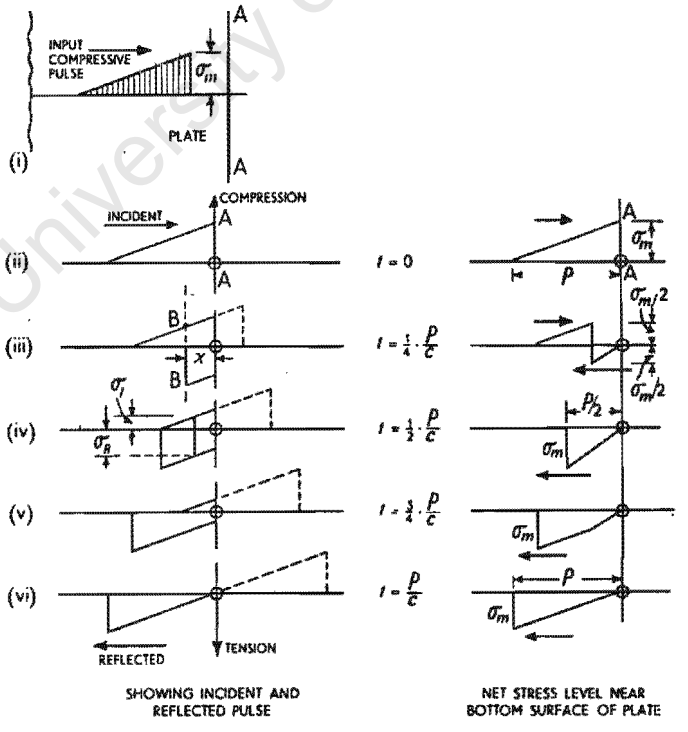

Figure 2.4 Stress wave reflection of a sawtooth pulse at various time intervals [after ref. 11].

When the intensity of loading causes stresses beyond the elastic limit, plastic stress waves are generated. These high-energy plastic stress waves, capable of causing large deformations in the target material, follow the higher velocity elastic stress waves[13]. Figure 2.5 shows the strain displacement for elastic wave followed by a plastic wave, where c_0 and c_1 are the speeds of the elastic and plastic waves respectively. The magnitude of the elastic and plastic wave front is ε_Y and ε_1 respectively. The principal energy absorbing mechanism in steel armour plate is plastic deformation by a concentrically expanding plastic bending waves[14].

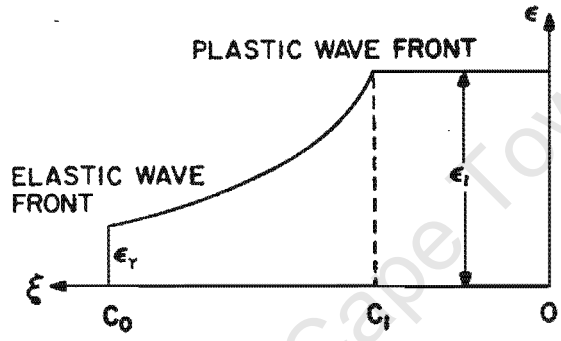

Figure 2.5 Strain distribution for elastic wave preceding a plastic wave [after ref. 13].

2.2.3 Dynamic Fracture

Griffith made the pioneering study in the field of fracture mechanics. Later the investigations by Irwin and Orowan led to the evolution of fracture energy concepts and the inclusion of plasticity effects[15 16]. Their work considered the conditions under which a crack will propagate in a material and the dynamic effects of the crack propagation. These theories and the mechanism of fracture are not discussed in this literature survey as the concept of dynamic fracture is introduced only to define the low velocity impact regime and outline the fracture energy requirements of ductile and brittle materials. The various fracture modes expected within the low velocity impact regime are discussed in section 2.3.

Fracture toughness or K_{ic} is a measure of a materials resistance to crack propagation. Specimens prepared with a starter crack are loaded quasi-statically to determine the K_{ic} value for a given material[17]. Generally, brittle materials have low K_{ic} values and fracture at low impact energies whereas ductile materials have high K_{ic} values and high impact energies are required to cause fracture[17]. Fracture of brittle materials occurs by a low energy absorbing mechanism in which the crack propagates between atomic planes in which the atomic planes are cleaved apart[17]. In ductile materials a high-energy absorbing mechanism of void formation and void coalescence leads to ductile tensile fracture[17 18].

In general fracture toughness decreases with decreasing temperature and increases with decreasing strain rate[17].

2.3 Classification of the Impact Regimes

The mathematical relationship between the stresses, strains, and their time dependence is known as the constitutive equation of a material. The general form of the constitutive equation would cover the total range of strain rates that could occur. However, due to the changing deformation mechanisms with changing strain rate, constitutive equations usually cover only a small range of strain rates[8]. The total strain rate range is thus divided into various impact regimes in which the deformation mechanisms and fracture modes are similar. Lindholm[9] described the generic characteristics of the impact regimes and thus categorised the various impact regimes as illustrated in Figure 2.1. Lindolm divided mechanical impact testing into five sub regimes, three of which are considered dynamic and two that are considered quasi-static. He described the general test method and testing considerations pertinent to each strain rate regime. Although distinct regimes are identified, their respective behavioural idiosyncrasies can overlap into grey areas in which combined effects can occur[10]. The three dynamic regimes are discussed in the remainder of this chapter.

Referring to Figure 2.1, the strain rate range extending between quasi-static loading up to and overlapping the elastic plastic regime is known as the low velocity impact

regime. A typical upper limit to the low velocity impact regime is 250m.s^{-1} [2]. Within this regime, indentation and perforation are largely dependent on the geometry and deformation of the global structure. Typical loading durations are in the millisecond regime[2]. A more detailed account of the low velocity regime is described in section 2.4.

The regime of elastic plastic response incorporates a range of impact velocities from 250 to 3000m.s^{-1}. The structural response to such short duration loading is localised and the structural response becomes secondary to the behaviour of the material within a small impact zone, typically 2 to 3 projectile diameters. Typical loading durations are in the microsecond regime[2].

Further increases in impact velocity result in localised stresses exceeding the target flow stress by an order of magnitude and invoke hydraulic material behaviour[2]. The constitutive models must incorporate the thermodynamic equations of state, as the impact process can no longer be assumed to be isothermal and analytical models must account for phase transformation effects[2].

There are various mechanisms by which an impacted material may fail. The exact failure mechanism depends on variables such as the material properties, impact velocity, projectile shape, method of target support and relative dimensions of projectile and target. Figure 2.6 illustrates the competing damage mechanisms for thin and intermediate thickness targets encountered in this study. Radial surface cracking occurs in material, such as ceramics, where the tensile strength of the material is low in comparison to the compressive strength. The bending stresses on the rear surface cause the plate to fail as the bending stresses exceeding the ultimate yield stress. Plugging occurs when a blunt penetrator travelling at a velocity close to the ballistic limit (velocity required for penetration) impacts with a finite thickness target, resulting in a cylindrical plug of nearly the same diameter being sheared from the target. Petaling is produced by high radial and circumferential stresses that occur at the projectile tip. Bending moments created by the displacement of the plate material being pushed by the striker cause the characteristic deformation patterns.

Petaling is most frequently observed in thin plates struck by conical or hemispherical projectiles at relatively low velocities. Petaling is accompanied by with large plastic flow and permanent flexure. The tensile strength of the material is reached and a star shaped crack develops around the tip of the projectile[2].

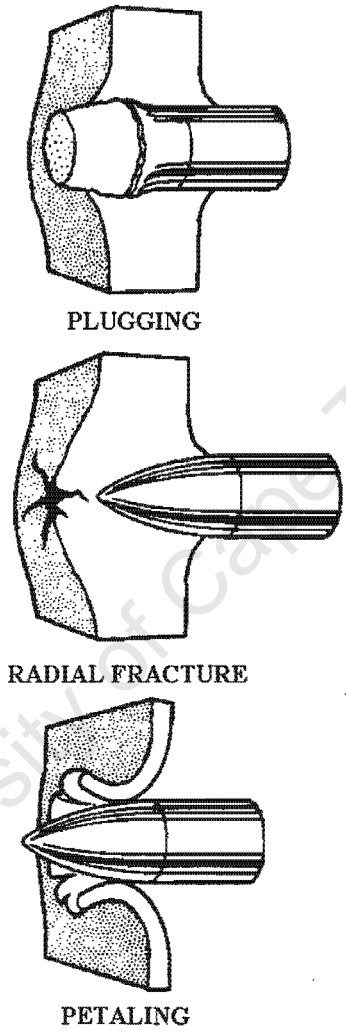

Figure 2.6 Damage mechanisms encountered in this investigation [after ref. 2].

2.4 The Low Velocity Impact Regime

The low velocity impact regime is described, incorporating the previously described dynamic fracture, stress wave and strain rate behaviour.

2.4.1 Definition of the low Velocity Regime

As an exact definition of the low velocity impact regime does not exist, a working definition is thus pieced together from the aspects of impact previously discussed. A reasonable bound on the low velocity impact regime, which is often described as the regime of tool drops and hailstones[19], is developed. An important feature of low velocity impact is that both structural and material responses of the global structure are considered in the analysis.

As discussed in 2.2.2 when two solid bodies impact upon on another vibrational waves are transmitted throughout the two impacted bodies. Elber[20 21] concluded that the static and low velocity load deflection curves for thin plate penetration are similar when the high frequency vibratory component is removed. Another definition of the low velocity impact is that the quasi-static and low velocity failure mechanisms are similar but differ in extent[22].

Both projectile and target play an equally important role in determining a systems response to impact[23 24]. The geometry of the projectile largely influences the stress distribution in both the target and projectile. For example a sharp projectile can produce concentrated point loading whereas a blunt and deformable projectile would produce a less intense stress distribution and may plastically yield throughout the loading duration further reducing the contact stress. The rigid and hemispherical tup used in this study falls in between these two extremes allowing the user to further simplify the impact event and gain a clearer understanding of the target materials impact response.

Strain rate dependence of the material within the low velocity impact regime is expected to occur. However, with reference to section 2.2.1 the literature on the low velocity regime suggests that the degree to which yield strength increases and fracture toughness decreases may not be distinguishable over the range of velocities attainable with a drop weight impact tower. Thus, the difference in strain to failure at $1m.s^{-1}$ may be indistinguishable from the strain to failure from a $5m.s^{-1}$ impact event.

2.4.2 Experimental Low Velocity Impact Investigations

A complete constitutive equation would take into account the geometry of the impacting bodies, elastic, plastic, and shock-wave propagation, work hardening, thermal and frictional effects, finite strains and deformations, and crack initiation and propagation in the colliding bodies[2]. Due to the large number of variables involved and the complex interactions that take place during an impact event analytical solutions can be quite formidable. Hence, the bulk of the work on impact dynamics is experimental in nature[2]. Impact testing provides us with a means of characterising materials impact response and correlating it to in service product performance. Thus it is imperative that the correct impact test is chosen for a particular application.

Brautman and Rotem[25] suggest that strain rate sensitive materials are especially sensitive to the test apparatus and that fracture energies are dependent on specific mechanisms that can differ from test to test. Roche and Kakarala[26] compare the performance of ten impact testing methods in five different classes namely pendulum, tensile, instrumented drop weight and driven dart. These comparative tests were performed using a wide range of materials of elastic modulus. They concluded that the results from different impact tests do not correlate although in some instances there is a fair correlation. Thus, the selection of an appropriate impact test should suitably simulate the test conditions and failure limits that would be expected in practice. Cantwell and Morton[27], mimic this remark in their review article, stating that the impact test should strive to simulate both the loading conditions and reproduce the failure modes that are expected in practice. For these reasons a complete review of the various impact testing apparatuses available is presented in the design chapter of this thesis and the selection of the instrumented drop weight tower apparatus as the best possible method of investigating low velocity projectile impact within the scope of this study is discussed. The split Hopkinson pressure bar (SHPB) is ignored as a possible impact testing apparatus as the SHPB obtains somewhat higher strain rates than were required for this investigation: $10^3\ s^{-1}$ as opposed to $10^2\ s^{-1}$ [28].

2.5 The Low Velocity Impact Behaviour of Glass Plates

When glass is subjected to projectile impact the specimen fracture may occur, assuming the loading intensity is large enough to cause fracture, in one of two ways[29]. Either, the specimen will fracture on the impacted surface due to the contact stresses. Alternatively, the specimen will fail due to the bending stresses on rear surface. The competing fracture processes are largely a function of the plate thickness[29]. As the thickness, and hence stiffness, of the beam is increased, the stresses on the rear surface, due to flexure, diminish while the contact stresses, on the front surface, increase. Thus, an optimum thickness exists whereby there is an equal probability of fracture occurring on the front and rear surface[30]. The bending and contact stresses as a function of thickness are illustrated in Figure 2.7 and the competing fracture processes for thick and thin glass plates are illustrated in Figure 2.8.

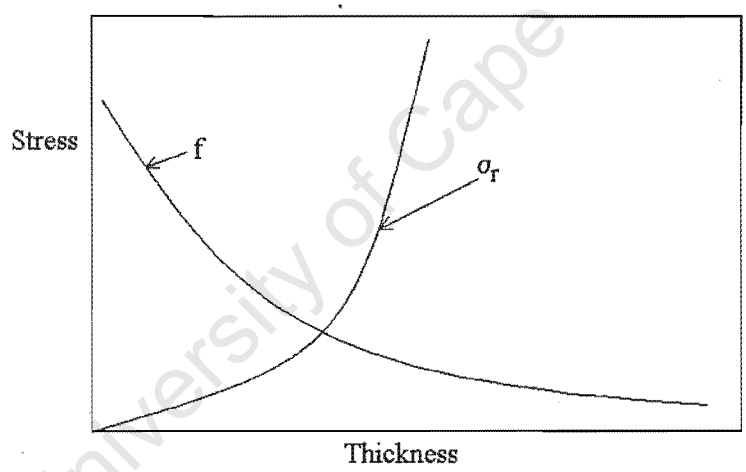

Figure 2.7 The effect of specimen thickness on the bending stress (f) and the contact stress (σ_r) [after ref. 29].

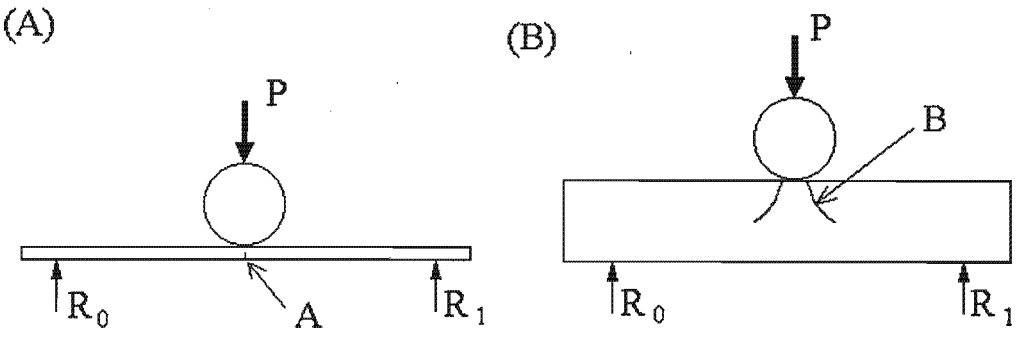

Figure 2.8 (A) A thin glass plate with a relatively low stiffness flexes during impact, relieving the contact stresses, and will normally break from a point on the lower face near A. (B) For a thick plate the flexibility is low, high contact stresses therefore form and fracture usually starts from the upper surface near B.

2.5.1 Hertzian Cone Fracture Due to Contact Stresses

Hertz[31] made the pioneering investigation into the fracture of glass due to indentation contact stresses. Hertz discovered that when a hard spherical indentor statically loads a flat glass specimen a cone crack of characteristic fracture is formed. According to Hertz theory this cone should form at the edge of the contact zone, were the tensile stress is at a maximum[32]. However, later work showed that this is not always the case and often this crack is formed just on the outside of the contact zone[33 34]. Attempts to explain this have incorporated the friction between the two impacting solids[33] and the statistical distribution of flaws[34]. If the intensity of the contact stress is great enough the ring crack will develop further to form a cone crack[32]. Auerbach[35] observed that for a glass plate the critical force required to initiate fracture (P_c) was related to the indentor radius (R) according to equation (2.1). Where A is known as Auerbach's constant.

$$P_c = AR \qquad \textbf{(2.1)}$$

Figure 2.9, after an investigation by Ball[36], schematically illustrates the events which occur during the impact of a thin glass plate by a steel ball.

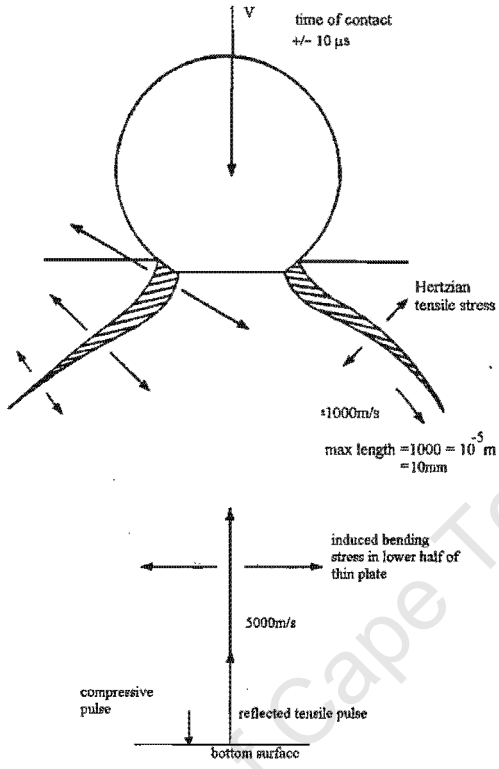

Figure 2.9 A schematic representation of the events which occur during the impact of a thin glass plate by a steel ball [after ref. 36].

2.6 Methodology for Instrumented Drop Tower Impact Testing

A review of the literature on instrumented drop weight testing is presented. The derivation of the force and energy versus deflection curves and the interpretation of the curves are discussed.

2.6.1 Derivation of the force versus deflection curve

The following derivation of the energy transfer during impact is taken from the GRC Model 930 I Dynatup Instruction Manual[37]. The following definitions appear in the derivation: P(t) = load measured by the tup tranducer, F(t) = total force acting on the tup, a(t) = the resultant acceleration of the crosshead, v_i = the crosshead velocity prior to impact, v(t) = resultant velocity of the crosshead, x(t) = resultant displacement of the tup and m = mass of the tup and crosshead.

The first step is to establish a force balance for the tup as shown in equation (2.2). This relationship provides a means of determining the instantaneous resultant acceleration of the crosshead with time according to the equation (2.3).

$$F(t) = mg - P(T) = m \times a(t) \tag{2.2}$$

$$a(t) = \frac{F(T)}{m} = g - \frac{P(t)}{m} \tag{2.3}$$

Once the resultant tup acceleration is known the resultant velocity v(t) and displacement x(t) can be calculated from the integration shown in equations (2.4) and (2.5). The boundary conditions x(0) = 0 and v(0) = V_{impact} and a Simpson's rule numerical integration scheme are utilised to integrate the acceleration-time trace and obtain the velocity-displacement history. Assuming a high sampling frequency is maintained, a high level of accuracy can be attained using this method.

$$v(t) = v_0 + \int_0^t a(t)dt = v_0 + gt - \frac{1}{m}\int_0^t P(t)dt \tag{2.4}$$

$$x(t) = \int_0^t \int_0^t a(t)dt = v_0 t + \frac{1}{2}gt^2 - \frac{1}{m}\int_0^t \int_0^t P(t)dt \tag{2.5}$$

The value of x(t) given in equation (2.5) is the position of the crosshead tip with respect to time, using the point of impact as the initial starting position. Assuming the tup to be a rigid body the value for x(t) corresponds to the deflection of the impacted plate. This relationship is described in equation (2.6) where $x_I(t)$ represents the indentation and $x_{BS}(t)$ represents the combined bending and shear of the plate.

$$x(t) = x_I(t) + x_{BS}(t) \tag{2.6}$$

Once the crosshead path is completely defined a simple energy balance is carried using the change in kinetic and potential energy, of the crosshead, with respect to time, to calculate the amount of energy absorbed by the plate at time *t* as shown in equation (2.7). The sum of these energies is equal to the total system energy. Definitons used to describe this energy balance are: K(t) = kinetic energy of the crosshead, P(t) = potential energy of the system, $E_a(t)$ = energy absorbed by the impacted plate and $E_t(t)$ = the total energy of the system. The initial point of impact equation (2.10) can be derived to describe the energy absorbed by the system as a function of time.

$$E_t(t) = K(t) + P(t) + E_a(t) = \text{constant} \tag{2.7}$$

Applying the initial conditions x(0)=0 and v(0) = V_{impact}. The initial kinetic energy is taken to be $\frac{1}{2} m \times V_{impact}^{\ 2}$, $E_a(0) = 0$, The potential energy P(0) is taken as = 0 at x(0). Equation (2.7) can be rearranged to solve for the constant.

$$E_t(0) = \frac{1}{2} m \times V_{impact}^{\ 2} = \text{constant} \tag{2.8}$$

Applying the constant to equation (2.7) and noting that if the potential energy was taken as 0 at x(o) then a negative potential develops as the crosshead penetrates the test specimen then equation (2.7) can be rewritten as:

$$E_t(t) = \text{constant} = \frac{1}{2} m \times V_{impact}^{\ 2} = -mgx(t) + \frac{1}{2} m \times V(t)^2 + E_a(t) \tag{2.9}$$

Solving for the total energy absorbed by the plate, equation (2.9) becomes

$$E_a(t) = \frac{m}{2}\left(v_{impact}^{\ 2} - v(t)^2\right) + mgx(t) \tag{2.10}$$

2.6.2 Instrumented impact data acquisition and evaluation

Data collection parameters and possible data acquisition problems

Conventional drop weight tester software require the user to select the expected load and time range. The load and time ranges have to be large enough to capture all the data and small enough to ensure a good plotting resolution[38]. The data acquisition system developed for this apparatus does not require the user to pre-select the load and time ranges, as data is sampled over a large load and time range and the relevant data is selected after the impact event and rescaled to the appropriate plotting dimensions.

The instrumented impact systems have two selectable methods of triggering data collection. The one method uses a velocity fork attached to the crosshead, which passes through a photodetector to provide a trigger signal. The other method uses a rise in the load signal above a preset threshold. The software developed for this system uses the threshold level technique. It is advisable that the threshold level be set at roughly 10% of the expected maximum load, this ensures that the trigger level is well above the background noise level[38].

Impact causes the components involved to oscillate at their natural frequency, often referred to as ringing[38]. These oscillations are often detected by the instrumentation. If the amplitude of the oscillations is significant relative to the amplitude of the load signal, difficulties in interpreting the relevant data points will be encountered. Techniques can be employed to reduce the effect of the oscillations. The first technique is to reduce the impact velocity. As the amplitude of the oscillations is proportional to the impact velocity by performing the test at a reduced impact velocity the effect of the oscillations will be reduced[38]. Another technique is to apply a thin layer of tape or elastomer to the point of impact. The layer of tape reduces the effect of the ringing by acting as a "damper" between the specimen and tape. The energy absorbtion of the tape will have to be taken into account in the analysis[38]. The author cautions against the use of this technique as the tape could effect a different fracture mechanism to that obtained when the tape is not used. Accurate filtering of

the data is another method of decreasing the effect of the ringing. Although the filter can improve the "readability" of the data, care must be taken to ensure that the data is not overfiltered, thus affecting relevant test data.

Data evaluation

The relative shape of the load-deflection curve is a representation of the deformation and fracture history of the specimen. It is imperative that the force-deflection curve can be interpreted correctly by the user. Thus, a typical force-deflection curve for a through penetration impact test on a ductile material is presented in Figure 2.10 and the different stages of impact are discussed. The force-deflection curve and accompanying discussion is taken from a study by Knakal and Ireland[39] that forms part of the ASTM STP 936 standard for instrumented impact tests.

In Figure 2.10 the five deformation stages and transition points are illustrated. The stages are described as follows:

Stage A – dynamic offset. The loading response is disturbed by the harmonic oscillations generated during the initial collision. The oscillations are usually small and insignificant.

Transition A – start of the linear load-deflection deformation.

Stage B – linear load deformation. The specimen is reacting as an elastically loaded structure and if the applied load were removed, the specimen would return to its original position. However, a localised plastic indent does form at the load point.

Transition B – yield. The onset of plastic or permanent deformation.

Stage C – first major permanent deformation. The damage is generally distributed over a large volume so a decrease in load is not observed.

Transition C – maximum load. This point is defined as the onset of deformation that does not result in an increased load. This point is usually associated with the first appearance of visible cracks on the tension surface of the specimen.

Stage D – stable or slow rate deformation. The deformation can be identified with localised thinning of the specimen around the circumference of the dart.

Transition D – end of the test. The start of unstable macrocracking or fracture.

Stage E – the portion of the curve giving no descriptive data. Showing the friction force exerted by the specimen on the probe as it slides through the puncture

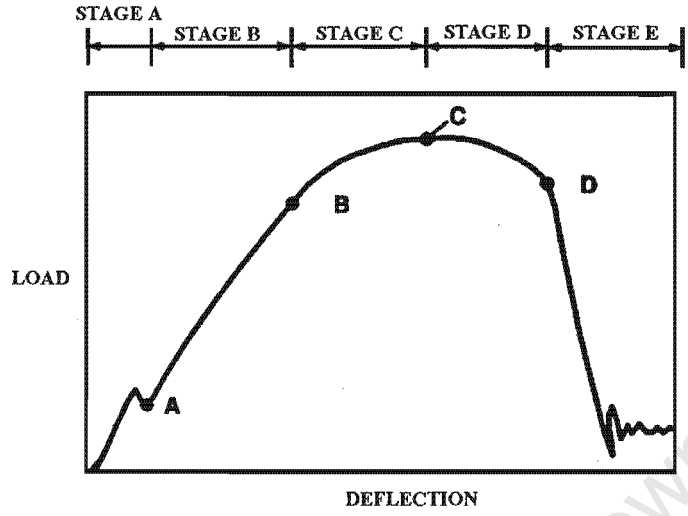

Figure 2.10 Idealised load-deflection curve showing the deformation stages and transitions for a puncture test on a ductile flat plate specimen [after ref. 39].

Knakal and Ireland[39] concluded the following regarding the use of the instrumented drop weight tester for the evaluation of a material impact behaviour.

1) The load-deflection record is an excellent indication of the specimen deformation process. Specific features of the force-deflection record can be used as distinct characteristics of the material response to projectile impact.
2) A single idealised load-deflection record (presented above), divided into different deformation stages, which are connected by transition points, can be used as a guide for data selection analysis of any record.
3) The following data can be derived from the force-deflection curve:
   (a) stiffness, which is the slope of the linear elastic load-deflection portion (Stage B) of the curve, and
   (b) load and deflection, values at the following transition points:
   The yield point (Transition B)
   The point of maximum load resistance (Transition C)

4) The load, deflection and energy values for transition C and D should be used only for the comparisons between specimens tested by exactly the same procedure.

5) Under no circumstance should any data obtained after transition D be used to represent material impact performance. The dart sliding through the fracture does not reveal useful data.

6) Care must be taken to avoid manipulating the data, using filtration techniques, to force any data analysis. When there are inherent oscillations of the load-deflection record, caused by specimen fracture mode and dart velocity is should be identified as "uncertain for data analysis".

7) Specimen thickness should be taken into account in any evaluation of the instrumented drop test i.e. to the slope of force-deflection for various specimen should be normalised according to a specific thickness.

Figure 2.11 shows the correlation between the characteristic points on the load-time plot, for a brittle material, and the different stages of fracture progression on the test specimens.

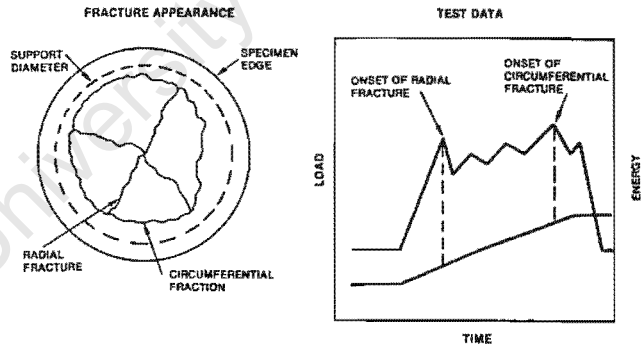

Figure 2.11 A comparison of the failure progression and force-deflection for a puncture test on a brittle material [after ref. 38].

A useful tool for characterising a material impact performance is the energy-deflection curve. As the force-deflection and energy-deflection curves are plotted on the same deflection axis, a direct correlation between a characteristic event on the force-deflection curve and the energy to cause the event can be made. An illustration of a typical load and energy-deflection curve for a non-puncturing impact test is shown in

Figure 2.12. The contact load increases with increasing deflection up to a point of maximum load and then decreases as the tup and crosshead rebound off the test specimen. Absorbed energy can be seen to increase continuously during the impact event until a peak value is reached at the point of maximum deflection and then decrease as the elastic energy built up during the impact is returned to the crosshead during plate rebound. The maximum total energy is thus made up of the absorbed and returned elastic energy components.

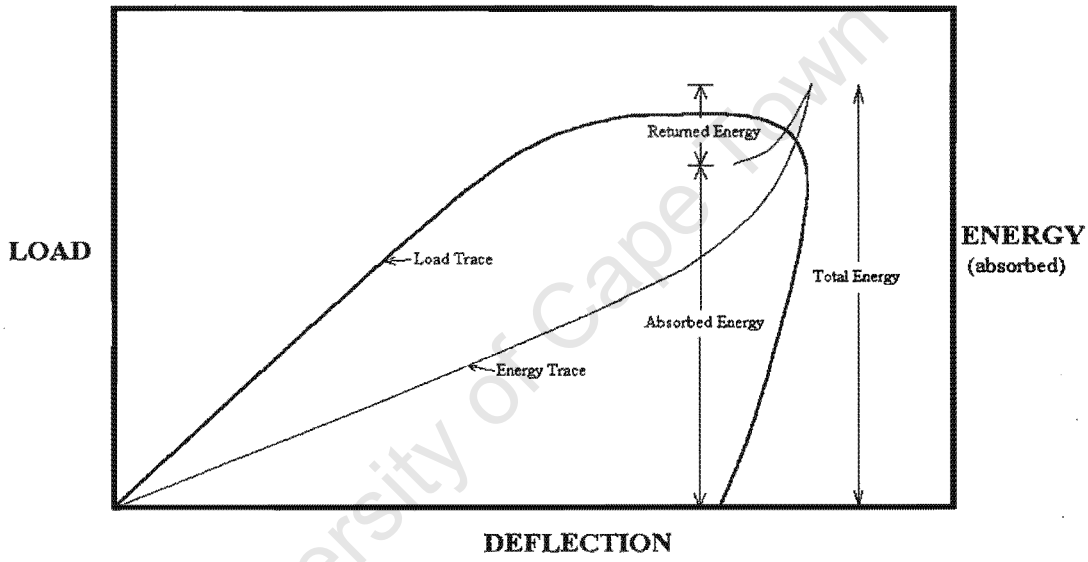

Figure 2.12 Illustration of absorbed energy and load versus tup deflection for a rebound impact event.

2.7 Review of the Low Velocity Impact Test Standards

The American Standard Test Methods (ASTM) relevant to low velocity impact testing are reviewed. A chronological order of the changes and developments in the testing methods is maintained to highlight the developments in impact testing and when these developments originated.

ASTM D256-81

ASTM D 256 covers tests for determining the pendulum impact resistance of notched plastic specimens. Appropriate use of both the Charpy and Izod impact testing apparatus is described. This test method describes a measure of the resistance to breakage by flexural shock and not the penetration resistance of the material. This standard had been revised more recently as D256-90b and D256-93a.

ASTM F 736-81

ASTM F 736-81 covers the test methods for impact resistance of monolithic poycarbonate sheets by means of a falling weight. Originally issued in 1981. The only reportable data mentioned is the energy to puncture a test specimen. A backup test configuration involving a three point beam specimen is suggested in the event that insufficient energy can be generated with the standard drop tower to puncture the specimen. The penetrator geometry and a table of recommended constraint diameters for a given plate thicknesses.

ASTM D 1822M-89

ASTM D 1822M-89 is the standard test method for tensile impact energy. This standard describes a pendulum type apparatus. The test specimen is supported by a crosshead, which in turn is attached to the pendulum arm. A striker anvil arrests the specimen at the bottom of the swing and the energy to fracture the specimen is measured as the integral of the force with respect to distance travelled by the specimen. The test method does not address the various combinations of force and distance that can provide and equivalent impact energy, and thus ignores the influence of strain rate.

ASTM D 3029-90

ASTM standard D 3029-90 describes the accepted procedure for determining impact resistance of flat, rigid, plastic specimens by means of a tup or falling weight. The recommended procedure is to determine the energy, in any combination of mass and height, which causes 50% of the specimens tested to fail.

There are three suggested geometries relating to the tup and constraining ring diameter. The operator is given the freedom to select the geometry that facilitates ease of sampling or initiating a different failure mode. The test standard recommends a drop range of between 0.3 and 1.4 meters.

ASTM acknowledges the visco-elastic nature of plastics but maintains that there is not a significant effect from the difference in the range of velocities attainable between the recommended drop heights. The standard concludes that within the limited velocity range recommended for this particular test a constant weight variable height test will yield the same results as a constant height variable weight method.

This test method is only recommended to provide a relative ranking of penetration resistance of materials under similar test conditions.

ASTM STP Series

There are two ASTM STP series that highlight the relevant information on instrumented impact testing of composite materials. These are Instrumented Impact Testing, ASTM STP 563 and Instrumented Impact Test Data Interpretation, ASTM STP 936. The standard addresses general issues relating to instrumenting a dynamic impact test. Issues discussed include how to remove the natural harmonic frequency response of the system from the load signal, removing inertial load effect from the signal and data evaluation. The issues discussed in this ASTM standard pertinent to this study are discussed in chapter 2.6.2.

3. The Low Velocity Impact Testing Apparatus

3.1 The Design of an Instrumented Low Velocity Impact Tester: Problem Definition

3.1.1 Design Statement

Design a test rig capable of evaluating the dynamic response of materials to low velocity impact with projectiles, under various impact conditions.

3.1.2 Design Requirements

The design must:

- allow the initial impact velocity to be variable between 0 and 10 $m.s^{-1}$
- permit the adjustment of the impact kinetic energy according to test demands
- acquire the penetration resistive force history for the impact event
- measure the velocity of the impacting projectile prior to impact
- utilise the load-time trace and impact velocity to determine the force-deflection and energy-deflection curves for the impact event
- allow the penetrator to be interchangeable, so that the effect of different projectiles shapes can be analysed
- facilitate the testing of various specimen thicknesses
- ensure that the clamping mechanism gives a constant clamping pressure for all tests and is not arduous and time consuming to operate
- incorporate a clamping mechanism that allows the test specimen to be rotated and thus facilitate multiple tests on one specimen
- feature a hoisting device that will lift the impacting crosshead to the necessary drop height.

3.1.3 Design Constraints

The design must:

- The design must not become a single purpose device that will subsequently become obsolete. The apparatus must therefore be designed in a modular fashion such that existing features can readily be expanded upon or exchanged without major modification being required.
- be significantly robust to withstand the high stresses imposed on the global structure during impact
- incorporate a computer software system to analyse the load trace for the impact event
- stick to a fixed budget, without a compromise on the accuracy of the test result
- allow for all wearing components to be readily accessible for routine inspection or replacement
- not involve any exceedingly complicated fabrication and hence excessively high fabrication costs or time
- utilise a simple and low cost hoist system.

3.1.4 Design Criteria

The design should:

- be as simple to operate as possible
- minimise vibration propagation inherent in an impact event
- be of a compact design so that a minimum amount of laboratory space would be required
- utilise as many standard components as possible, particularly the wearing components.

3.2 Concept Formation for the New Impact Testing Apparatus

The various low velocity impact testing apparatuses are reviewed. Conclusions as to the advantages and disadvantages of the various impact test methods are presented and discussed.

3.2.1 Pendulum Impact Tester

The pendulum impact tester is illustrated in Figure 3.1 below. There are two ASTM recommended pendulum impact tests namely the Charpy and Izod tests. The Charpy test was originally developed to investigate the dynamic fracture toughness of metals. The test apparatus is comprised of a striking hammer that swings in a fixed arc prior to impacting with the specimen. The potential energy of the pendulum is converted to kinetic energy as the pendulum descends from its starting point. A fraction of this incident kinetic energy is absorbed or dissipated during fracture of the specimen. The absorbed impact energy is inferred from the height of continued pendulum travel, and thus potential energy remaining in the system, following the impact event. Driscoll[40] in his review article found that the conventional Charpy and Izod tests were inadequate as they provide only single value measurements and the test is not representative of an actual in service projectile impact. Thus, modern pendulum impact testers incorporate the use of instrumented striking hammers[41] Relevant information, such as the energy to initiate and propagate crack growth, can thus be calculated from integrating the transient load signal.

The Charpy and Izod tests differ only in the method of specimen clamping. The Charpy impact specimen is freely supported in a horizontal position with the notch in a centralised position as illustrated in Figure 3.2. For the Izod test, the specimen is clamped in the vertical position like a cantilever beam with the notch aligned just above the anvil jaws as is shown in Figure 3.3. The Izod and Charpy specimen clamping methods induce different stress fields. High bending stresses are produced in the Charpy configuration as opposed to largely shear stresses in the Izod test.

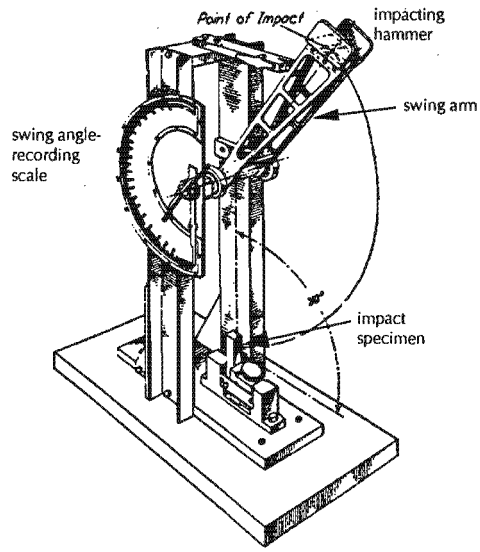

Figure 3.1 Illustration of a pendulum impact tester.

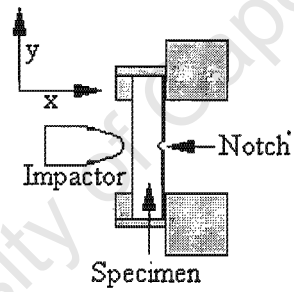

Figure 3.2 Schematic view of the Charpy impact fixture and specimen.

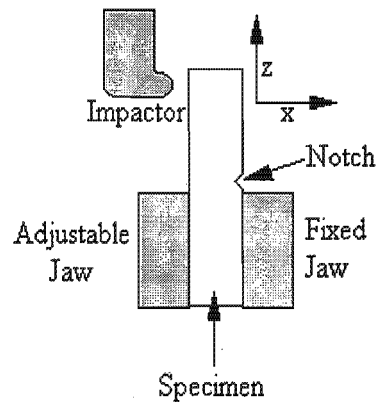

Figure 3.3 Schematic view of the Izod clamping fixture and specimen.

Advantages:

- simple mechanical design
- ease of operation
- minimal operating variables
- requires only a small laboratory space
- easily interpreted result
- low cost apparatus.

Disadvantages:

- not representative of an in service projectile impact
- gives only a singular measurement of impact resistance
- no information as to the mode of failure
- impact velocities varied only over a very small range.

3.2.2 Gas Gun

An inert gas is pressurised, in a reservoir, to a predetermined pressure. The high pressure gas is released by either bursting a membrane or releasing a solenoid[42]. A projectile is accelerated down the barrel of the gas gun by the rapidly expanding air. The velocity of the projectile, prior to impact, is measured using either optical sensors or breakwires[42 43].

Initial attempts to measure the penetration force history involved the use of ultra high speed cameras to record the discrete displacement history. However, this method was found to be inaccurate[4]. Subsequently a technique known as laser Doppler anemometry has been employed to determine the force history for the impact event[4]. However, this technique is complex and requires the use of costly photo-detectors, high speed storage oscilloscopes and data analysis computers.

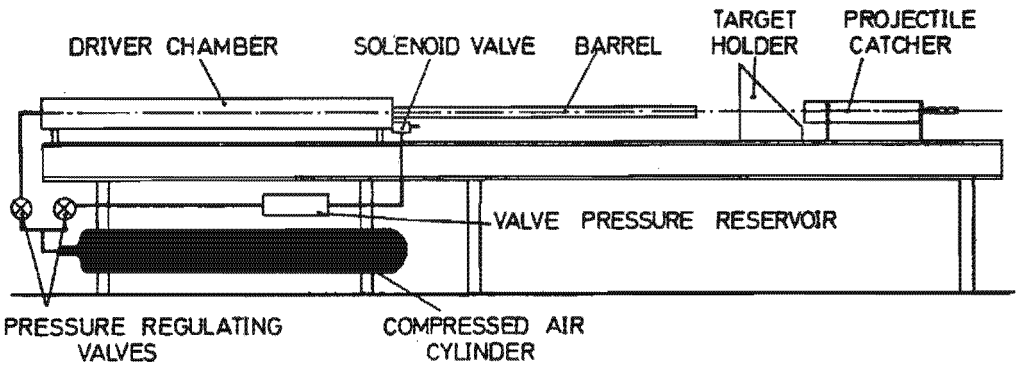

Figure 3.4 Schematic view of a typical air gun apparatus [after ref. 42].

Advantages:

- high velocity range
- increased upper bound velocity limit at which test can be performed.

Disadvantages:

- usually only small, light particle tests can be performed
- difficulties and high costs associated with determining the penetration force trace for the impact event
- determining the final velocity for either the rebound or through penetration cases is often complex and inaccurate.

3.2.3 Falling Dart

A typical instrumented falling dart is schematically illustrated in Figure 3.5. The dart is released from a pre-selected height and falls under the influence of gravity towards the clamped specimen. Originally, the falling dart apparatus did not incorporate the use of an instrumented dart. The height required to cause 50% of all specimens tested to fail was obtained using a trial and error approach. With increased technology, the falling dart was instrumented with a velocimeter to calculate the initial impact velocity and either an accelerometer or a load cell to calculate the transient load trace. The load trace is communicated to a data acquisition computer either by complex transmitter or trace wires.

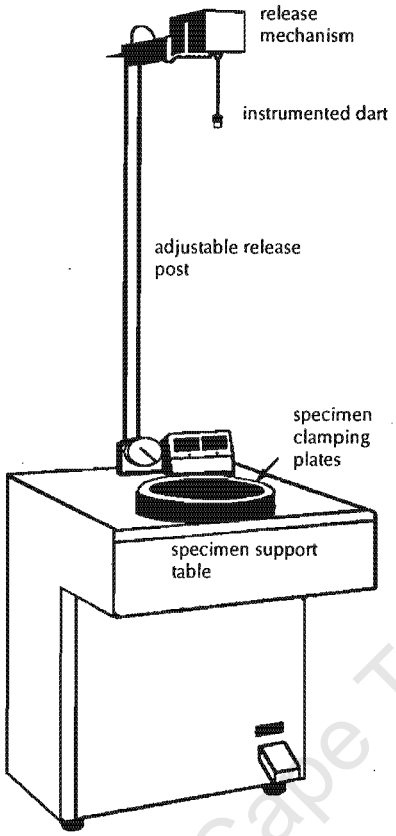

Figure 3.5 Schematic view of an Instrumented falling dart apparatus.

Advantages:

- simple mechanical design
- uncomplicated test procedure.

Disadvantages:

- the electronics required to transmit the load trace for the impact event from the unconnected dart to the data acquisition system is complex and costly
- the line of flight of the free falling is easily affected by the trace wires used to transmit the load trace, thus influencing the point of impact with the specimen
- the dart weight is limited to low masses, usually under 1.5 kg.

3.2.4 Servo-controlled Hydraulic Ram

The servo-controlled system is built around a hydraulically driven penetrating rod. The hydraulic system accelerates the penetrating rod to a predetermined velocity. The shape and size of the penetrating rod tip can be varied to influence the impact conditions. A displacement transducer measures the displacement of the penetrating rod and a load cell strategically positioned between the penetrating tip and the remainder of the penetrating rod measures the impact load trace. A data acquisition system processes this data and a load-deflection curve is obtained for the impact event.

Advantages:

- large range of impact velocities
- the in service impact event is accurately simulated
- very low velocity test can be performed[44]
- high reproducibility of impact test.

Disadvantages:

- complex mechanical design
- high costs associated with the hydraulic propulsions system
- large laboratory space is required.

3.2.5 Instrumented Drop Weight Tester

The Instrumented drop weight tower, illustrated in Figure 3.6, is an apparatus that relies on gravitational acceleration to supply a known energy and velocity to a free falling impacting crosshead. A hemispherical protrusion or tup attached to the crosshead, impacts with a specimen supported by selectable clamping conditions. The potential energy of the system is determined by variable combinations of drop height and crosshead mass, with drop height determining the velocity prior to impact.

Current instrumentation includes the use of either an accelerometer or load cell and a velocimeter. The accelerometer or load cell measures either the crosshead

deceleration or transient contact force respectively. The velocimeter measures crosshead velocity prior to impact. Using the impact velocity and the undeflected specimen as initial conditions, the transient load trace can be integrated to determine both the crosshead velocity and displacement as a function of time. The transient load trace can then be plotted as a function of the tup displacement. The crosshead kinetic energy is then calculated using the velocity with respect to time function. Thus the amount of energy transferred between the tup and specimen can be calculated.

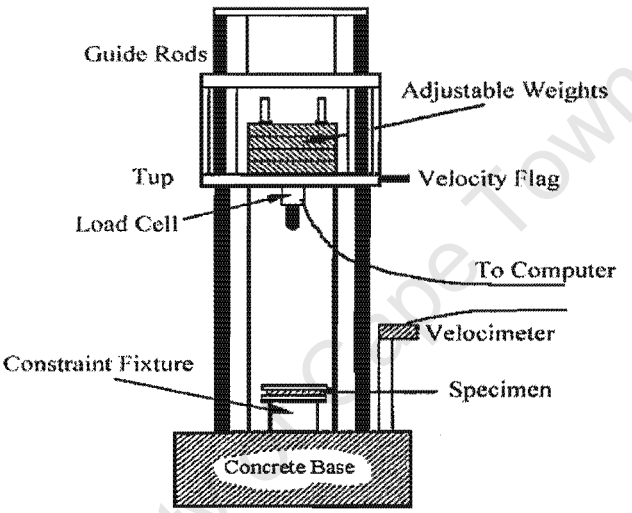

Figure 3.6 Schematic of a conventional instrumented drop weight tower.

Advantages:

- highly variable impactor masses
- simple and reliable construction
- high reproducibility of impact test
- true representation of an in service impact event
- simple to operate

Disadvantages:

- high laboratory roof required for high velocity drop towers
- conventional drop weight testers have a minimum projectile mass limit of approximately 11kg
- upper impact velocity limit of 5m.s^{-1}, due to height constraints.

3.3 Possible Design Solutions

Having analysed the advantages and disadvantages associated with all the impact testing apparatuses the design objective was to develop a dynamic apparatus that would satisfy all the requirements, constraints and criteria as discussed in Chapter 3.1. Ideally, the design solution would incorporate as many of the positive aspects, of the discussed apparatuses, as possible.

Three adaptations of pre-existing designs were considered viable for obtaining the desired impact criteria. The methodology, advantages and disadvantages of these systems are discussed and the most dynamic impact apparatus based on its merits was thus selected.

3.3.1 Solution A

This solution is based on the typical pendulum impact tester, but the emphasis of the design is on adapting the pre-existing apparatus so that it mimics a typical impact event more closely.

Figure 3.7 illustrates the proposed pendulum impact testing apparatus. The conventional impact anvil, used for the Charpy and Izod test, is replaced with a penetrating rod (tup). Different impact velocities can be obtained by releasing the swing arm from varying drop angles. A load transducer positioned between the tup and the impact hammer is used to obtain a load trace for the impact event. An angular displacement transducer attached to the pendulum axle measures the angular displacement of the swing arm. The impact resisting force can thus be plotted as a function of the tup displacement. By integrating the force-displacement curve the total energy absorbed by the test specimen can be calculated.

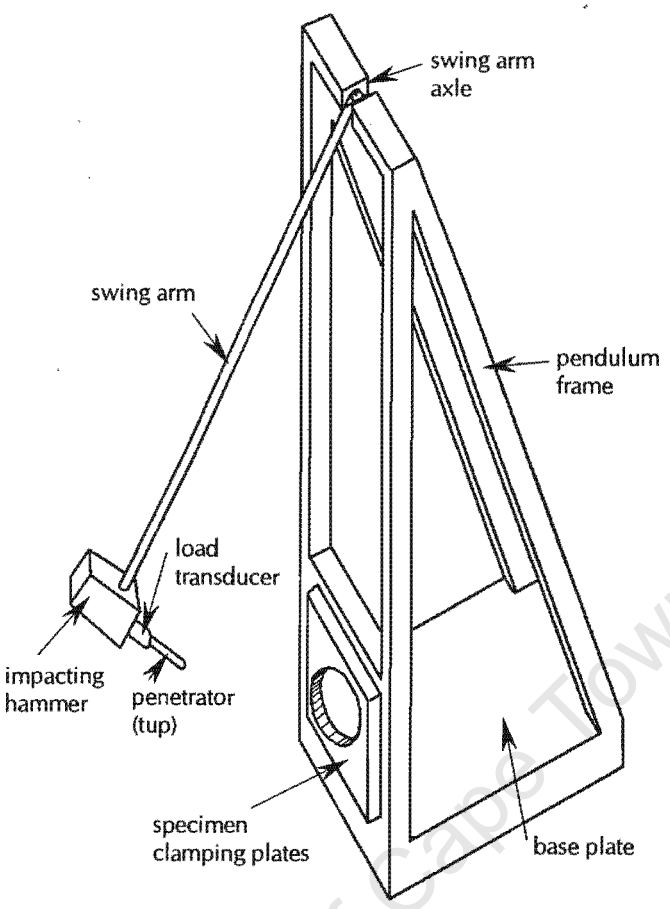

Figure 3.7 Schematic of the proposed impact pendulum.

Advantages:

- simple mechanical design
- low cost associated with construction
- ease of operation.

Disadvantage:

- complex impact process, as the penetrator is moving in an arc
- large laboratory space required for the swing arm and pendulum frame
- only a small range of impact velocities can be tested on a pendulum system
- the actual kinetic energy involved in the impact event is difficult to calculate, due to the dynamics of a complex pendulum.

3.3.2 Solution B

Figure 3.8 illustrates the modified conventional drop weight tower that is considered to be a possible solution. The design incorporates two parallel cylindrical guide rails along which the crosshead travels. The proposed modifications include the extension of the guide rails, which conventionally measure 2 to 3m, to 4.5m, thus increasing the upper velocity limit.

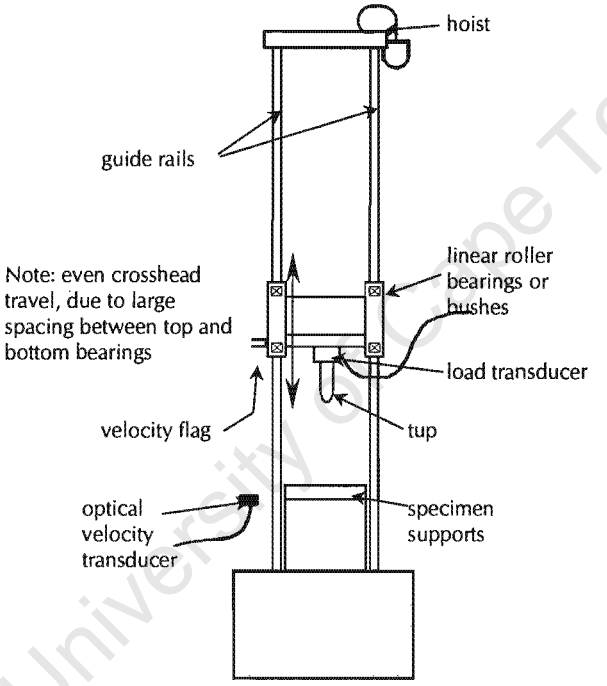

Figure 3.8 Schematic illustration of the conventional instrumented drop weight tower.

Advantages:

- the crosshead mass and impact velocity are easily varied
- although a high ceiling is required only a small laboratory floor space is required
- the design is tried and tested and teething problems associated with original designs can thus be avoided
- the apparatus can be used to obtain Charpy and Izod impact energies.

Disadvantages:

- to ensure that the crosshead falls evenly, the top and bottom bearings, or bushes, need to spaced relatively far apart. This design constraint and the mass of the four bearings ensures that a low crosshead mass is not possible. Thus, low energy tests on polymer sheets and brittle materials can not be accurately performed on this apparatus
- ensuring the guide rails remain parallel over the 4.5m would be an overwhelming task and would involve costly high precision machining
- high costs: The two 4.5m high precision guide rails required would result in this design being extremely costly
- the maximum specimen diameter that can be tested is limited to the distance between the guide rails.

3.3.3 Solution C

Solution C is illustrated in Figure 3.9. The design is based on the conventional drop weight tower except that the conventional guide rails have been replaced with a linear guide rail. This change facilitates the use of a cantilever type crosshead. A singular rail bearing, 4.5m in length is used to facilitate the crosshead motion. The problem of maintaining the parallelism of the guide rails is thus avoided. The load cell attachment, velocity measurement system and data acquisition remains unchanged from the conventional drop weight tower.

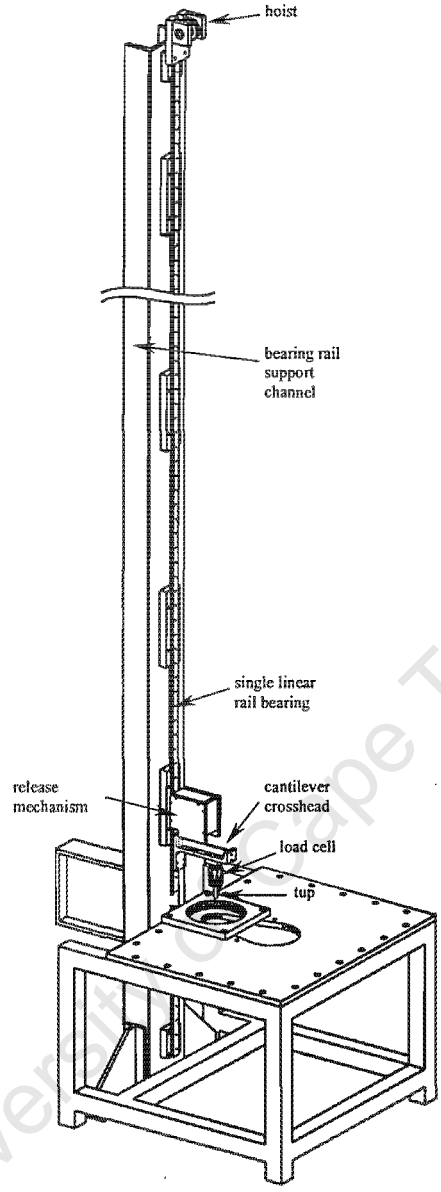

Figure 3.9 Schematic of a modified instrumented drop weight tower.

Advantages:

- due to the lower mass of the linear carriages, the mass of the impacting crosshead is significantly reduced, increasing the sensitivity of the apparatus
- the crosshead mass and impact velocity are easily varied
- although a high ceiling is required only a small laboratory floor space is required
- the apparatus can be used to obtain Charpy and Izod impact energies
- the problem of maintaining the parallelism of the two guide rails over 4.5m is avoided

- by increasing the size of the cantilever crosshead, there is no limit to the specimen size that can be tested
- the linear bearing carriages can support high moments ensuring smooth, even travel on the bearing track
- the use of a single linear rail bearing as opposed to two linear guide rails significantly reduces the total cost of the apparatus
- the linear rail is made up in sections. Sections of the rail that wear faster can be replaced singularly as opposed to replacing the whole rail in the case of the conventional drop weight tower.

Disadvantages:

- butt-joining the individual lengths of bearing track requires high precision track mounting blocks, requiring very low machining tolerances
- due to the originality of the design careful attention must be taken to ensure that possible design oversights are avoided.

3.4 The New Test Apparatus Design Solution

On the basis of the advantages and disadvantages of the possible design solutions the following design solution was chosen.

Description:

A laboratory test apparatus to be used for investigating the low velocity impact resistance of plates, under varying impact conditions.

Figure 3.10 The instrumented low velocity impact testing apparatus with (1) column mounted bearing rail, (2) the crosshead and linear bearing carriages, (3) clamping base and clamping plates, (4) signal processing unit, (5) computer used for data acquisition, (6) the digital storage oscilloscope.

Hardware:

- overall dimensions: length = 5000mm
  width = 450mm
  bredth = 450mm
- bearing system: IKO Linear Way Series
  LWL and LWLF 24 miniture series
- crosshead: length = 170mm
  width = 40mm
  breadth = 100mm
- hoist drive: 100W 12V Dc electric motor
  direct couple to 50:1 worm gearbox
- crosshead travel: stroke = 450mm

Test Specimens:

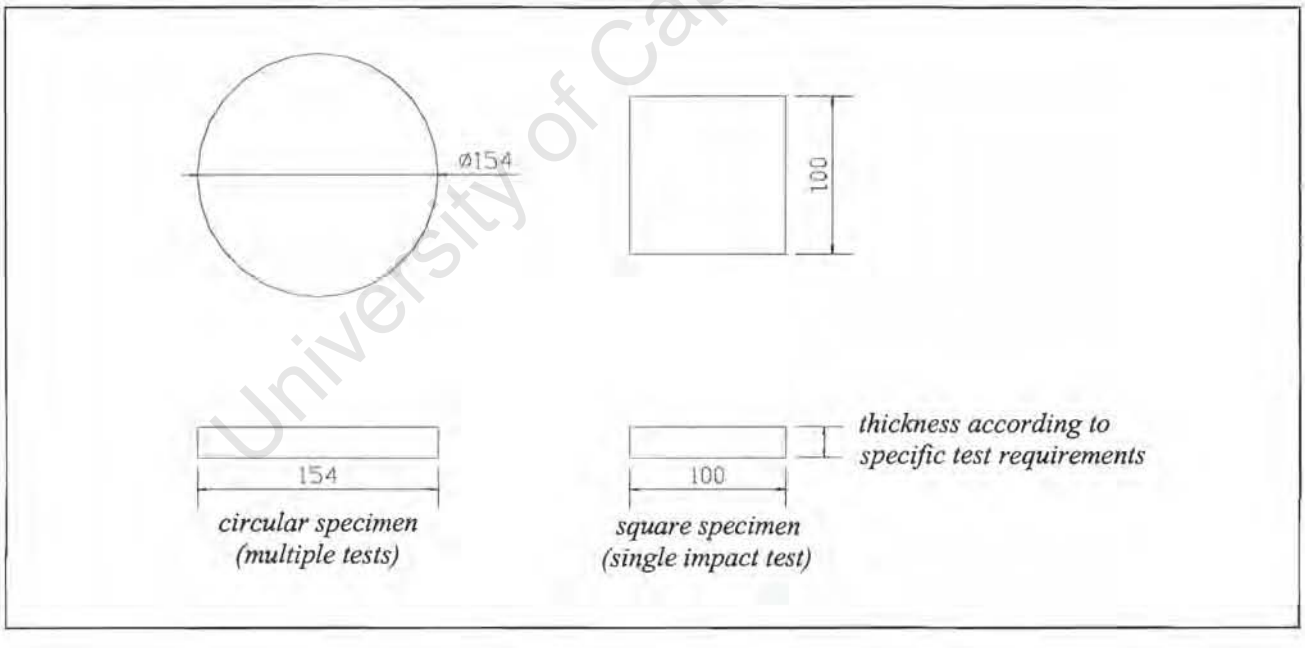

Figure 3.11 Recommended test specimen dimensions for clamped circular and square specimens.

3.5 Discussion of the Instrumented Drop Weight Tower

The design of the instrumented drop weight tower satisfies all the requirements, constraints and criteria as discussed in Chapter 3.1. The design will be discussed under several sub-headings with reference to the partial isometric sub-assembly drawing at the end of this chapter. For greater clarity, photographs of the components have been included in their relevant sections. The data acquisition system and the software that was developed are also discussed. If detail of the apparatus components is required, relevant component drawings have been included in Appendix A.

3.5.1 The Basic Layout

Reference should be made to the isometric sub-assembly drawing at the end of chapter 3.5. The drop weight tower has been built in two separate sub-sections. The impacting crosshead travel system (1-8) and the specimen clamping unit (9-11).

The butt-jointed bearing rails (2) are joined and mounted on the bearing aligning blocks (3). These blocks are attached to a vertical support channel (4), which in turn is fastened to the laboratory floor and wall by means of gusset plates (12). The gusset plates are separated from the floor and wall by means of a thin vibration absorbing cork layer. The crosshead is fastened to the bearing carriages (5) and is free to travel in a linear motion along the length of the bearing rail. A winch mechanism driven by a 100W 12V dc motor hoists the crosshead to the desired drop height. The specimen clamps (9) are bolted to the drop tower base plate (10). The base plate is fastened to the drop tower frame (12).

3.5.2 The Cantilever Crosshead

The cantilever and conventional crosshead systems, and the forces involved during impact, are illustrated in Figure 3.12 and Figure 3.13 respectively. These illustrations are used to explain the complications involved in using a cantilever type crosshead and aid in the discussion of how these complications were overcome.

The emphasis of the crosshead design was on reducing the crosshead mass and in so doing increasing the sensitivity of the apparatus. The crosshead is thus manufactured out of high strength grade 7075 aluminium and incorporates the high flexural rigidity of a T section in the crosshead beam. The total of the mass of the crosshead, load cell, load cell mounting block, tup and two bearing slide units is 1.2kgs. This is in contrast to the minimum total crosshead weight of 11.5kgs for a Dynatup conventional drop weight tower.

Due to the symmetry of the conventional crosshead the center of gravity is in the same plane as the force acting on the tup during impact, as illustrated Figure 3.13. Because the penetration resistance force and the crosshead mass act in the same plane, no rotational couple is established during the impact event. This ensures that the crosshead travels evenly, both during the impact event and rebound, in the case of a low-blow impact. To ensure the even travel of the unsymmetrical cantilever crosshead, the crosshead must be balanced in such a way that the center of gravity acts in the same plane as the force acting on the tup during the impact event. This is achieved by attaching a balancing block to the free end of the crosshead, as depicted in Figure 3.12. This ensures that the forces act in the same plane, similar to the conventional crosshead. No couple is established and the even motion of the crosshead is ensured.

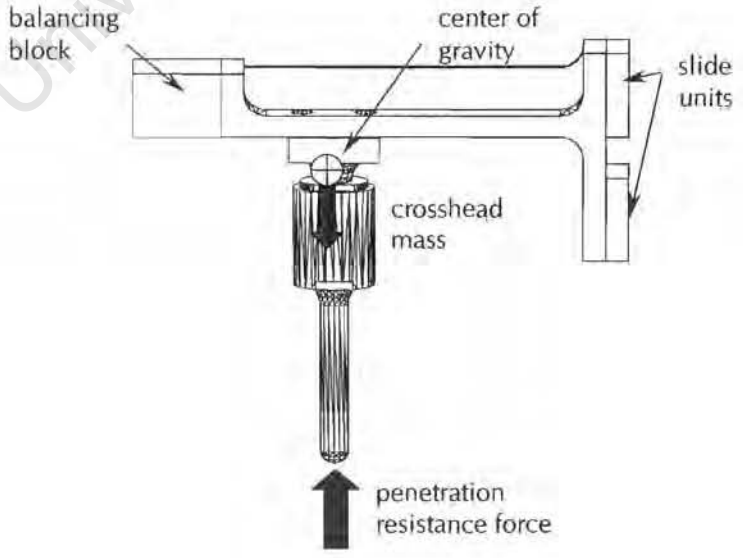

Figure 3.12 The cantilever crosshead and forces involved during impact.

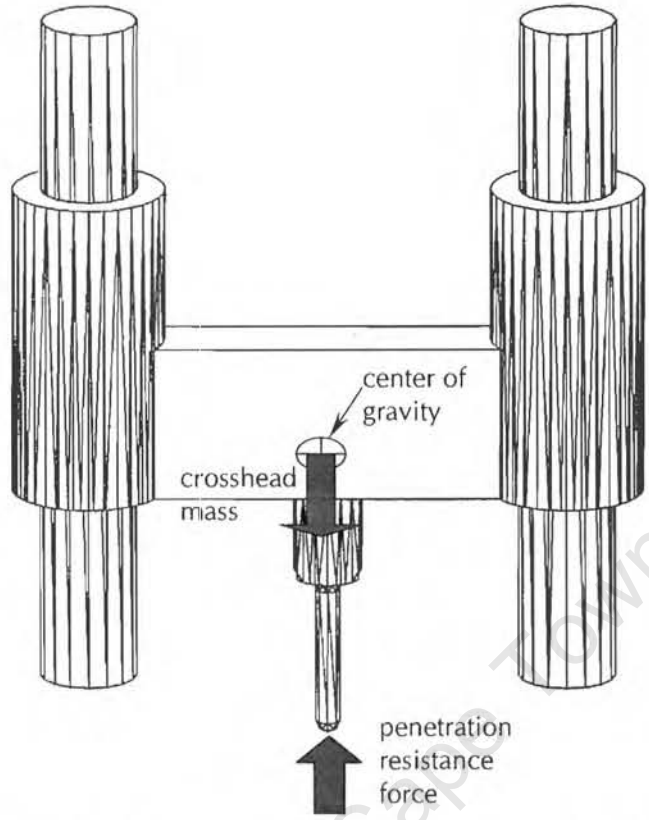

Figure 3.13 Conventional crosshead system and the force involved during the impact event.

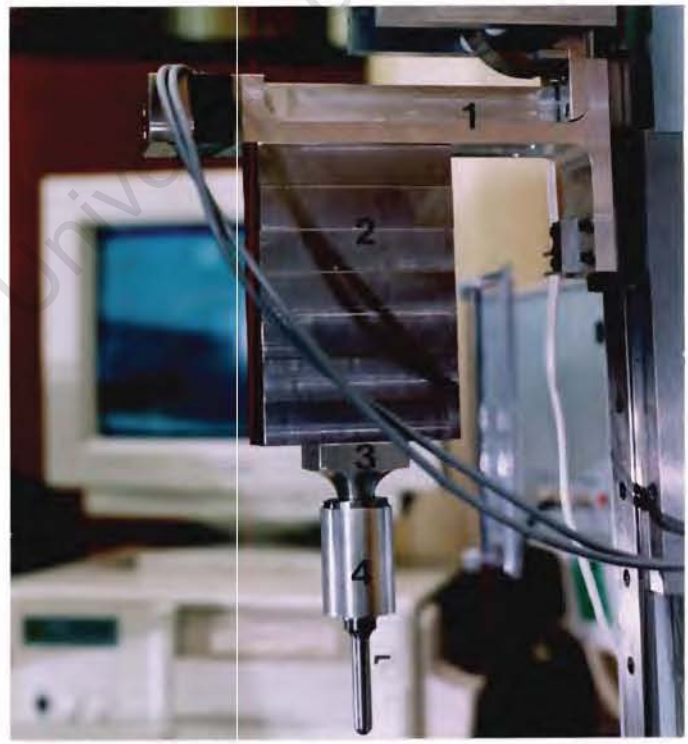

Figure 3.14 The (1) cantilever crosshead, (2) weight addition blocks, (3) load cell mounting block, (4) load cell and (5) tup.

3.5.3 The Bearing System

An IKO Linear Way Series (LWLF24) rail bearing unit was chosen to facilitate the linear motion of the crosshead. The load rating and essential operating information used to select the required bearing can be found in Appendix B.

The forces and moments that act on the bearings prior to impact are illustrated Figure 3.16. The loads exerted on the bearings by the 20 kg crosshead were calculated to be well within the dynamic and static load ratings of the LWL bearings.

Figure 3.15 illustrates the static moment load to which the slide units resists motion. The moment T_x illustrated in Figure 3.15 and Figure 3.16, established due to the weight of the crosshead, is calculated to be well below the static moment rating for a single bearing unit. The effect of this moment is further reduced by using two slide units thereby converting the moment into reaction forces R_1 and R_2 illustrated in Figure 3.16. T_0 and T_y moment are expected to be nominally zero as no out of plane forces are exerted on the crosshead.

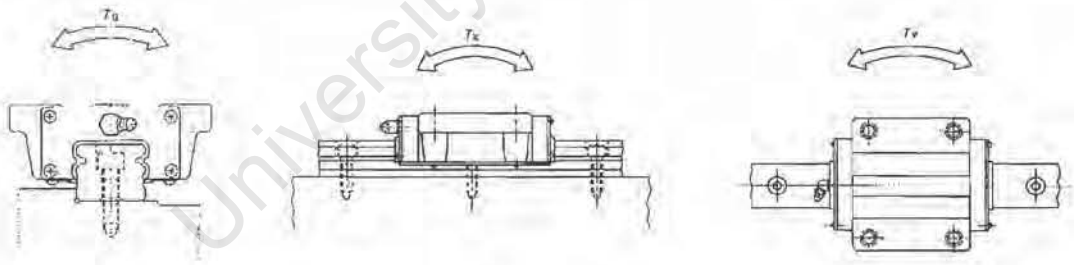

Figure 3.15 The moment loads to which the linear roller bearings resist motion.

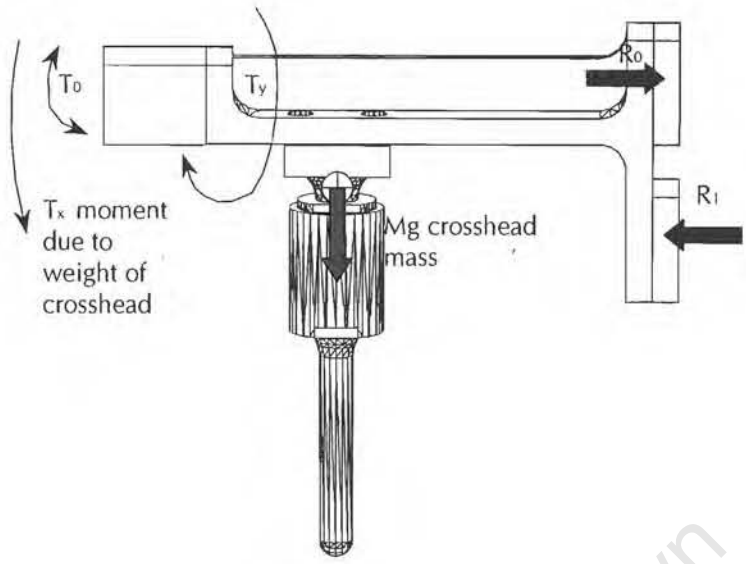

Figure 3.16 The forces and moment acting on the bearing carriages prior to impact.

The maximum track length available is 680mm. The 4.48m of bearing track is thus made up of six 680mm tracks and one 400mm track. The butt jointed bearing tracks are aligned and mounted on mounting blocks. A high precision recess is machined into the mounting blocks to aid in the alignment of the bearing tracks. Figure 3.17 illustrates the bearing tracks in position on the mounting bocks

Figure 3.17 The bearing tracks in position on the mounting blocks.

3.5.4 The Impact Force Measurement

Three techniques of acquiring the impact force history have been used on existing impacting testing apparatuses. The current apparatus employed the use a column load cell transducer to determine the impact load trace. The two other techniques considered are the use of an accelerometer or laser doppler anemometry.

The accelerometer is used to acquire the deceleration history for the impact event. The acceleration time curve and the mass of the crosshead is then used to calculate the impact resistance force. The use of an accelerometer was not considered feasible due to the high costs of an accelerometer robust enough to cope with the extreme accelerations during impact.

Laser doppler anemometry (LDA) was also considered as a means of acquiring the impact load trace. The application of LDA to calculating the impact force history was made by Birch and Jones[4]. The technique involves measuring the frequency of laser light reflecting off the surface of the impacting projectile. The frequency of the reflected light is proportional to the instantaneous velocity of the projectile. LDA is a complex technique that involves costly photo-detectors, lasers and high frequency oscilloscopes, for these reasons it was decided that LDA was not a feasible means of acquiring the impact force history.

It was decided that the most cost effective and practical solution would be to design and manufacture a column strain gauge load cell specifically for this apparatus. A decision had to be made as to whether to use a quartz load cell or strain gauge load cell. It was decided to use a strain gauge load cell to avoid the problem of signal drift[45] experienced with quartz load cells. As the load cell would have to withstand the high forces expected during impact, a robust column load cell was designed to measure the impact load trace.

Male and female threads are machined onto the load cell column so that is can be fastened in position between the crosshead and tup. Flat faces are machined onto the

sides of the load cell column to accommodate the strain gauges. The strain gauges are glued into position and wired in a Wheatstone bridge circuit. Wiring the strain gauges in a Wheatstone bridge configuration ensures the linearity of the load cell output. The Wheatstone bridge circuit also ensures the load cell output is not affected by changes in the ambient temperature. The load cell and strain gauge arrangement is illustrated in Figure 3.18. The load cell was calibrated by compressing the load cell on a tensile testing machine and measuring the voltage output at various compressive forces. The load cell calibration coefficient was calculated to be $6569N.V^{-1}$. The load cell calibration curve can be found in Appendix C

Figure 3.18 The load cell column and outer casing (removed), illustrating the strain gauges arrangement.

3.5.5 Tup Geometry

Figure 3.19 illustrates the hemispherical head tups used in this study. The tups are manufactured with hemispherical heads having the same diameter as the tup shaft. A male thread is machined onto the shaft and the tup is threaded into position on the load cell. The tups were manufactured from silver steel. The tups were heat treated at 780 °C for thirty minutes followed by water quenching and then tempered at 150 °C for one hour. Using this heat treatment a Rockwell hardness of between 62 and 65

was achieved for all the tups used. Five tups were manufactured for this study. A 12.7mm hemispherical head tup was manufactured to comply with the ASTM standard and four tups with shaft diameters varying from 4 to 10 mm, with 2mm increments, were manufactured to investigate the effect of projectile shape on impact. The shaft length measures approximately 50mm. This length proved sufficient to analyse a complete impact event.

Figure 3.19 The hemispherical head tups used in this study.

3.5.6 Impact Velocity Measurement

The impact velocity measuring system is illustrated in Figure 3.20. The velocity fork attached to the crosshead occludes an optical limit switch prior to impact. A clock counter circuit is started and stopped as the two prongs of the velocity fork pass through the optical limit switch. The distance travelled by the velocity fork and time elapsed on the clock counter is used to determine the initial impact velocity.

Because the distance between velocity fork and tup changes as weight blocks are added, the optical limit switch is located on a slide rail. The height of the optical switch must be adjusted to ensure that both prongs of the velocity flag pass through

the switch before impacting with the specimen. Thus, assuming a tolerance of 1mm is maintained between the second prong of velocity flag passing through the optical switch and the tup touching the plate, the initial impact velocity measured is actually the velocity of the crosshead approximately 6mm from the impact test specimen. This inaccuracy proved to be negligible.

Figure 3.20 The velocity measurement system with (1) the velocity flag, (2) the optical limit switches and (3) the height adjustment rail.

3.5.7 The Release Mechanism

Due to data acquisition constraints, the crosshead release had to be triggered by the software. The release mechanism is thus triggered by a computer activated solenoid. As the pulling force of the 12V solenoid is limited, the release mechanism had to be

designed in such a way that the weight of the crosshead would not influence the performance of the trigger. The trigger consists of two interlocking blocks, the solenoid pulls one of the block out of position allowing the remaining block to swing freely thus releasing the crosshead catch. The trigger mechanism, both in the locked and released position, is illustrated in Figure 3.21.

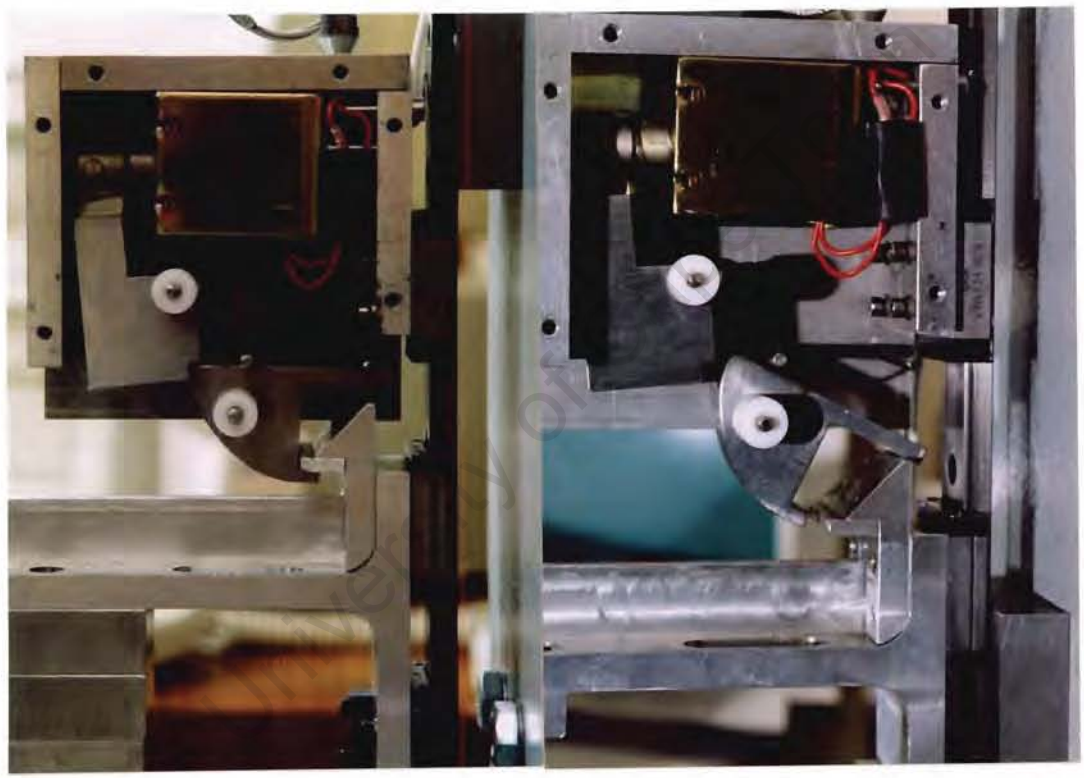

Figure 3.21 The trigger mechanism , with the side plate removed, before and after the crosshead is released.

3.5.8 The Specimen Clamping System

Two specimen-clamping systems were designed for the apparatus.

The clamping system most commonly used in the ASTM STP 936 requires a 4inch square specimen to be clamped between a 3inch annular clamping plate and anvil. The specimen is securely clamped into position such that the specimen has a support

moment as a boundary condition. The clamping system complying with the ASTM standard is illustrated in Figure 3.22.

For the second clamping method, 155mm diameter specimens are clamped between a recessed annular anvil and a clamping plate. This system clamps the plates on a circular contact radius of 70mm giving a support moment at the boundary condition. In order to determine the approximate fracture threshold velocity for a single impact test, the clamping plates can be aligned so that the impact point is 40mm from the centre of the specimen. Thus, by rotating the specimen, numerous tests can be performed on one specimen until the approximate threshold for failure is determined.

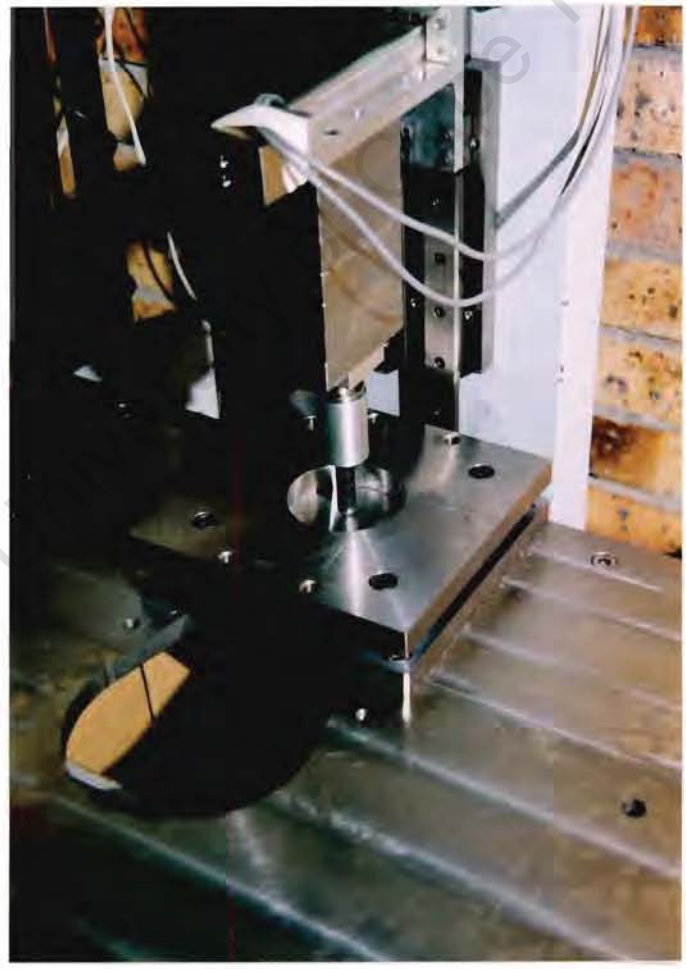

Figure 3.22 The specimen clamping base and clamping plate for the ASTM compliant system.

3.5.9 The Hoist Mechanism

A hoist system capable of hoisting a 20kg crosshead to a pre-selected drop height was developed. A 100W, 12V Dc motor and gearbox combination was directly coupled to a deep groove pulley. The complete hoist system is illustrated in Figure 3.23.

Figure 3.23 A view of the hoist arrangement showing the (1) 12V motor, (2) gearbox and (3) pulley.

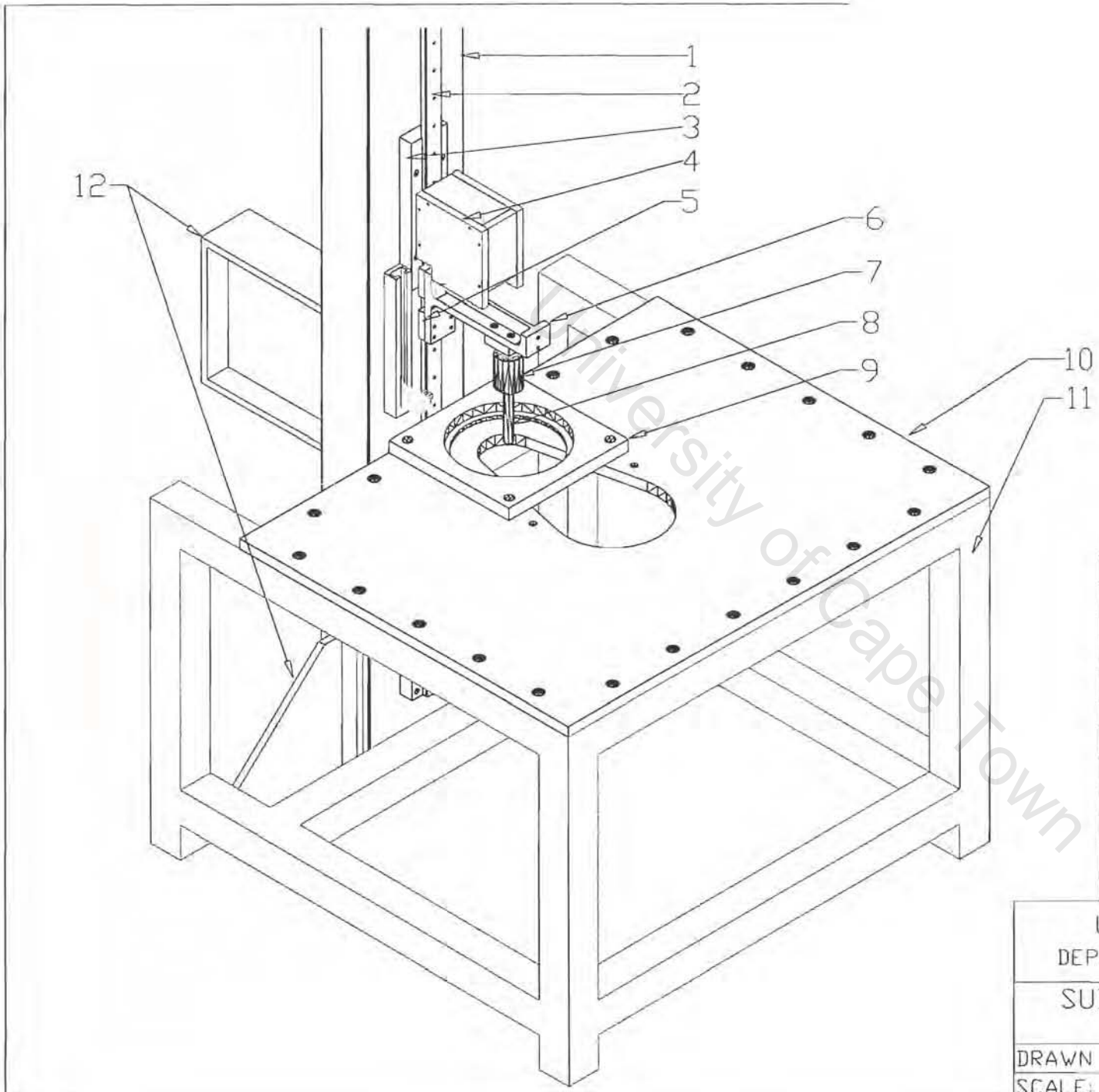

1	support channel
2	linear rail bearing
3	bearing mounting blocks
4	crosshead release system
5	bearing slide unit
6	crosshead
7	load cell
8	penetrator (tup)
9	specimen clamping base
10	base plate
11	mounting frame
12	gusset plates

UNIVERSITY OF CAPE TOWN
DEPARTMENT OF MATERIALS ENGINEERING

SUBASSEMBLY DRAWING OF DROP WEIGHT TOWER

DRAWN BY: P. CARTMEL	DATE: 06/08/97
SCALE: DNS	

3.6 The Data Acquisition System

A complex data acquisition system and software package was developed to analyse the load trace for the impact event. Three curves are generated by the software, namely; the force-time, force-deflection and energy-deflection curves. The data acquisition system is illustrated in Figure 3.24.

The voltage measured on the load cell Wheatstone bridge is amplified by a high-speed amplifier. The processed signal is then communicated to an Eagle Technologies PC30GA analogue to digital input board which is interfaced with an IBM compatible 486DX4-100 computer.

The PC30GA board is capable of sampling data at a speed of 100 kHz on 16 channels. For this investigation, only one channel is used to sample the load cell voltages. Twelve digital input output ports (DIO) are available on the PC30GA card. Thus the velocimeter clock counter output is communicated as a 12 bit binary number to the DIO ports. The 5V output signal required to activate the solenoid is achieved via a digital to analogue (D/A) outputs available on the PC30GA card.

Figure 3.24 The data acquisition system showing the signal processing box (1), data acquisition computer (2) and the digital storage oscilloscope (3).

3.6.1 The Impact Analysis Software

The essential aspects of the software, the methodology and the operating procedure are presented and discussed. A more comprehensive description of the software processes can be found in Appendix D.

As the software package is started, the computer sets the transfer mode, sampling frequency and channel on which to sample the load cell voltages. The main window opens as the software package is started. Two principal variables are required by the software, the total mass of the crosshead and the load cell calibration coefficient. As the strain gauges on the load cell can degrade or detach from the load cell column it is recommended that the load cell be recalibrated at regular intervals. On the main window that is now open the mass of the crosshead is entered into a labelled text box. If no value is entered, the software uses a default value of 4.6kg to perform the calculations. If this is not the true mass of the crosshead the deflection calculations will be incorrect.

To commence testing the operator presses on the "start test" command box and a sampling procedure window opens. The user must enter the load cell calibration coefficient, in the labelled text box, and the "perform test" command box must be clicked. The software then presents a safety message box telling the user to stand clear of the apparatus and press "enter" to commence testing.

After the user presses enter, allowing the test to commence, a series of procedures takes place. Firstly, the voltages on the load cell are sampled for a second to determine the offset value on the load cell. The offset value is the average voltage measured on the load cell when no load is applied. After the offset value is calculated, sampling is started and a 5V output is transmitted to the solenoid relay. The 5V output triggers the solenoid relay and a 12V voltage is relayed to the solenoid thereby activating the solenoid and releasing the crosshead. Conventional drop weight tower software starts sampling after the velocity flag passes the optical limit switches, triggering a sampling procedure. This places a lower velocity limit on the

tests that can be performed by the apparatus. It was felt that this constraint would limit the usability of the apparatus, as impulse testing, for example, could not be performed. For this reason, sampling is started before the crosshead is released and continued for 2 seconds, thus ensuring that the impact event will be captured, in the data sample, irrespective of the impact velocity. As the time taken for the crosshead to travel the length of the drop tower is measured to be approximately 1 second, the 2 second sampling period is adequate to ensure all the impact information is captured. Conventional software packages require the user to input the expected impact test duration, the data for the impact event is then sampled at optimum frequency for the specific test. The drawback associated with this system is that preliminary tests have to be performed to aid the user in predicting the impact duration. In addition, if for some reason, the impact duration is prolonged and the impact duration is longer than the user prediction, the complete test will not be captured.

Sampling takes place at a set frequency of 100 kHz. The time difference between data points is thus 10 microseconds. According to the dynatup software manual[37] even the most ductile material requires no more than 25 milliseconds for the entire impact event and a very brittle plastics can sometimes fail in as short a time as 1 millisecond. The impact curves will thus be plotted with a minimum of 100 points for brittle impact tests and a maximum of 2500 for a ductile test. Although, a higher resolution would have been preferred the sampling frequency proved to be sufficient to accurately plot the relevant graphs such that the yield and maximum load points can be adequately interpreted.

The data for the 2 second sampling period is stored in an array variable. After sampling is completed, the clock counter result i.e. the time taken for the velocity fork to pass through the optical limit switch is communicated to the PC30GA board. The software converts the 12-bit clock counter result into a time in milliseconds and the initial impact velocity is calculated.

The sampled data must be analysed to obtain the relevant data. As the load cell is compressed during impact, the voltage readings on the load cell during impact are negative. The software thus analyses the sampled data to find values below a pre-selected threshold. The data points (a user specified value) before and after the threshold is intersected, are stored in the impact data array. This ensures that all the data points for the impact event are analysed. The initial offset value is subtracted from the sampled voltages to ensure that the voltage at the start of impact corresponds to a zero force. The concepts of offset correction and sub-threshold data capture are illustrated in Figure 3.25 and Figure 3.26. Figure 3.25 shows a fraction of a 2 second voltage trace, with an exaggerated offset voltage, before the irrelevant data is omitted and offset correction is taken into account. Figure 3.26 shows the relevant voltage trace for the impact event, with offset correction taken into account.

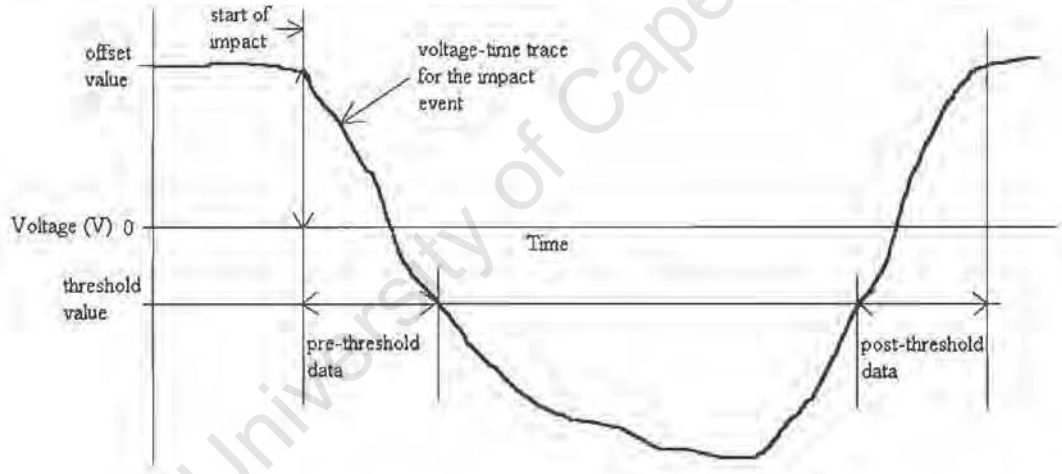

Figure 3.25 A fraction of the 2 second load cell voltage trace, illustrating the load cell offset and the threshold voltage.

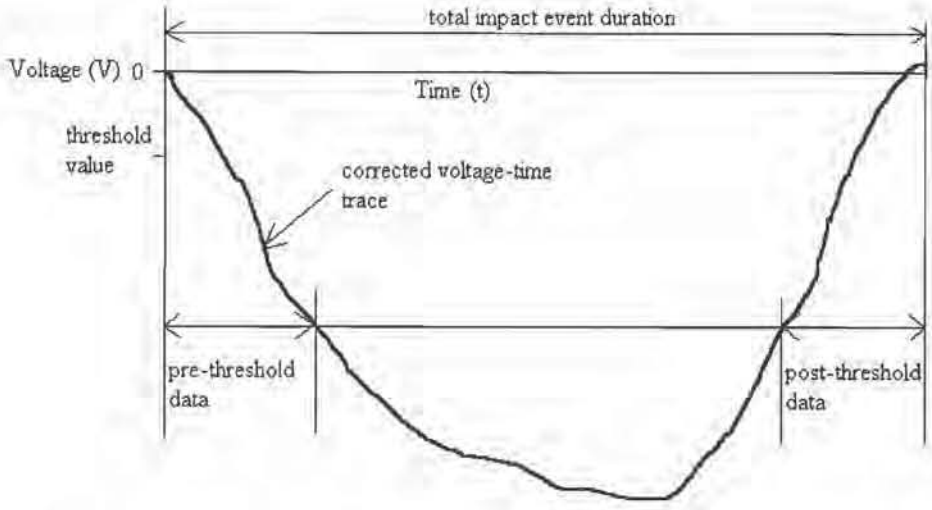

Figure 3.26 The relevant fraction of the load cell trace with the load cell offset correction taken into account.

After the offset correction is taken into account, the relevant voltages are multiplied by the calibration coefficient to convert the voltages to forces. The measured force is applied to equation (2.2) to calculate the total force exerted by the tup onto the impact specimen. From this force, the acceleration history can be calculated according to equation (2.3). The calculated acceleration history is then integrated according to equation (2.4) and (2.5) and the boundary conditions are applied to calculate the velocity and displacement history respectively. The velocity and displacement traces as a function of time are calculated and applied to equation (2.10) to calculate the energy absorbed by the plate during impact. The high frequency electrical noise component of the force data is smoothed out using a low pass smoothing algorithm. The smoothed force data or energy absorbed can then be plotted as a function of the tup displacement.

Typical voltage-time, force-time, force-deflection and energy-deflection functions generated by the software for a rebound impact is illustrated in Figure 3.27, Figure 3.28, Figure 3.29 and Figure 3.30. Note that the default pre and post threshold values shown in Figure 3.27 are adjusted in Figure 3.28 so that only the relevant impact data is analysed.

If the user wishes to plot numerous curves on one graph the data for a singular test can be saved using the "copy data" function and plotted on a graphing application.

Advantages of this data acquisition system and software package are:

- the user can adjust the pre-threshold length to ensure the load trace runs through the origin
- the expected time range does not have to be predicted, thus, making the package more user friendly and ensuring the entire test is captured
- as the sampling is started before the crosshead is released as opposed to the conventional software, that is started by the velocity flag passing an optical limit switch there is no lower velocity limit on the test that can be performed.

The drawbacks associated with the data acquisition system and software package are:

- because the sampling frequency is set at 100 kHz the plotting resolution for short duration test is not optimised
- the software process is slow. This is due to the large array of data that is stored during the 2 seconds of sampling.

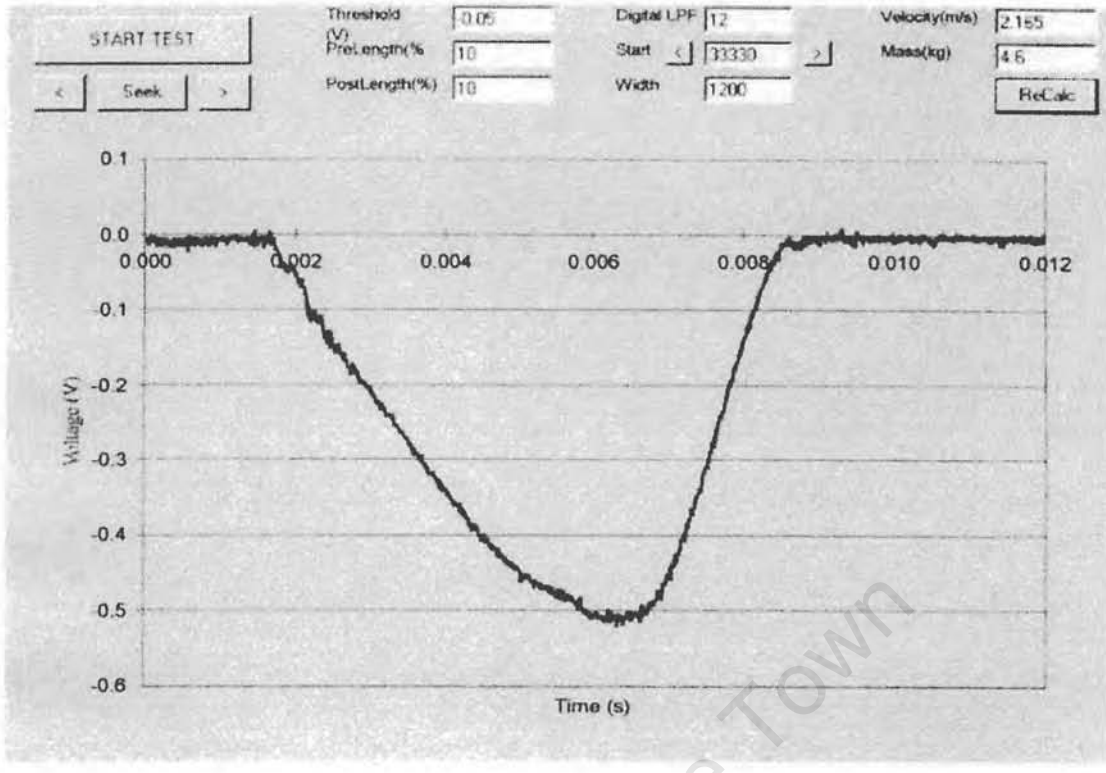

Figure 3.27 A fraction of the 2 second voltage sample for a rebound impact, plotted as a voltage-time curve.

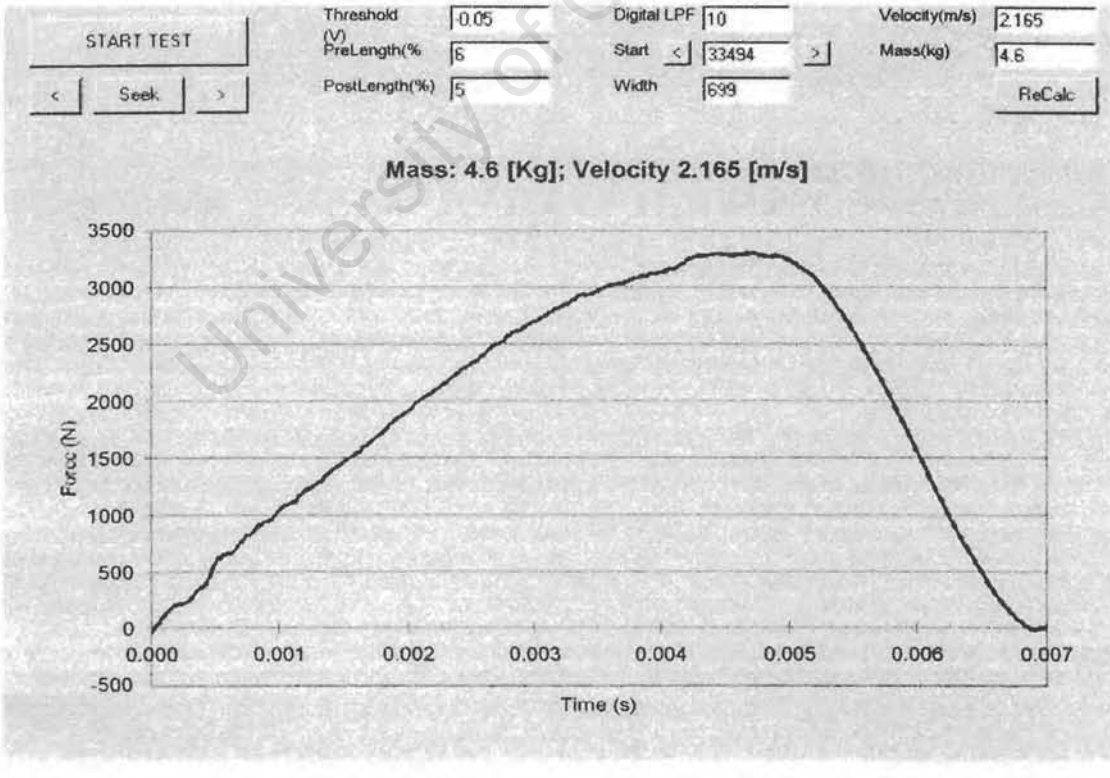

Figure 3.28 The force-time curve. Note: the force data has been smoothed and the pre and post-threshold variables have been adjusted to ensure only the relevant data is captured and the load trace goes through the origin.

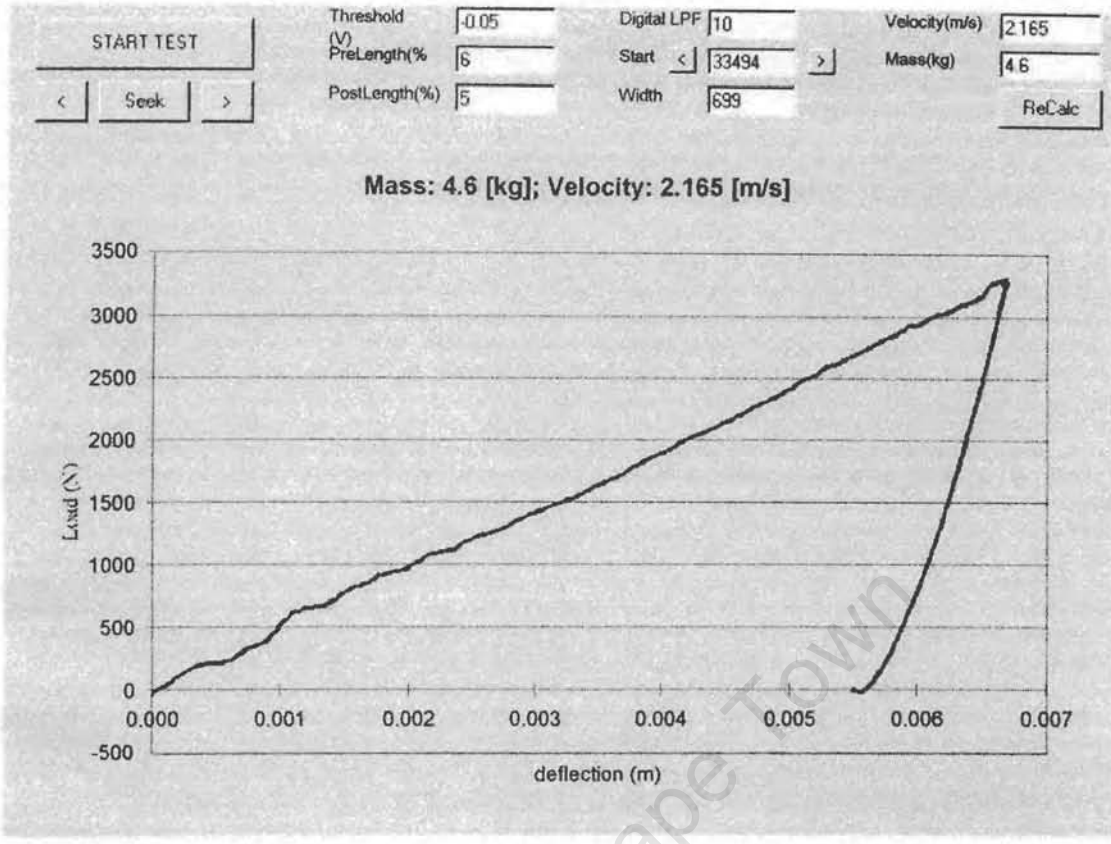

Figure 3.29 A typical force-deflection curve.

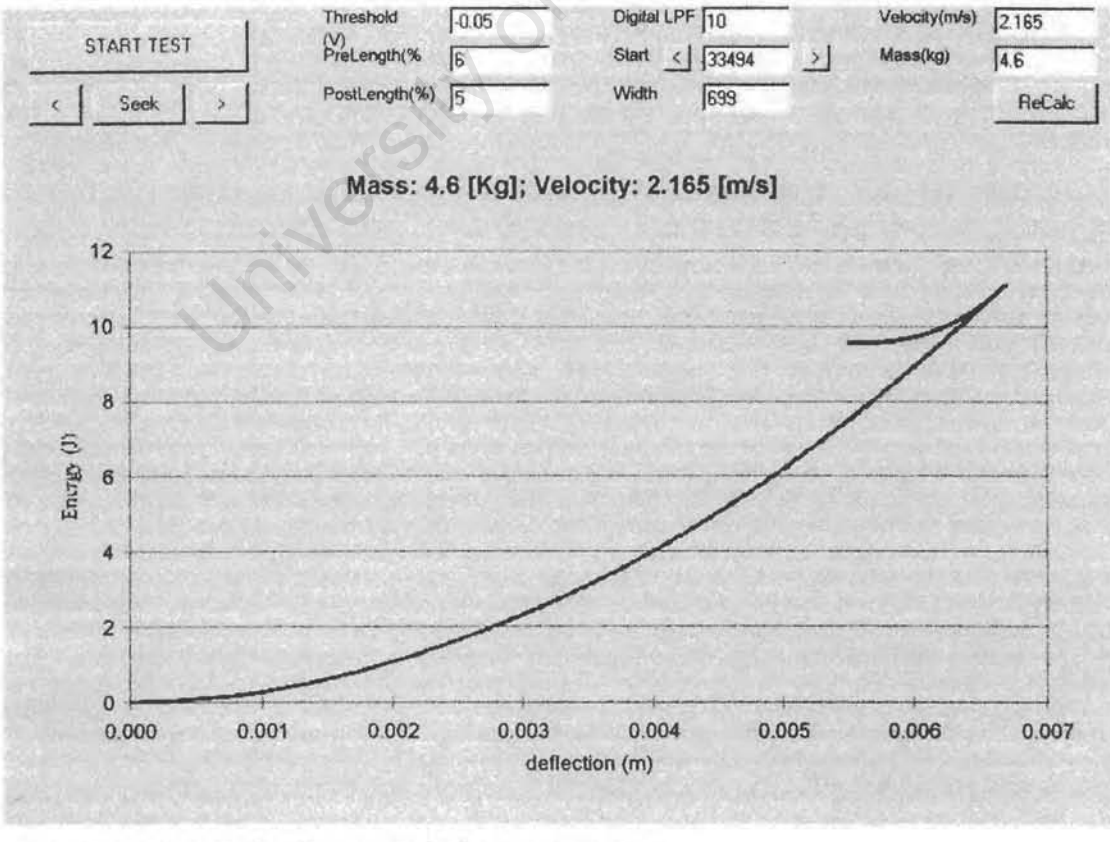

Figure 3.30 A typical energy-deflection curve.

3.7 Experimental Procedure

This section presents the impact analysis methodology used in this study. A guide to using the impact testing apparatus and the calibration of the load cell is presented.

3.7.1 Test Rig Operation

A step by step guide to performing an impact test using the instrumented drop weight tower is presented. It is assumed that a test specimen conforming to the dimensions specified in Figure 3.11 has been machined. It is also assumed that the load cell calibration procedure has recently been performed and the crosshead mass has been measured using the recommended weighing system described below.

The crosshead mass can be calculated in one of two ways. Either, the weight of the each component of the crosshead system is individually weighed and the sum of the components is entered as the crosshead mass. Alternatively, a digital scale is positioned on the clamping base and the crosshead assemblage is rested on the scale. The total crosshead mass can thus be read off the digital screen. Both of these systems gave equally accurate results.

Operating procedure:

1. Run the instrumented drop tester software.
2. Switch on the signal-processing unit.
3. Clean the specimen-positioning anvil and clamping plate, such that all debris that may affecting the uniformity of specimen clamping pressure, is removed.
4. If the circular test specimen is to be tested, position the specimen in the recessed anvil. If a square test specimen is to be tested, position the specimen centrally over the annular clamping anvil.
5. Position the clamping plate above the specimen and screw in the clamping bolts. Tighten each clamping bolt to 5Nm torque.
6. Adjust the velocity measurement block height such that the when the tup is resting on the test specimen the upper prong of the velocity fork is directly in line with the lower optical limit switch.
7. Measure the mass of the crosshead.

8. Enter the crosshead mass value, into the labelled text box.
9. Move the crosshead into the required position using the labelled toggle switch on the data acquisition box.
10. Click on the "start test" command box and wait for the sampling form to load.
11. Enter the load cell calibration coefficient, into the labelled text box on the sampling form.
12. Click the "perform test" command box and wait for the "commencing test warning" message box to appear.
13. Click "OK" and wait for the test to be performed and the data for the test to be processed.
14. From the "view" menu select the force-time curve.
15. Adjust the pre and post threshold length values such that only the impact event data is capture as discussed in chapter 3.6.1.
16. Adjust the Low pass smoothing value such that the shape of the force-time curve does not differ from the voltage-time curve but that a smoother plot is obtained.
17. View the force-deflection and energy-deflection curves, note the values of interest, and make the necessary deductions.
18. If the user desires to plot the graphs using a more efficient graphing tool, select the "copy graph data" function from the File menu. The data can either be pasted directly into a spreadsheet for graphing or pasted into wordpad and saved as a text file.
19. To analyse the test specimen, remove the clamping plate and perform the required inspections.
20. To perform further testing repeat steps 3 through to 19.
21. Once testing has been completed, switch off the signal processing unit and close the data acquisition package.

3.7.2 Load Cell Calibration

The load cell is compressed over a 0 to 20kN range at 0.5kN increments using a tensile testing machine. The voltage, as calculated by the data acquisition system, is

measured using the "offset value" function on the sampling form of the software package at each compression increment. The compressive force is then plotted against the measured voltage and the best fit straight line for the plotted points is calculated. The slope of the best fit straight line determines the load cell calibration coefficient in Newtons per Volt.

4. EXPERIMENTAL WORK

4.1 Experimental Motivation

The emphasis of this project was on designing and manufacturing an apparatus to analyse the projectile impact resistance of thin plate specimens. Thus, the experimental procedure was weighted towards performing tests to investigate the validity of the impact test result and demonstrating the performance capabilities of the instrumented impact testing apparatus. A secondary aspect of the performance capability investigation was to analyse the impact response of selected materials to low velocity impact.

In order to analyse the performance of the impact apparatus, the majority of the tests would be performed on a ductile material. It was felt that the longer impact duration, for ductile impact, and thus improved plotting resolution, would give a superior illustration of the performance of the impact test rig. The plotting resolution issue is discussed in section 3.6.1. In which, it was concluded that although the sampling frequency upper bound of 100kHz is sufficient to make the critical inferences, the small sample of data points captured for the brittle material impact event did not do justice to the capabilities of the impact rig and data acquisition system.

The ductile material chosen for this investigation was aluminium grade 1200. This decision was based on the typically ductile behaviour of this grade of aluminium and its relatively low cost and high availability.

A secondary element of this study was to analyse the projectile penetration resistance of combinations of a ductile and brittle material acting simultaneously. Conventional plate glass was chosen as the brittle and aluminium grade 1200 was chosen as the ductile material. The tests that were performed are discussed further in section 4.4.

The test rig operating procedure and the methodology for analysing the impact response of a test specimen are discussed in section 3.7.

4.2 Impact Apparatus Performance Evaluation

The results acquired using the impact testing rig were verified by comparing the actual deformation for a rebound impact event, measured on the impacted specimen, to the deflection as measured by the impact testing rig data acquisition system.

It was felt that this was the best method of demonstrating the accuracy of the data acquisition system. The tup deflection is a function of the crosshead mass, impact velocity and the penetration resistance load trace. If one of the dependent variables is inaccurate, the displacement calculation will be incorrect. The crosshead mass is measured independently. Thus, the accuracy of the deflection calculations is dependent on the accuracy of the penetration resistance load trace and impact velocity. If the displacement measured by the apparatus corresponds with the actual plastic deformation, over a range of impact parameters, the impact velocity and penetration resistance load trace is proved accurate.

Figure 4.1 illustrates the force-deflection curve for a rebound impact event. X_{total} is the measure of the total plastic deformation that took place during the impact event. Figure 4.2 shows a sectional profile of the plastic deformation after a rebound impact. The total plastic deformation is a measure of the dishing deformation and the localised indent. The value X_{total}, measured by the data acquisition system and on the specimen must correspond for the data acquisition system to be proved accurate.

The plastic deformation agreement tests were performed using a 12.7mm hemispherical head tup. Tests were performed on both 3mm and 6mm thick plates using three different crosshead masses. The crosshead was released from 1.5m, 2.5m and 3.5m. A minimum of five tests for each set of test parameters was performed. The average difference and percentage error between the actual deformation and the measured deformation were calculated for each set of test parameters.

Specific reproducibility tests were performed on 3mm and 6mm thick aluminium specimens releasing a 2.9kg crosshead from three drop heights. Three tests were performed at each impact velocity and the force-deflection curves for each series of

tests was plotted on the same set of axes to illustrate the close correlation of the data for identical tests.

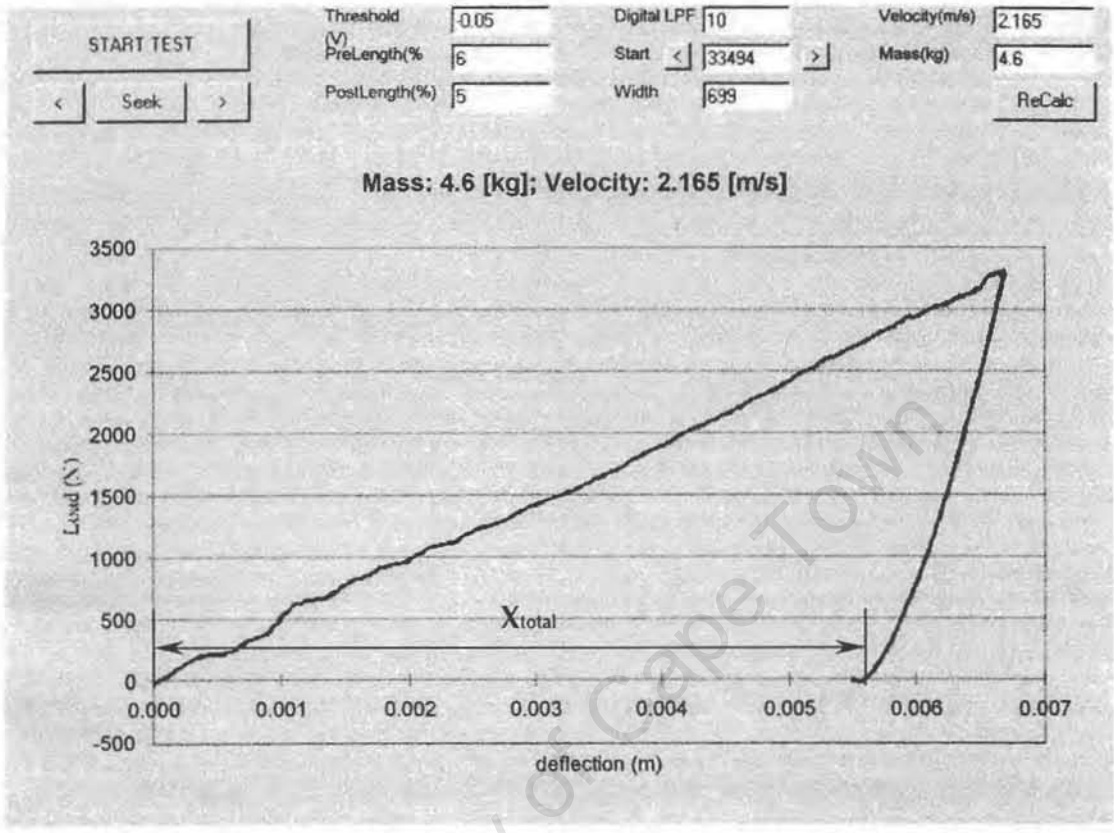

Figure 4.1 The total plastic deformation as measured by the impact testing apparatus.

$$X_{total} = X_{dishing} + X_{indent}$$

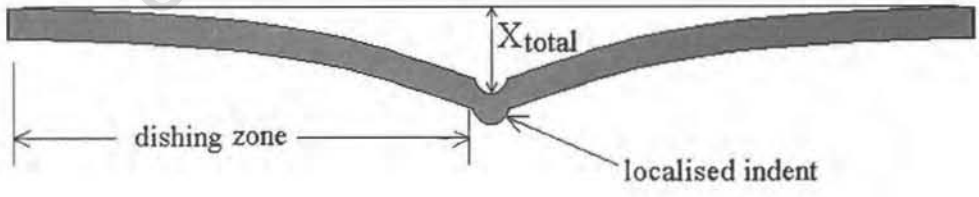

Figure 4.2 A sectional profile of the dishing and indentation deformation due to a rebound impact.

4.3 Impact Behaviour of Ductile Plates

The impact response of ductile materials to changing impact parameters was investigated. The emphasis of these tests was on demonstrating the acquired impact response was in accordance with the observed and expected impact response with respect to the literature. The system variables that influence the impact response of the test specimen are, the initial impact velocity, kinetic energy, projectile shape and specimen thickness. To test the influence of an individual system variable, tests were performed varying the individual variable and keeping the remaining system variables constant.

The variables kept constant were chosen such that a complete range of impact phenomena i.e. from rebound to through penetration would be exhibited by varying the remaining variable over the range available. The constant parameters used when an individual parameters influence was being analysed were as follows:

- Tup; 12.7mm diameter hemispherical head
- Impact velocity; $5m.s^{-1}$
- crosshead mass; 4.6kg
- plate thickness: 3mm

Table 4.1 presents an experimental matrix of the test performed and the impact parameters for the various tests. The influence of an impact parameter was analysed by plotting a force and energy-deflection curve, for each set of variables, on the same set of axes so that the effect of the changing parameter could be graphically inspected. As the impact apparatus results were already proved highly reproducible, only one force-deflection and energy-deflection curve for each set of impact parameters was plotted.

Influence of impact velocity				
impact velocities (approximate)	3.5m.s^{-1}	5.0m.s^{-1}	6.0m.s^{-1}	7.0m.s^{-1}
plate thickness	3mm			
tup Diameter	12.7mm			
crosshead mass	4.6kg			
Influence of crosshead mass				
crosshead masses test	2.5kg	2.9kg	4.6kg	7.55kg
plate thickness	3mm			
tup Diameter	12.7mm			
impact velocity	5m.s^{-1}			
Influence of changing plate thickness					
plate thickness tested	0.9mm	2mm	3mm	4.5mm	6mm
crosshead mass	4.6kg				
tup Diameter	12.7mm				
impact velocity	5m.s^{-1}				
Influence of changing tup diameter				
tup diameters tested	4mm	6mm	8mm	10mm
impact velocity	5m.s^{-1}			
plate thickness	3mm			
crosshead mass	4.6kg			

Table 4.1 The experiment matrix for tests performed to analyse the impact behaviour of aluminium grade 1200 plates.

4.4 Impact Behaviour of Laminated Ductile and Brittle Plates

The impact resistance of a brittle and ductile material acting as a laminated plate was investigated. Conventional float glass was chosen as the brittle material and aluminium grade 1200 was used as the ductile material. Glass was chosen due to its low fracture toughness and typically brittle behaviour. It was felt that the impact apparatus's ability to effectively analyse the effect of placing a low fracture toughness glass in combination with a high fracture toughness ductile material would serve as an effective demonstration of the impact testing apparatus's capabilities.

The projectile impact response of 6mm laminated plates made up of a combination of 3mm glass and aluminium plates were investigated. Both permutations of glass acting as the front and rear surface were investigated. The response of the laminated plates was compared to individual 6mm glass and aluminium plates.

Due to the low energies at which the glass plates fail, a low crosshead mass was favoured for this investigation. However, it was discovered that the lowest possible crosshead mass did not give the most accurate results. Thus, a slight compromise on the impact energy of the test was made in favour of an improved accuracy and a 2.2kg crosshead was used for the laminate investigation. A 12.7mm hemispherical tup was used for all the tests performed. Tests were performed at three impact velocities covering the entire velocity range. In order to confirm the validity of the results multiple tests were performed for each set of impact parameters. Table 4.2 illustrates the different laminates investigated and the various test parameters.

Laminates investigated			
3mm glass front plate and 3mm aluminium rear plate			
3mm aluminium front plate and 3mm glass rear plate			
6mm aluminium plate			
6mm glass plate			
Impact parameters			
Velocities tested (approximate)	$3m.s^{-1}$	$5m.s^{-1}$	$7m.s^{-1}$
Tup Diameter	12.7mm		
Crosshead mass	2.2kg		

Table 4.2 Experimental matrix for the laminated plate tests.

5. RESULTS

5.1 Evaluation of the Low Velocity Impact Testing Apparatus

5.1.1 The Plastic Deformation Correlation Tests

The results of the test conducted to verify the agreement of the actual deformation with the deformation as measured by the impact analysis software are presented in this section. The mean and standard deviation were calculated from each set of tests performed. From the average actual deformation measured on the specimen and deformation measured by the impact testing rig, the average difference and percentage error were calculated. The test parameters and results for the tests performed are illustrated in Table 5.1 and force-deflection curves for the 2.9kg crosshead tests are illustrated in Figure 5.1. A standard 12.7mm diameter hemispherical head tup was used for the entire series of tests.

It was found that the impact testing apparatus could accurately measure the actual plastic deformation that took place during a rebound impact event. The error percentage results varied from a low of 0.48% to a high of 15.9%. It is noted that the high percentage error of 15.9% was attained for the particularly sensitive case of the 1.2kg crosshead impacting on a 6mm thick plate.

Minor deviations in measured and actual deformation for identical tests were observed. In most cases the deviation increased with increasing drop height. The deviation in measured and actual deformation is attributed to the minor deviations in impact velocity from the same drop height. The deviation in impact velocity is attributed to changes in minor changes in bearing lubrication for each test. From Figure 5.1 it can be seen that the deviation in measured plastic deformation was directly related to the variation in impact velocity from the same drop height. This is best illustrated by the tests performed on 3mm thick plates, for the 3.5m release height tests, the relatively large deviation in impact velocity correlates with the large deviation in measured plastic deformation. Whereas for the 1.5m release height tests the small deviation in

impact velocity correlates with small deviations in measured plastic deformation. In all cases, an increase in impact velocity corresponds with an increase in measured deformation.

From a set drop height, the impact velocity increased with an increase in the mass of crosshead.

test performed		average actual deformation (measured on the plate using a particular vernier calliper)		average deformation measured by software		average difference	
	average velocity ($m.s^{-1}$)	mean (mm)	standard deviation	mean (mm)	standard deviation	(mm)	% error from actual deform-ation
3mm plate 1.2kg crossead	4.28	4.14	0.114	4.46	0.089	0.32	7.72%
	6.58	7.30	0.2	7.72	0.130	0.42	5.75%
	6.89	7.4	0.187	8.10	0.071	0.7	9.45%
3mm plate 2.9kg crosshead	4.59	8.20	0.100	8.16	0.089	0.04	0.48%
	6.34	11.80	0.187	11.98	0.164	0.18	1.51%
	7.74	15.58	0.277	15.7	0.561	0.12	0.8%
3mm plate 4.6kg crosshead	4.9	11.32	0.100	11.85	0.120	0.53	4.68%
	6.024	15.0	0.137	15.71	0.158	0.71	4.73%
	Through penetration occurred						
6mm plate 1.2kg crosshead	4.60	1.38	0.084	1.6	0.071	0.28	15.9%
	5.90	2.35	0.156	2.7	0.130	0.42	14.8%
	6.44	2.61	0.114	2.92	0.164	0.40	11.8%
6mm plate 2.9kg crosshead	4.60	3.08	0.130	3.32	0.084	0.24	7.79%
	6.30	5.28	0.084	5.64	0.114	0.36	6.81%
	7.7	7.00	0.158	7.28	0.084	0.28	4%
6mm plate 4.6kg crosshead	5.05	5.64	0.089	5.82	0.100	0.18	3.19%
	6.91	9.22	0.084	9.84	0.114	0.62	6.72%
	7.87	10.52	0.148	10.88	0.089	0.36	3.3%

Table 5.1 The actual plastic deformation and measured deformation correlation results.

5.1.2 Reproducibility of Impact Test Results

Reproducibility tests were performed using a 2.9kg crosshead impacting on 3mm and 6mm thick aluminium specimens. Three tests were performed from each release height. The crosshead was released from 1.5m, 2.5m and 3.5m thus covering the full range of crosshead travel available. The force-deflection results of the tests are illustrated in Figure 5.1. For identical tests, highly reproducible force-deflection curves were observed. From Figure 5.1 it is noted that the initial impact velocity does not alter the shape of the force-deflection curve pre the yield point.

From a set release height, minor variations in impact velocity were observed. A corresponding variation in the measured displacement was found for the variations in velocity from the same drop height. For all the tests the deviation in velocity increased with increasing release height. The increased in impact velocity deviation with increasing release height is attributed to the variation in bearing friction acting over a longer period of time. A maximum variation in velocity of 0.15m.s^{-1} was observed from a release height of 3.5m.

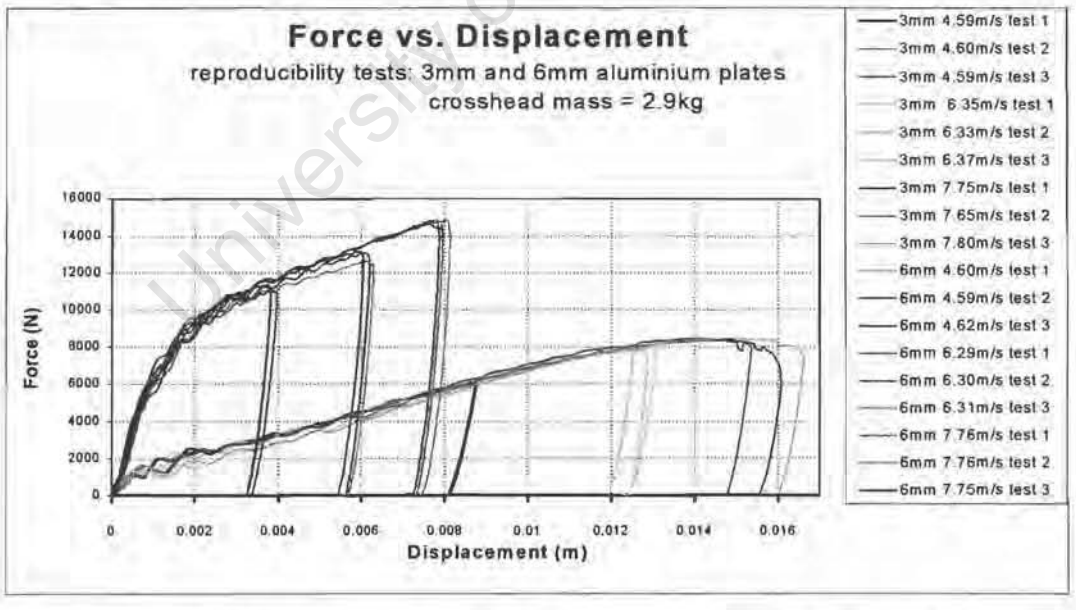

Figure 5.1 Force-deflection curves for the reproducibility tests performed on 3mm and 6mm aluminium plates using a 2.9kg crosshead.

5.2 The Low Velocity Impact Response of a Ductile Material

The impact response of aluminium grade 1200 to changing impact parameters was investigated. The influence of four system parameters namely, the projectile shape, impact velocity, projectile mass and specimen thickness was analysed.

5.2.1 Influence of Impact Velocity

The tests to analyse the influence of impact velocity on a ductile material's impact response were performed using a 12.7mm diameter tup attached to a 4.6kg crosshead impacting on 3mm thick test specimens. To obtain a wide range of impact velocities the crosshead was released from four release heights, facilitating four different impact velocities ($3.84 m.s^{-1}$, $5.01 m.s^{-1}$, $5.88 m.s^{-1}$, $6.85 m.s^{-1}$).

Figure 5.6 illustrates the force and energy-deflection curves generated by the impact apparatus for the various impact velocities. A sectional profile view for each test is illustrated in Figure 5.7. Rebound impact events occurred for the 3.84 to $5.88 m.s^{-1}$ tests and through penetration occurred for the $6.85 m.s^{-1}$ test. Agreement of the actual and measured impact response is illustrated by the force-deflection curves and the sectional profile illustration.

Identical pre-maximum load point force-deflection curves were observed for the different impact velocities. Impact velocity had no influence on the yield point that occurred at approximately 2000N and 1.9mm of tup displacement. The dishing extent increased with increasing impact velocity although very similar dishing profiles were observed for all the tests. This was particularly apparent for the 5.88 and $6.85 m.s^{-1}$ tests where the dishing profiles are almost identical. A greater variation in the degree of plate thinning at the localised indentation with increasing velocity was observed. An appreciable degree of plate thinning was observed for the $5.88 m.s^{-1}$ test.

For the $6.85 m.s^{-1}$ test the approximately 97 Joules of the initial 107 Joules of kinetic energy was absorbed during the impact event and through penetration occurred at

17mm of tup displacement. The point of maximum load occurred at 8300N and 14mm of tup displacement.

For all the rebound tests very small rebound displacements were noted. This is in accordance with the energy-deflection curves where it is noted that the energy absorbed during impact is only slightly less than the initial kinetic.

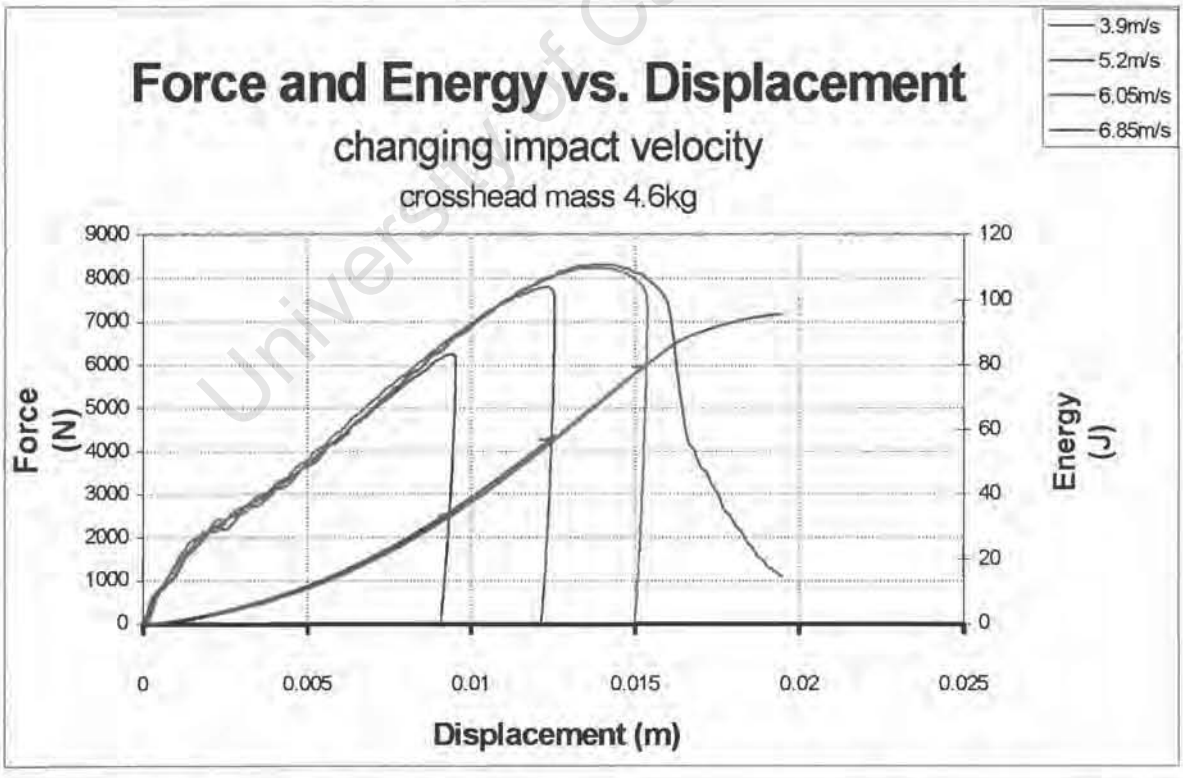

Figure 5.2 The force and energy versus deflection curves illustrating the effect of impact velocity on the impact response of the test specimens as measured by the impact testing apparatus.

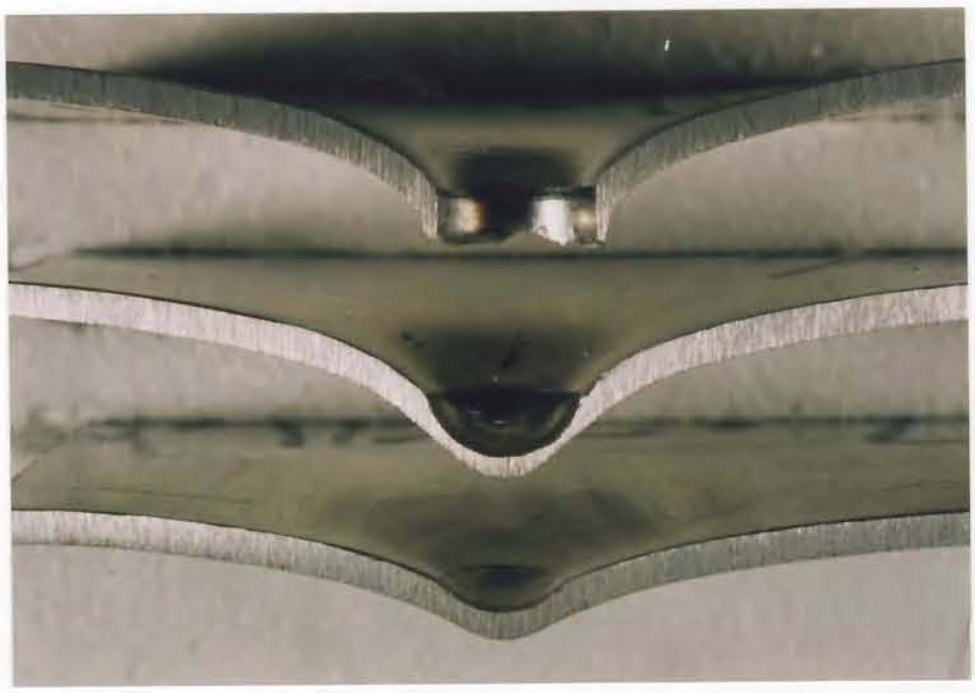

Figure 5.3 Sectional profiles of the impacted plates for the changing impact velocity tests (plates in order of decreasing velocity, top plate 6.85m.s^{-1}, 5.88m.s^{-1}, 3.85m.s^{-1}). Tests performed using a 4.6kg crosshead and 12.7mm tup.

5.2.2 Influence of Crosshead Mass

The tests to analyse the influence of crosshead mass on the impact response of ductile plates were performed using a 12.7mm diameter tup impacting on 3mm thick plate. The crosshead was released from approximately 1.6m to facilitate a 5.2m.s^{-1} initial impact velocity. The effect of four crosshead masses (7.55kg, 4.6kg, 2.9kg, 2.5kg) was investigated.

Figure 5.4 illustrates the force and energy-deflection curves generated by the impact apparatus for the various crosshead masses. A sectional profile view for each test is illustrated in Figure 5.5. According to the force-deflection curves and sectional profile of the test specimens, the influence of crosshead mass closely resembled that of impact velocity. Rebound impact events occurred for the 2.5 to 4.6kg crosshead impact tests and through penetration occurred for the 7.55kg crosshead.

Irrespective of crosshead mass, identical gradients for the force-deflection curves were observed during the linear elastic-loading phase. A distinct change in slope, indicating the onset of plastic yielding, was observed at 1700N and 1.5mm of tup displacement. As with the changing velocity tests the dishing extent increased with increasing impact velocity although very similar dishing profiles were observed for all the tests. A greater variation in the degree of plate thinning at the localised indentation with increasing crosshead mass was observed.

For the 7.7kg case the through penetration occurred after approximately 17mm of tup displacement. The point of maximum load was reached at 8500N and 14mm of tup displacement. For the 7.55kg crosshead test 97 Joules of the initial 103 Joules of kinetic energy was absorbed during the impact event. As with the changing velocity test very small rebound displacements were noted, this is confirmed by the energy deflection curve where the amount of energy absorbed during the rebound impact events was slightly less than the initial kinetic energy.

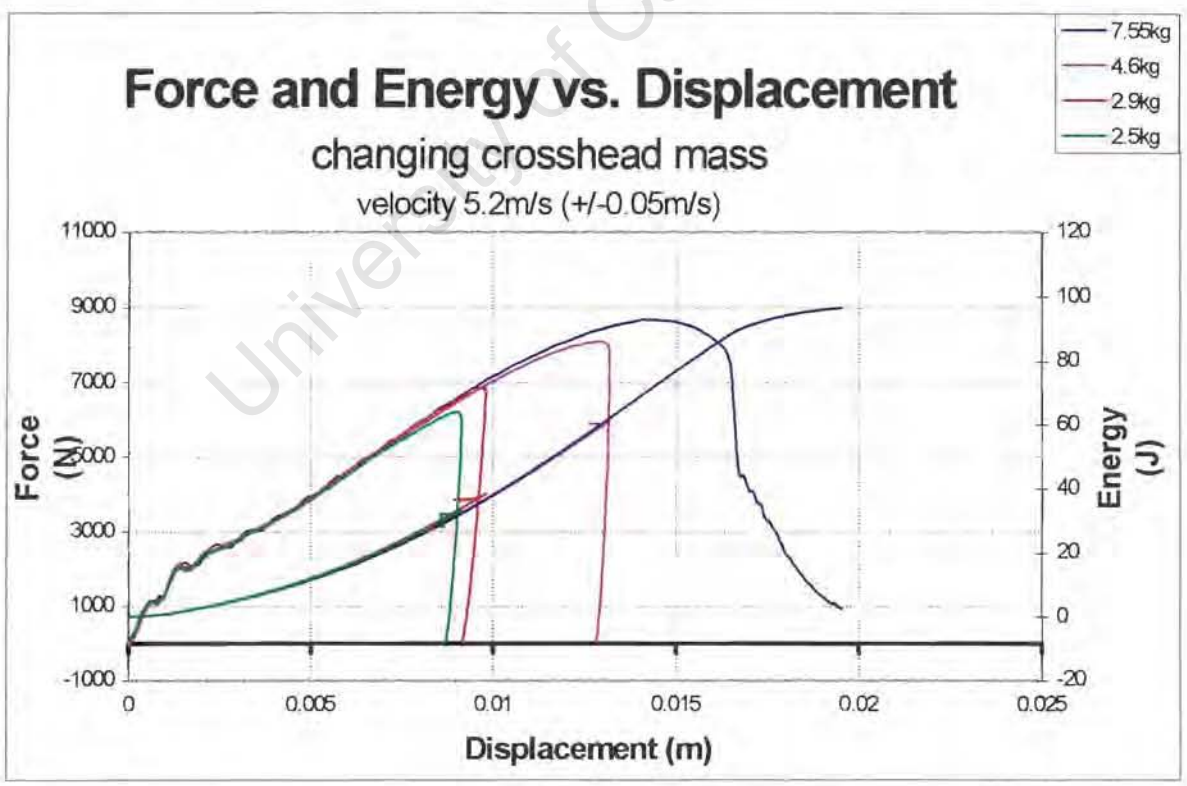

Figure 5.4 The force and energy versus deflection curves illustrating the effect of crosshead mass on the impact response of the test specimens as measured by the impact testing apparatus.

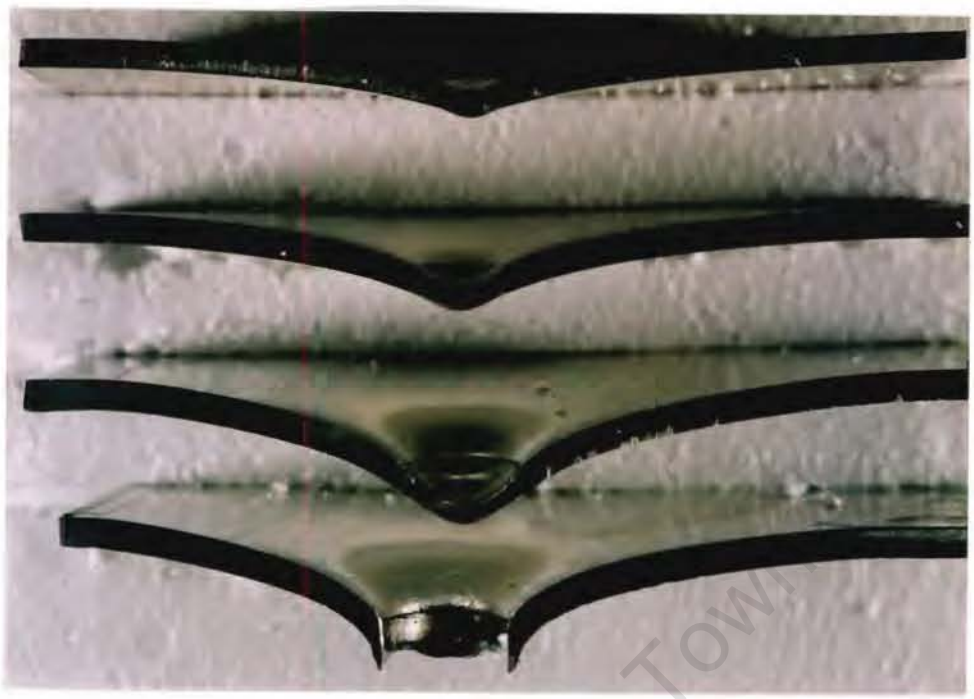

Figure 5.5 Sectional profiles of the impacted plates for the changing crosshead mass tests (plates in order of increasing mass, top plate 2.5kg, 2.9kg, 4.6kg, 7.55kg). Test performed at 5.2m.s^{-1} using a 12.7mm tup.

5.2.3 Influence of Tup Diameter

The tests to analyse the influence of the tup diameter were performed using a 4.6kg crosshead impacting on 3mm thick plates. The crosshead was released from approximately 1.6m facilitating a 5.1m.s^{-1} impact velocity. Four tups of varying hemispherical diameter (4mm, 6mm, 8mm, 10mm) were utilised for these tests. The changing crosshead mass with changing tup, although marginal, was accounted for.

The force and energy-deflection curves generated by the impact apparatus for the various tup diameter tests are shown in Figure 5.6. A sectional profile view for each test is illustrated in Figure 5.7. Through penetration occurred for the 4 to 8mm tup impacts and a rebound impact occurred for the 10mm tup impact. The agreement as to the impact response can be observed on the force-deflection curves and the sectional profile illustration.

In the initial indentation stage, the tup diameter had very little influence on the gradient of the force-deflection curves until a yield point was reached at 1800N and a displacement of 1.8mm. After the yield point the gradient of the force-deflection curves decreased with decreasing tup diameter. Increased maximum load with increasing tup diameter was recorded.

For the 4mm and 6mm tup impact events very little dishing occurred. Hence, the displacement to cause through penetration was notably less than the displacement for the 10mm tup rebound impact. The high pressure associated with the smaller contact area for the 4 and 6mm tups was sufficient to cause shearing of a plug, of similar diameter to the tup, from the plate as opposed to the formation of dishing and plate thinning at the localised indent. The plug sheared from the test specimen for the 4mm tup case was of similar thickness to that of the original plate material with slight thinning of the plug at the circumference. The plug formed in the 6mm case was marginally thinner than the plate material and showed significant thinning at the circumference. From the energy-deflection curve, the energy required for plugging (18J and 32J respectively) in the 4mm and 6mm tup diameter cases is significantly less than the high energy dishing and plate thinning mechanism that dominated the 8mm tup impact event (53J).

From the sectional profiles in Figure 5.7 the amount of dishing significantly increased with increasing tup diameter. For the 10mm tup impact an appreciable degree of plate thinning and localised bending in the vicinity of the loading area occurred. For the 8mm tup impact the degree of plate thinning was sufficient to fracture a thin dome shaped plug from the plate material.

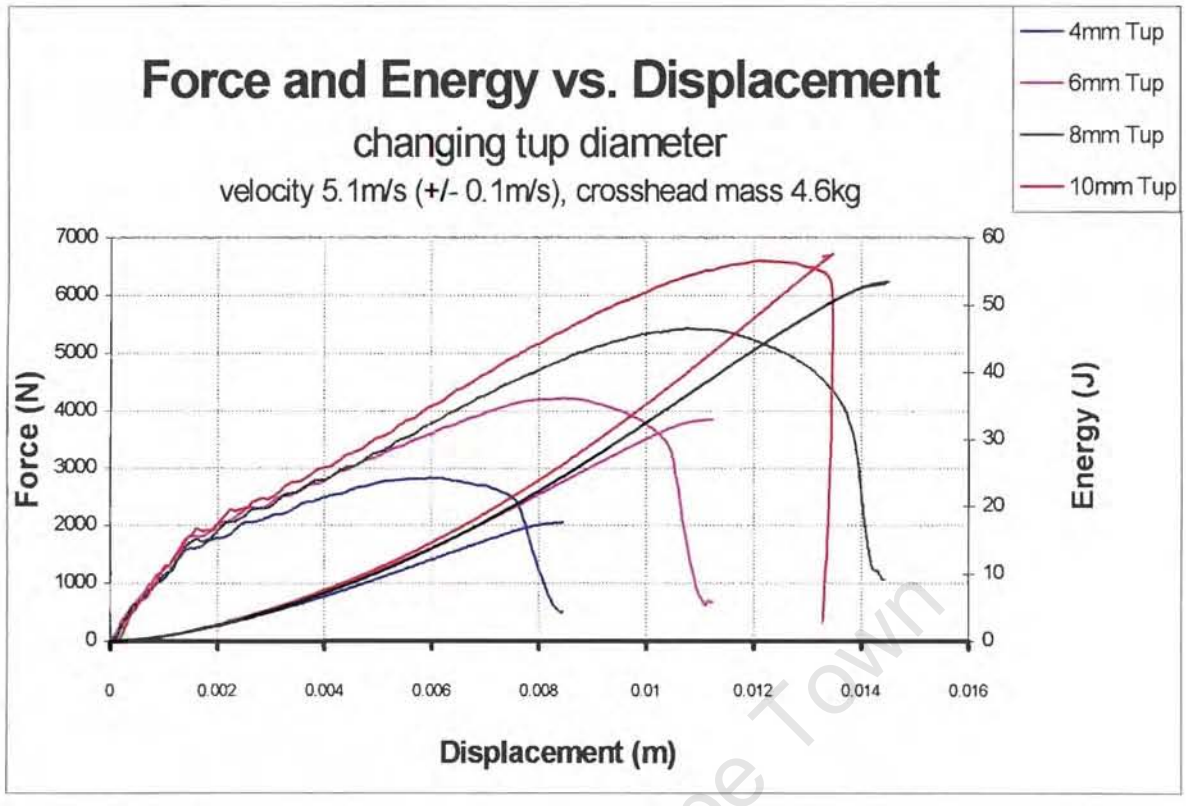

Figure 5.6 The force and energy versus deflection curves illustrating the effect of tup diameter on the impact response of the 3mm aluminium specimens.

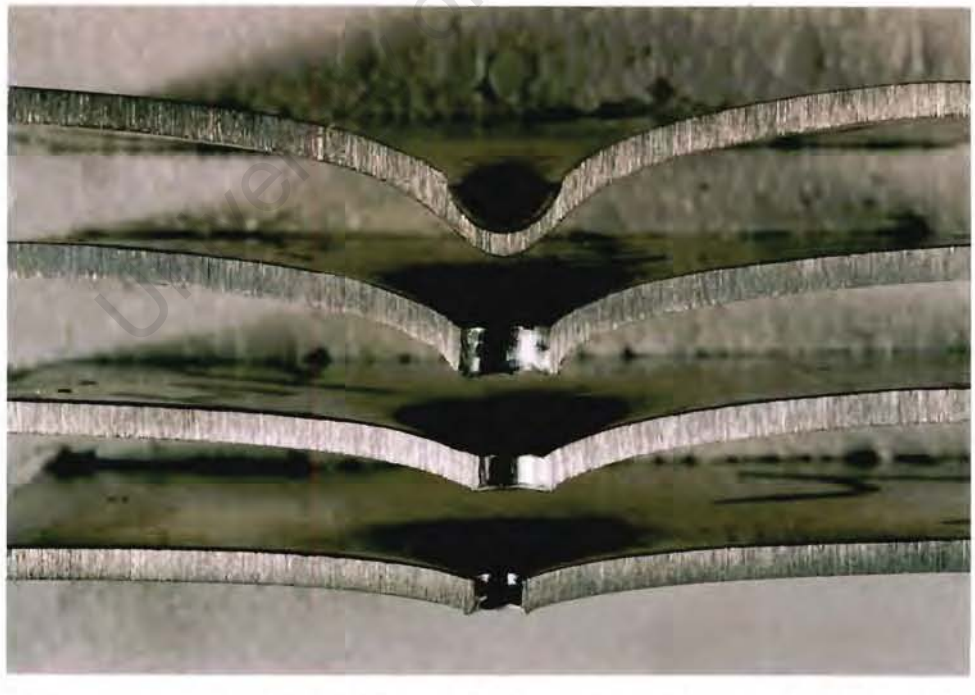

Figure 5.7 Sectional profiles of the impacted plates for the 10, 8, 6 and 4mm tup diameter tests (decreasing tup diameter from the top). Test were performed using a 4.6kg crosshead with a 5.1m.s^{-1}.

5.2.4 Influence of Specimen Thickness

The tests to investigate the influence of specimen thickness on the impact behaviour were performed using a 4.6kg crosshead, released from approximately 1.6m facilitating a 5.2m.s^{-1} impact velocity. Five different specimen thicknesses were tested (6, 4.5, 3, 2 and 0.9mm) and a standard 12.7mm diameter tup was used for all the tests.

The force and energy-deflection curves generated by the impact apparatus for the plate thickness tests are shown in Figure 5.8 and the sectional profile for the 6, 4.5, 3 and 2mm plate thickness tests are illustrated in Figure 5.9.

Through penetration occurred for the 0.9 and 2mm plate thickness tests and rebound impacts occurred for the 3, 4.5 and 6mm plate thickness tests. Although the sectional view of the 0.9mm thick plate is not shown in Figure 5.9, due to problems encountered in sectioning the thin plate, however, the impact response is visible on the force-deflection curve. Agreement of the force-deflection curve and the observed impact behaviour was noted for all the tests performed.

The gradient of the force-deflection curves increased significantly with increasing plate thickness. This is attributed to an increase in relative stiffness with increasing plate thickness.

For the 6mm thick plate test, the localised indentation dominated the impact response as opposed to dishing. However, dishing increased appreciably with decreasing plate thickness hence the increase in measured tup displacement with decreasing plate thickness. The effect of the increase in plastic deformation with decreasing plate thickness is to lessen the load resistance and thus maximum load point, as is seen on the force-deflection curve. The 3mm thick plate showed significant localised thinning at the edge of the tup contact area as opposed to the 4.5 and 6mm thick plates where minimal plate thinning was observed.

The maximum load decreased notably with decreasing plate thickness and an increase in the displacement to maximum load was observed. Although vastly different impact responses were noted for the 3, 4.5 and 6mm thick plate tests similar absorbed impact energy values were noted for the various tests. Approximately 57 Joules of the 62 Joules of kinetic energy was absorbed for each specimen thickness. For the 2 and 0.9mm thick plates, the absorbed impact energy is significantly decreased from the tests in which rebounds occurred as the total kinetic energy was not transferred to the plates and the crosshead motion was arrested by a stoppage block.

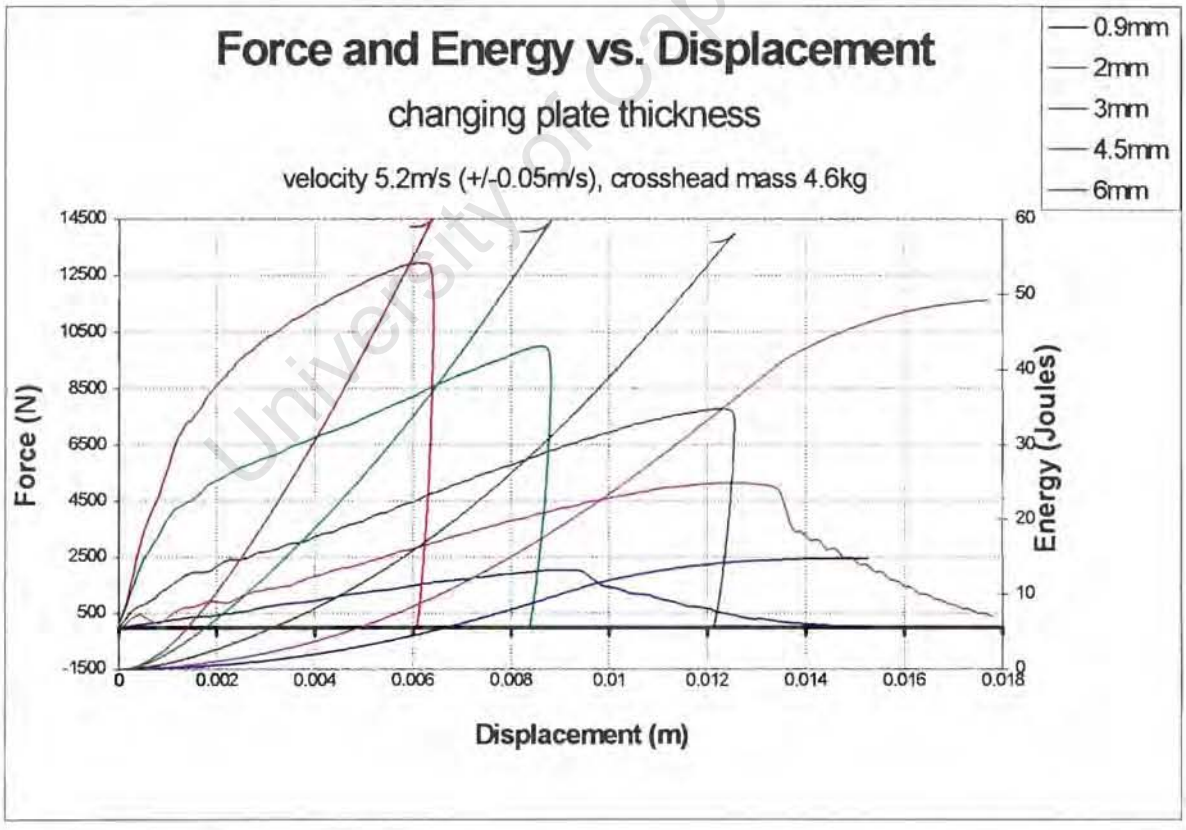

Figure 5.8 The force and energy versus deflection curves illustrating the effect of changing test specimen thickness as measured by the impact testing apparatus.

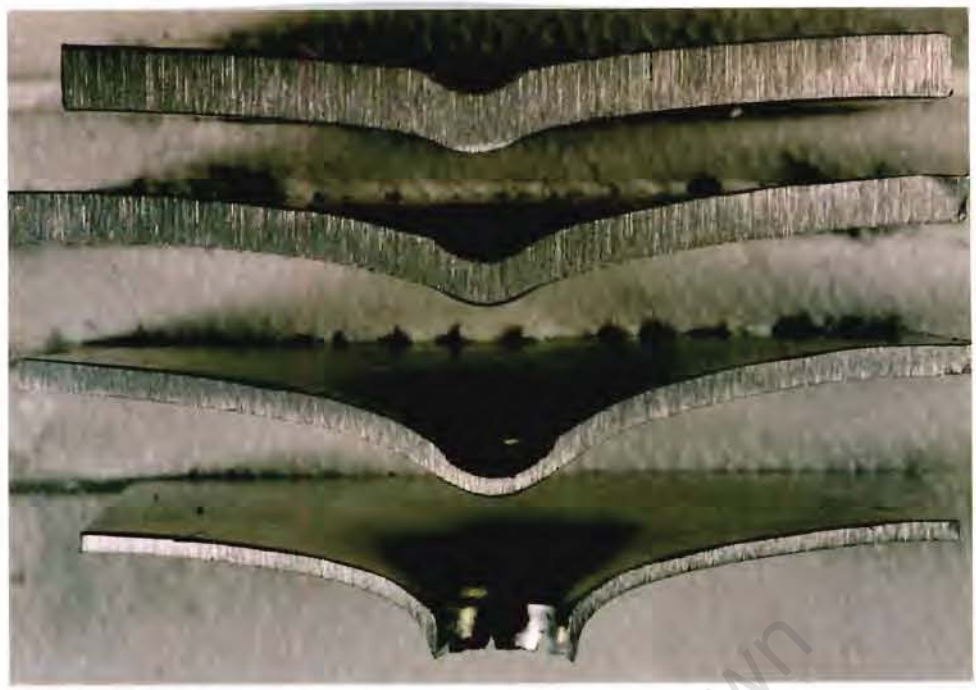

Figure 5.9 Sectional profiles of the varying plate thickness tests (decreasing plate thickness from the top, 6mm, 4.5mm, 3mm, 2mm). Test performed using a 4.6kg crosshead with a 12.7mm tup, with an impact velocity of 5.2m.s^{-1}.

5.3 The Low Velocity Impact Response of Brittle and Ductile Material Laminate Plates

The results of tests conducted to investigate the impact response of laminated plates made up of 3mm thick glass and aluminium plates are presented. The impact response was compared to that of 3 and 6mm thick aluminium plates and a 6mm thick glass plate. The influence of placing the glass on the distal or impacted side of the laminate was also investigated. For the purpose of discussion, the laminate with glass acting on the impacted side will be referred to as the glass-front laminate and the laminate with glass acting on the distal side will be referred to as the glass-rear laminate.

Tests were performed from three consecutive drop heights (1m, 2m, 3.5m) using a 2.2kg crosshead and a 12.7mm diameter tup. Multiple tests were performed for each set of parameters and laminates to verify the observed trends. Tests were repeated until the impact velocity for each laminate tested was equal to within two decimal places, thus eliminating the effect of minor variations in impact velocity on the measured deformation. The exact impact velocity and variation in velocity is illustrated on the force-deflection curves. Due to the high reproducibility of the test results it was felt that

plotting the results of multiple tests would unnecessarily confuse the readability of the graphs, thus, one test for each laminate was plotted on the graphed results. To demonstrate the reproducibility of the observed trends and justify the decision to plot only one test for the 3 and 7m.s^{-1} tests, two tests results are plotted for the 5m.s^{-1} impact velocity tests.

Figure 5.10 illustrates the force and energy-deflection curves for the 5m.s^{-1} laminate tests. From the Figure 5.10, it is seen that the glass-aluminium laminates and the 3mm aluminium plate exhibited very similar responses, the 3mm glass plate had no significant influence on the impact response of the laminate plate. The major influence of the glass is observed in the first 4mm of projectile displacement. Thus, for greater clarity, the force and energy-deflection curve for the first 4mm of penetration is illustrated in Figure 5.11.

The highest gradient, on the force-deflection curve, for the initial stage of penetration (pre 0.5mm displacement) was observed for glass-front laminate. A slightly reduced gradient is noted for the glass-rear laminate. The laminate plate force-deflection gradient, for the initial stage of penetration, was significantly higher than that of the 3mm aluminium plate.

The glass-front laminate yielded at approximately 2000N and 0.5mm of projectile displacement, a distinct drop in the load resistance was associated with the yielding. After the load resistance decrease, the impact resistance increased to levels slightly higher than that of the singular 3mm aluminium plate. The difference in the load resistance of the glass-front laminate and the 3mm aluminium plate decreased with increasing tup penetration until approximately 5mm of deflection, where no significant difference in the load resistance of the two plates could be observed.

The glass-rear laminate initially yielded at a similar position to the glass front laminate, however in contrast to the glass-front laminate, the load continued to increase after the observed yield point and a secondary yield point was noted for the glass rear laminate

at 2500N and 1.2mm of projectile displacement. After the secondary yield point the load resistance decreased to similar levels to that of the singular 3mm aluminium plate.

From Figure 5.10 it can be seen that the largest deformation was recorded for the singular 3mm aluminium plate as opposed to the laminated plates. The increased deformation for the singular aluminium plate is attributed to the decreased energy absorption during the initial stages of impact, the kinetic energy remaining in the crosshead is thus absorbed by increased plastic deformation during the final stages. The difference in absorbed energy after the initial stage is illustrated in Figure 5.11 where after 4mm of penetration the laminate plates have absorbed approximately 9 Joules as opposed to 7 Joules absorbed by 3mm aluminium plate. The final tup displacement for the glass-front laminate was slightly higher than the glass-rear laminate. This is attributed to the glass crushing that took place on the front face, as opposed to further plastic deformation of the aluminium plate, facilitating an increase in the tup displacement. The degree of glass crushing on the glass-front laminates is illustrated in Figure 5.15. The thickness of the crushed glass layer was measured for the glass-front test and the found to be slightly reduced from the initial 3mm plate thickness.

The force-time curves for the $5m.s^{-1}$ tests are illustrated in Figure 5.12. The 6mm glass plate can be seen to fracture completely within 100 microseconds. A rapid increase in the load was observed and an initial yield and secondary yield indicating the onset of radial and circumferential fracture[38], respectively, is visible. After the onset of circumferential fracture a rapid drop in the load resistance occurred. As with the force deflection curves the 3mm aluminium plate and the glass-aluminium laminates exhibited similar force-time traces.

The difference in total absorbed impact energy for the laminate plates and 3mm aluminium plates was indistinguishable for all the impact velocities tested. Although different fracture mechanisms were observed, for the $5m.s^{-1}$ tests, both the laminates and the aluminium plate absorbed approximately 28 Joules of the initial 29.2 Joules of kinetic energy.

The trends discussed for the $5m.s^{-1}$ tests were continued for the 3 and $7m.s^{-1}$ impact velocity tests and are illustrated in Figure 5.13 and Figure 5.14 respectively. However, the influence of the glass on the impact behaviour of the laminates appeared to diminish with increasing impact velocity and the aluminium plate increasingly dominated the impact response. From Figure 5.14, illustrating the $7m.s^{-1}$ test, it was noted that for the glass-rear laminate test, the load resistance did not increase after initial yielding and the secondary yield observed in the 3 and $5m.s^{-1}$ did not occur. The $3m.s^{-1}$ test exhibited similar total tup displacement trends to the $5m.s^{-1}$ in that the largest deformation was recorded for the 3mm aluminium plate followed by the glass-front plate. However, this was not the case for the $7m.s^{-1}$ tests where approximately 13mm of tup displacement occurred for the laminate plates and the singular 3mm aluminium plate.

Figure 5.15 and Figure 5.16 illustrate the fracture patterns for the glass component of the glass-front and glass-rear laminates respectively.

For the glass-front fracture pattern, the number of radial cracks decreased and the number of circumferential cracks increased with increasing impact velocity. The fracture pattern for the $3m.s^{-1}$ test exhibited an incomplete ring of circumferential cracks at a radius similar to that of the annular clamping ring. The $5m.s^{-1}$ fracture surface also exhibited an incomplete outer ring of circumferential cracks, similar to those seen in the $3m.s^{-1}$ fracture pattern, and an almost complete ring of circumferential cracks on a smaller radius. An imprint of crushed glass is visible in the centre of the plate. The $7m.s^{-1}$ fracture pattern exhibited a more complete outer ring of cracks and a complete inner ring of circumferential cracks.

As with the glass-front fracture pattern the number of radial cracks decreased and the number of circumferential cracks increased with increasing impact velocity for the glass-rear fracture pattern. Extensive star cracking was observed.

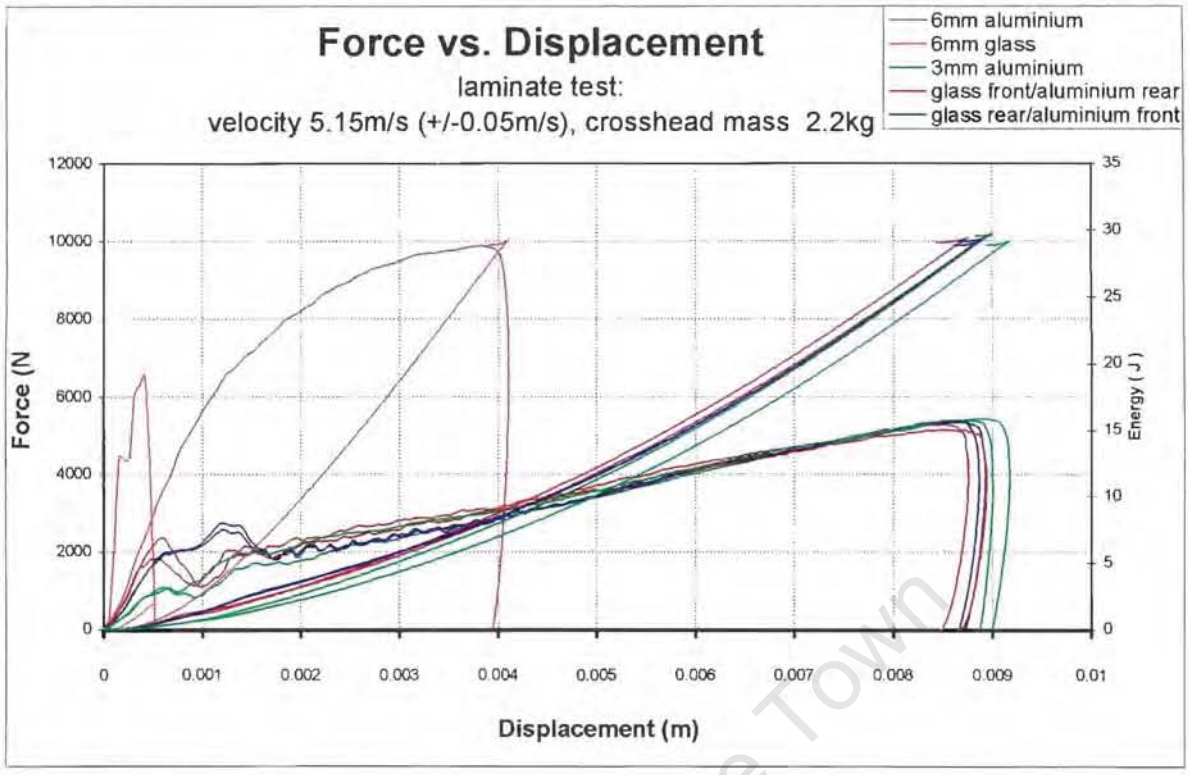

Figure 5.10 Force-deflection and energy-deflection curves (initial impact velocity 5m.s^{-1}). Test performed using a 2.2kg crosshead and 12.7mm tup.

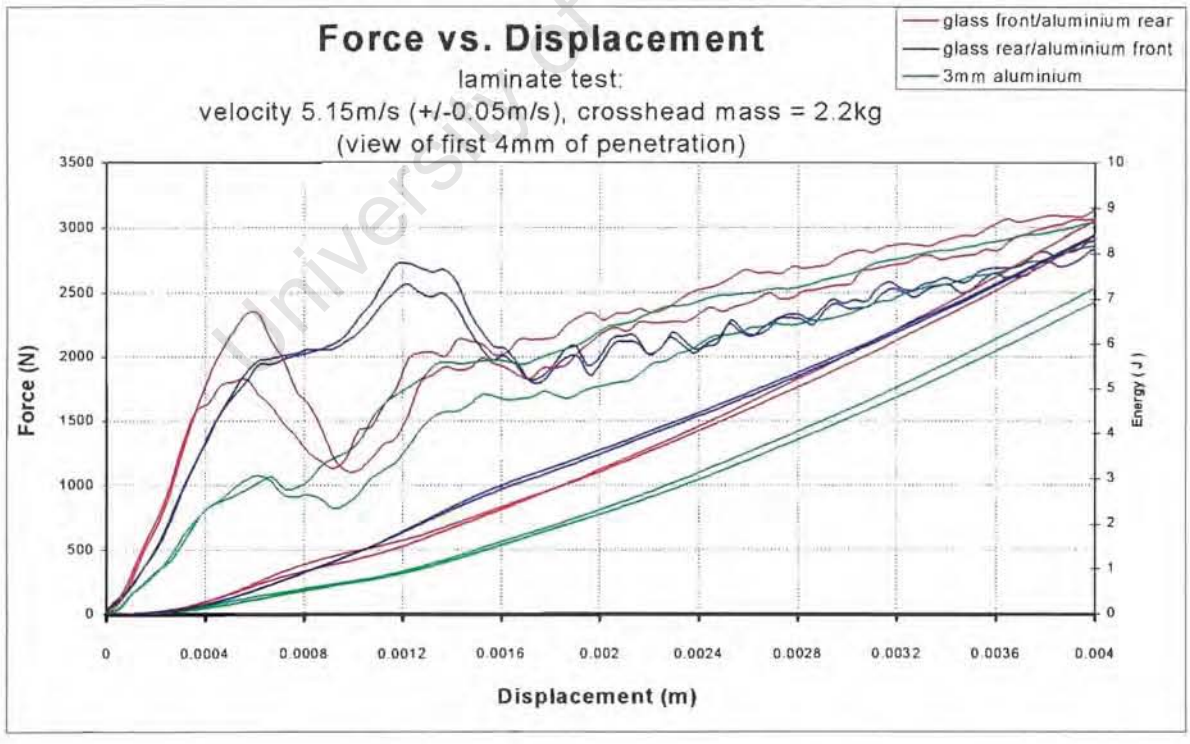

Figure 5.11 Force-deflection curve for the first 4mm of projectile penetration (impact velocity 5m.s^{-1}). Test performed using a 2.2kg crosshead and 12.7mm tup.

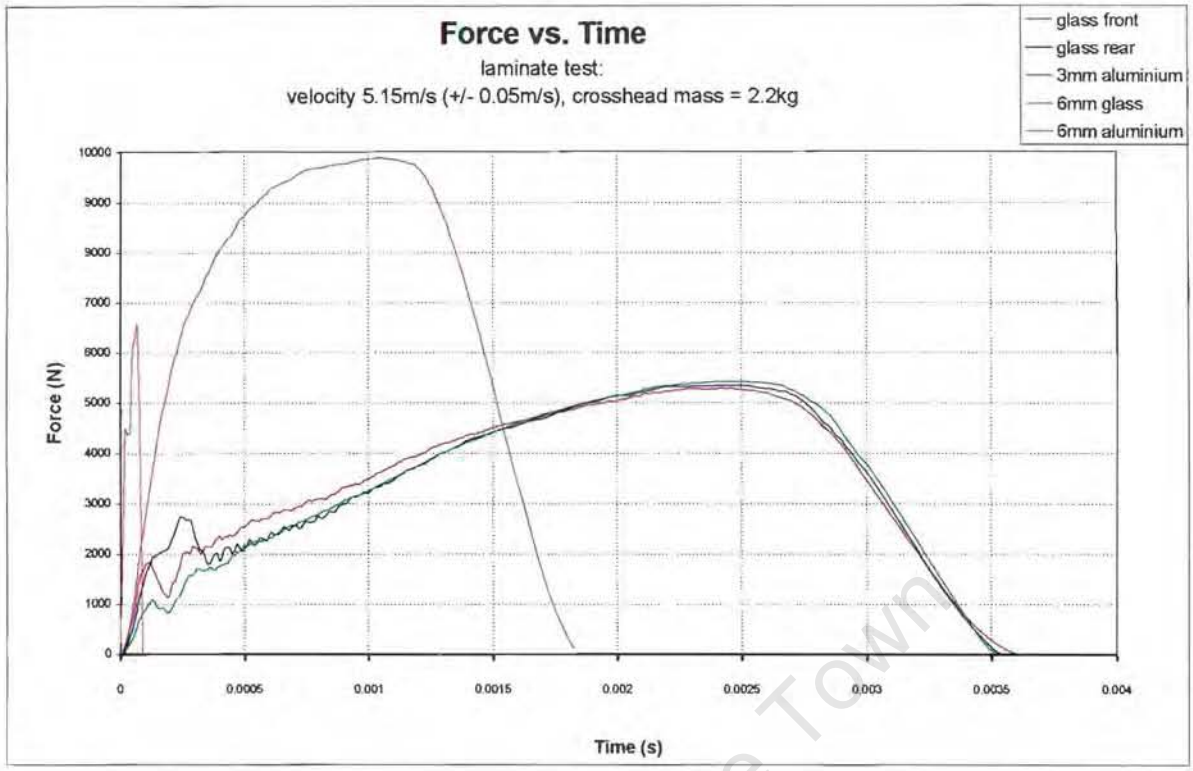

Figure 5.12 Force-time curves (initial impact velocity 5m.s^{-1}).

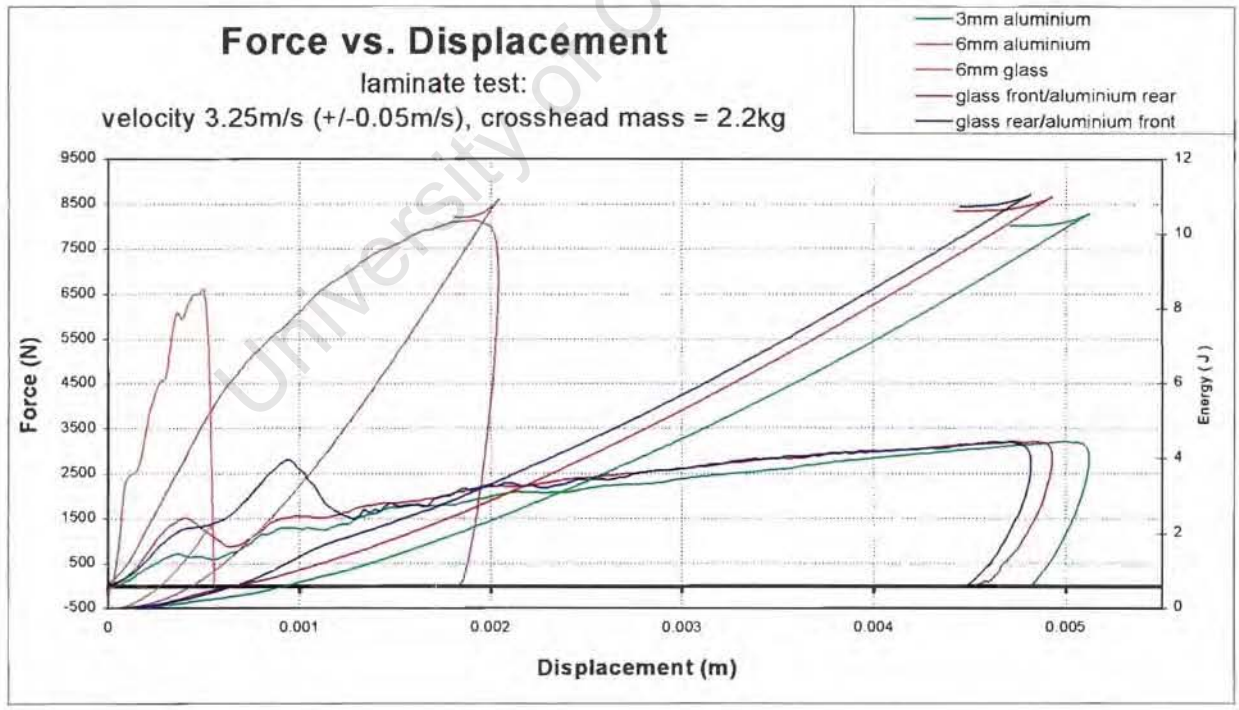

Figure 5.13 Force-deflection and energy-deflection curves (initial impact velocity 3m.s^{-1}). Test performed using a 2.2kg crosshead and 12.7mm tup.

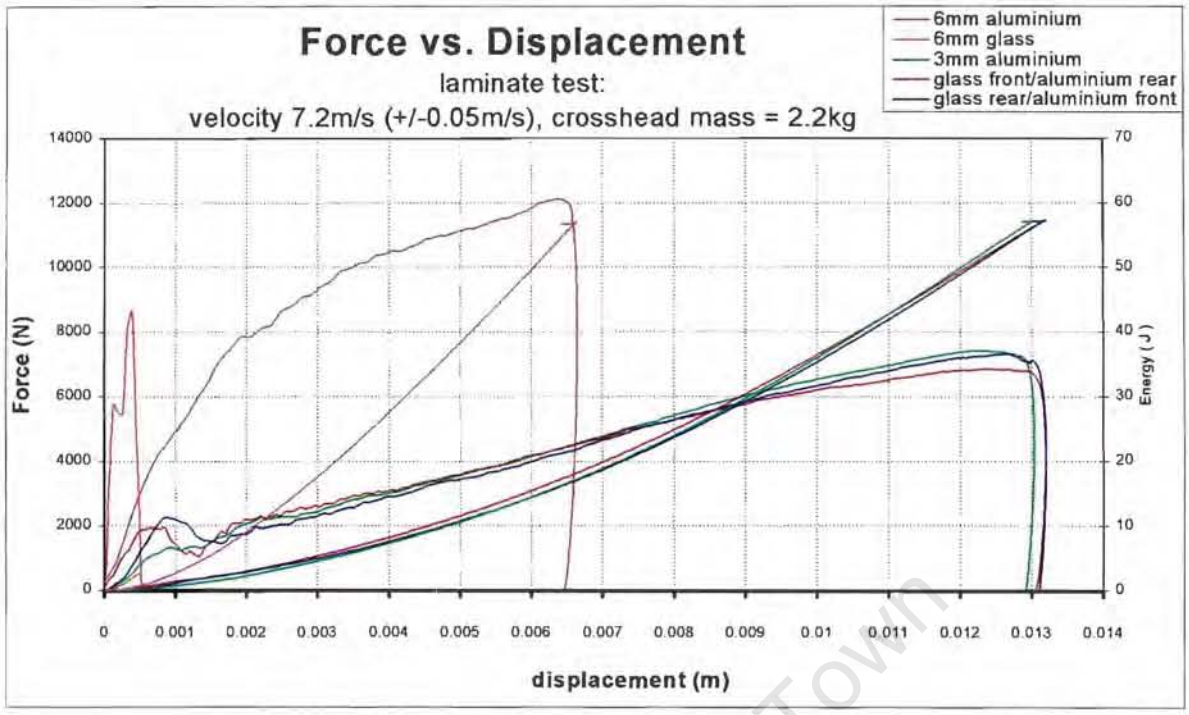

Figure 5.14 Force-deflection and energy-deflection curves (initial impact velocity 7m.s^{-1}). Test performed using a 2.2kg crosshead and 12.7mm tup.

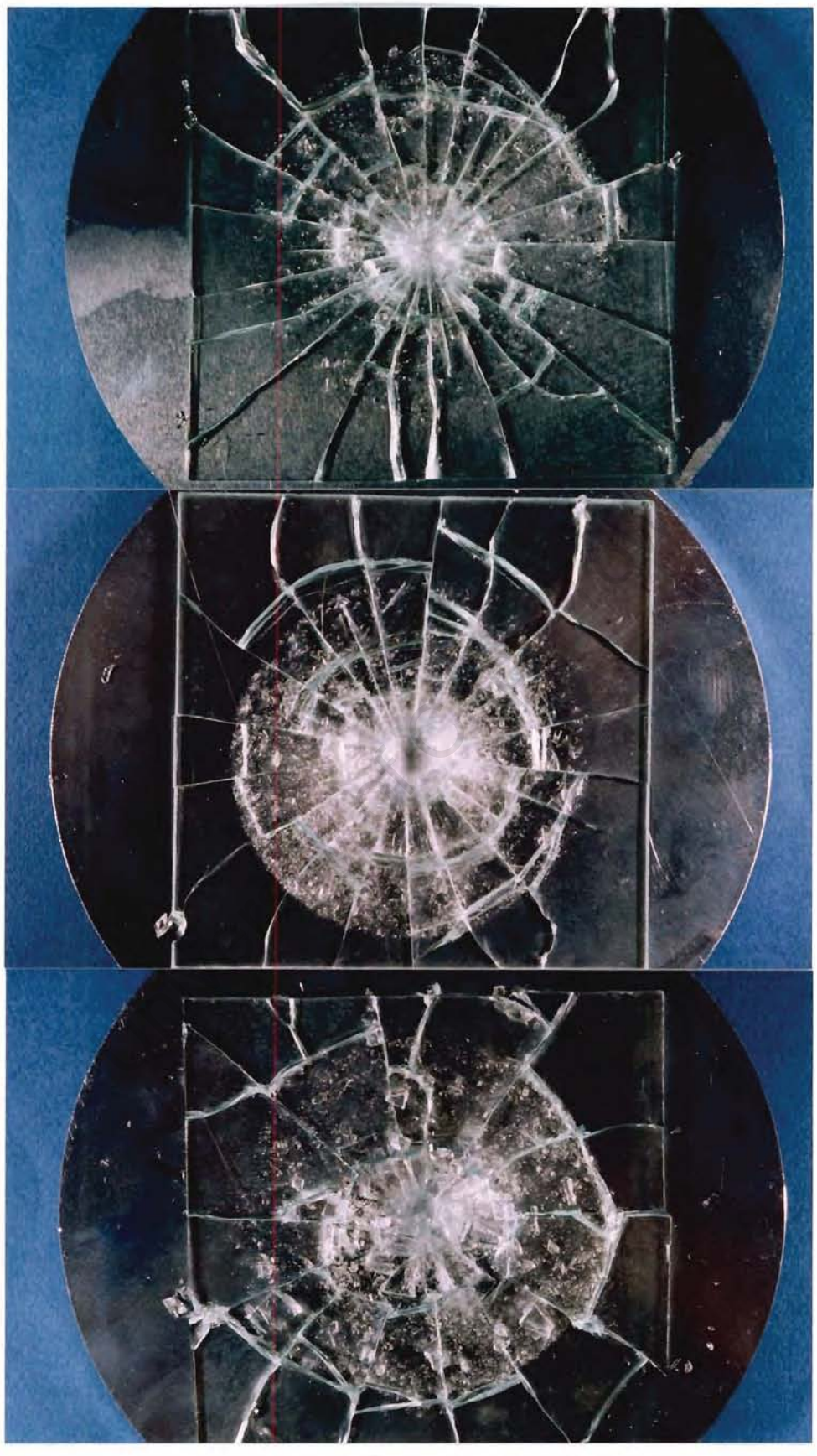

Figure 5.15 The fracture patterns for the glass-front laminates, increasing impact velocity from 3m.s^{-1} at the top of the page (3m.s^{-1}, 5 m.s^{-1}, 7m.s^{-1}).

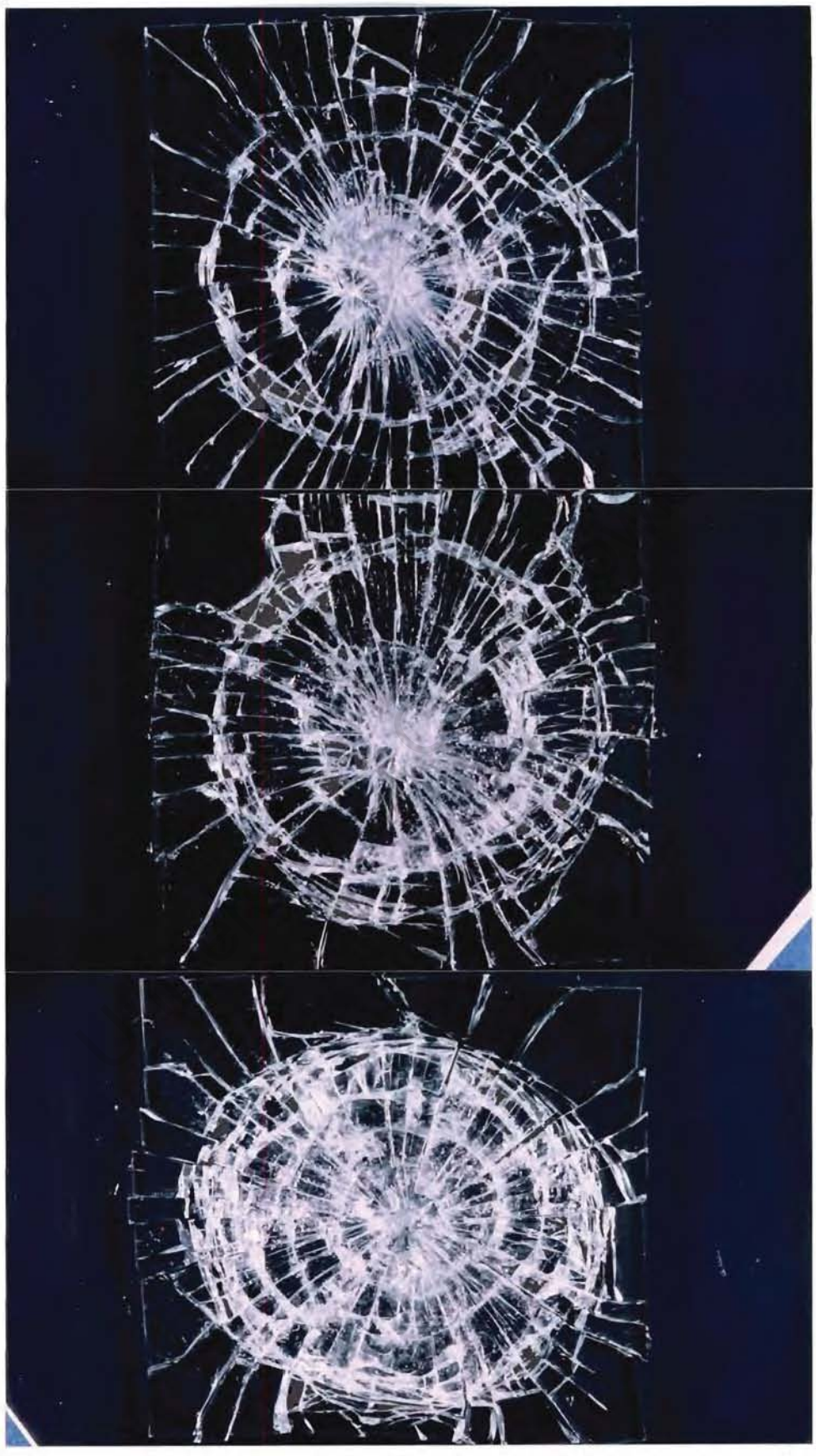

Figure 5.16 The fracture patterns for the glass-rear laminates, increasing impact velocity from 3m.s^{-1} at the top of the page (3m.s^{-1}, 5 m.s^{-1}, 7m.s^{-1}).

6. DISCUSSION

6.1 Introduction

The response of a material to projectile impact is critically dependent on a number of parameters. An understanding of the relative effect of these parameters can help in finding an optimal material or specimen thickness for a particular impact resistant application. The principal parameters defining the projectile impact behaviour of a thin plate test specimen are the projectile shape, impact velocity, kinetic energy and specimen thickness. An impact testing apparatus was designed and constructed to simulate a typical projectile impact event and analyse the influence of the principal impact parameters.

The following discussion describes the impact testing apparatus's ability to accurately simulate and analyse a typical impact event. The results of specific tests conducted to investigate the influence of the principal impact parameters and demonstrate the impact testing apparatus's capabilities are discussed. A second part of this discussion evaluates an investigation the into the apparatus's ability to investigate the impact response of combinations of glass and aluminium acting as laminates.

6.2 Evaluation of the Test Rig

The purpose of the plastic deformation investigation was to prove the accuracy and reproducibility of the results acquired using the impact testing apparatus. The results of the plastic deformation correlation tests show that the impact apparatus could accurately measure the degree of plastic deformation that took place during an impact event. It was felt that in the absence of a more appropriate test the agreement of the measured and actual plastic deformation sufficiently proved the accuracy of the impact apparatus and data acquisition system.

It was found that the closest correlation between the measured and actual plastic deformation was obtained for the 2.9 and 4.6kg crosshead tests. The increased percentage error associated with the 1.2kg crosshead tests was attributed to the increased relative effect of the rail bearing friction with the low crosshead mass.

The increase in the influence of bearing friction with decreased crosshead mass, also influenced the impact velocity. It was noted that the impact velocity decreased with decreasing crosshead mass for identical release height tests. It is felt that the decreasing impact velocity, with decreasing crosshead mass, adds credibility to the hypothesis that the relative effect of bearing friction increases with decreasing crosshead mass and is therefore accountable for the increased inaccuracy of the 1.2kg crosshead tests.

Minor variations in both the measured and actual plastic deformation were noted for test performed with identical test parameters. This phenomenon was attributed to the minor variation in impact velocity from the same crosshead release height. This deduction is justified by the fact that for the entire plastic deformation test series if a minor increase in impact velocity was measured a corresponding increase in the measured and actual deformation was observed. The impact apparatus was thus not analysing identical impact events and variations in the measured plastic deformation are expected. The impact apparatus's ability to measure small variations in impact velocity and accordingly predict a change in the plastic deformation, a change that in all cases was verified by the actual plastic deformation measured after the impact event, is seen as a very positive indication of the success of the impact testing apparatus.

The results of the reproducibility test illustrated in Figure 5.1 show that almost indistinguishable force-deflection curves were obtained for tests performed with identical impact parameters. The only variation in the force-deflection curves was noted after the point of maximum load, where minor variations in the maximum displacement and total plastic deformation were observed. As discussed previously the deviation in the measured displacement was attributed to slight deviations in impact velocity. The similarity of the force-deflection curves for set parameter impact tests sufficiently indicates the impact testing apparatus ability to accurately reproduce test results and it is seen as an indication of the success of the impact testing apparatus.

6.3 Ductile Plate Impact Behaviour

For the entire series of ductile plate tests, the impact apparatus accurately predicted the observed impact response, as was illustrated by the force-deflection curves and the sectional profile views for the various tests. The apparatus's ability to generate force-deflection curves that agreed with the observed trends was in itself seen as an indication of the success of the design.

The changing crosshead mass and changing impact velocity had a very similar effect on the impact response of the test specimens. Almost identical force-deflection trends were observed for the changing crosshead mass and changing impact velocity tests. This agrees with the ASTM D3029-90, albeit for composites and plastics, that suggests that similar results will be obtained for both changing mass constant velocity and changing velocity constant mass tests.

In both investigations, the initial slope of the force-deflection curves, during the linear elastic loading stage, was not influenced by changes in either, the crosshead mass or impact velocity. This observation is in accordance with the findings of Knakal and Ireland[39] who concluded that the linear elastic stage is and indication of the material stiffness and should therefore not be affected by a change in impact velocity or change in mass.

The changing specimen thickness tests illustrate the impact apparatus's ability to measure the specimen stiffness. The test rig correctly displayed an increase in the slope of the force-deflection curve for the linear elastic stage with increasing specimen thickness and thus stiffness.

Very small rebound displacements were noted for all the rebound tests. This was in accordance with the energy-deflection curves where the energy absorbed during the impact events was always slightly less than the initial kinetic energy of the crosshead. This was seen as an indication of the credibility of the energy-deflection curve, as most of the energy would be absorbed by plastic deformation and the remaining energy would be absorbed by secondary energy absorbing mechanisms such as

sound generation and stress wave dispersion. Although it is noted that Knakal and Ireland[39] observed that the utility of the energy values is doubtful unless the test conditions of probe geometry, probe size and specimen support anvil size are directly relatable to the intended use. They concluded that it is better to evaluate the material impact performance by independent consideration of the co-ordinates of load and deflection.

The series of tests performed give an adequate illustration of the impact apparatus's ability to analyse the influence of changing impact parameters on a material response to impact loading. From the generated force-deflection curves, essential features could be used to distinctly characterise the material behaviour under impact loading. The stiffness of the material, strain to failure and the load and deflection values at the yield and point of maximum load could be determined from the force-deflection curves.

6.4 Ductile and Brittle Laminate Plate Impact Behaviour

The impact apparatus was capable of measuring the impact response of aluminium-glass laminates. The effect of placing the glass plate on the impact or distal side of the laminate was discernible on the force-time and force-deflection curves.

Definite trends in the impact performance were noted for the laminate tests. The author postulated that the effect of placing the glass plate on the distal side of the laminate would be to effect a glass fracture due to high bending stresses on the rear side of the plate. This hypothesis was based on the assumption that the aluminium plate would relieve the contact stress on the glass plate. This hypothesis is based on the work by Ball[30] in which he investigated the effect of a soft interlayer on the impact resistance of laminates glass plate. Ball concluded that the interlayer has a protective effect on the rear layer of glass by dispersing the contact stresses and thus inhibiting the Hertzian cracking at the interface[30]. For this mode of fracture, it was assumed that the onset of radial and circumferential cracking would be visible on the force-deflection curve in a similar manner to that of a singular glass plate. Cheresh and McMichael[38] in their paper on instrumented data interpretation, state that the onset of

radial cracking is associated with a sudden drop in the load resistance, following the drop in load resistance a steady increase in load resistance can be expected until the onset of circumferential cracking which is associated with a second drop in load resistance. The primary and secondary yield point visible on the rear-laminate force-deflection curves, for the 3 and 5m.s^{-1} test, is seen as proof of the assumption that the onset of radial and circumferential cracking would be visible on the force-deflection curves. The observed trend was seen as a positive indication of the apparatus's ability to measure a response in accordance with the expected impact behaviour. A secondary yield in the 7m.s^{-1} test was not observed, it is postulated that the decreased impact duration and increased intensity of the stress waves transmitted from the aluminium plate to the glass plate resulted in the radial and circumferential cracks occurring at similar tup displacements.

The glass component of the glass-front laminates was expected to fracture due to high bearing stresses on the front face. This prediction is based on the assumption that the aluminium plate would not facilitate bending of the glass plate and thus increase the intensity of the contact stresses on the front face of the glass laminate. The force-deflection curve for the glass-front laminate tests showed a singular yield point and an increase in load resistance and secondary yield was not observed. From the force-deflection response and the inspected fracture surface it is postulated that the formation of a cone crack and the subsequent cone crushing dominated the impact response as opposed to the formation of radial and circumferential cracks that dominated the response of the singular glass and glass-rear impact tests.

From the energy deflection curves, the total energy absorbed for the laminates and the 3mm aluminium plate was similar for all velocities tested. However, the energy-deflection curve could be analysed at different stages of penetration to measure the difference in energy absorbed by the various fracture processes. This is best illustrated by Figure 5.11, the 5m.s^{-1} force-deflection and energy-deflection curve for 4mm of tup penetration, where the energy absorbed for the two laminate plates is approximately 1.5 Joules more than for the 3mm aluminium plate.

The force-deflection curves for the tests performed on the singular glass test illustrate the impact apparatus's ability to measure a short duration impact event. For all velocities tested a force-deflection curve typical of a brittle material impact response was observed. The yield point indicating the onset of radial cracks and a yield point indicating the onset of circumferential fracture was observed in all cases. Fracture was observed at similar tup displacements for all velocities tested. This is seen as an indication of the lack of strain rate sensitivity within the range of velocities tested on the impact testing apparatus.

7. Conclusions and Recommendations

An apparatus for analysing the material response to low velocity projectile impact has been designed and constructed. All of the requirements, constraints and criteria initially set for design were met. A cantilever crosshead was utilised for the impact apparatus thereby facilitating the use of a lighter crosshead, and more sensitive impact tests. The impact testing apparatus is equipped with a data acquisition system and software package that is capable of generating a force-time, force-deflection and energy-deflection curve for the impact event.

The force-deflection record for through penetration events is in agreement with the idealised force-deflection record proposed by Knakal and Ireland[39] in the ASTM standard for drop weight testing. The five stages of projectile penetration and the transition points are easily identifiable on the load-deflection record generated by the impact testing apparatus.

A series of tests performed to investigate the impact testing apparatus's ability to accurately measure the total plastic deformation proved highly successful. The percentage error between deformation measured by the apparatus and the actual deformation that took place varies from a low of 0.48% to a high of 15.9%. It is noted that the tests performed with the lowest possible crosshead mass (1.2kg) yielded markedly higher percentage errors than the slightly heavier crosshead (2.9kg) tests.

Reproducibility tests were performed using a 2.9kg crosshead mass. Multiple tests were performed from three different release heights. Almost indistinguishable force-deflection records were recorded for identical tests. Minor variations in the force-deflection records for the post maximum load point stages were observed. This variation was attributed to minor variations in impact velocity from the same release height, as the test in which no variation in impact velocity occurred identical force-deflection records were generated by the impact apparatus.

The test performed to analyse the effect of changing impact parameters on the material impact behaviour illustrated the performance capabilities of the impact testing apparatus. For the entire test series, the force-deflection record is in agreement with the observed impact response. From the force-defection record, the critical data defining the impact material response to impact loading is easily distinguishable. The stiffness of the material, strain to failure and the load and deflection values at the yield and point of maximum load can be determined from the force-deflection curves.

The laminate tests to investigate the effect of placing glass on the impact or distal side of an aluminium-glass laminate proves the apparatus's ability to analyse more complex tests. The force-deflection curves for the laminates tested show distinct characteristic trends. These trends are in accordance with the expected impact response hypothesised from the literature on the behaviour of glass under impact loading. The apparatus is capable of generating a force-deflection record for the 6mm glass, short duration impact event. The force-deflection curve generated for the 6mm glass test corresponds with the typical force-deflection curve for brittle impact proposed by Cheresh and McMichael[38]. However, it is noted that although the sampling frequency is high enough to plot the force-deflection curve and obtain the necessary data, a higher sampling frequency is preferred so that a higher plotting resolution can be achieved.

The energy-deflection curves, for the laminate test, shows that although the total absorbed impact energy was similar, the curves can be utilised to determine the extent of the different energy absorbing mechanisms at various stages of penetration.

The impact testing apparatus is ready and able to investigate the impact behaviour of various composites, in a further study on the methods of resisting low velocity projectile impact penetration.

[1] Zukas J.A., "Numerical Simulation of Impact Phenomena", **Impact Dynamics**, Zukas J. A. (Ed.), John Whiley and Sons, New York, 1982.

[2] Zukas J.A., "Penetration and Perforation of Solids", **Impact Dynamics**, Zukas J. A. (Ed.), John Whiley and Sons, New York, 1982.

[3] Roche, J. L., Kakarala, S. N., "Methodology for Selecting Impact Tests of Composite Materials in Automotive Applications", **Instrumented Impact Testing of Plastics and Composite Materials**, ASTM STP 936, Kessler S. L., G. C. Adams, Driscoll S. B., Ireland D. R., American Society for Testing and Materials, Philadelphia, 1987, pp 24-43.

[4] Wu E., Sheen H. J., Chen Y. C., Chang L. C., "Penetration Force Measurement of Thin Plates by Laser Doppler Anemometry", **Experimental Mechanics**, 1994, pp. 93-99.

[5] Macaulay M.A., **Introduction to Impact Engineering**, 1st Edition, Chapman and Hall, London, 1987.

[6] Harding J., "The Effect of High Strain Rate on Material Properties", **Materials At High Strain Rates**, Blazynski T.Z. (Ed.), Elsevier Applied Science, London, 1987, pp 133-187.

[7] Murr L.E., "Metallurgical Effects of Shock and High-Strain-Rate Loading", **Materials At High Strain Rates**, Blazynski T.Z. (Ed.), Elsevier Applied Science, London, 1987, pp 1-45.

[8] Nicholas T., "Material Behaviour at High Strain Rates", **Impact Dynamics**, Zukas J. A. (Ed.), John Whiley and Sons, New York, 1982.

[9] Lindholm U. S., **Techniques in Materials Research**, Bunshah R. F. (Ed.) Vol. 5, Interscience, New York, 1971.

[10] Zukas J.A., "Stress Waves In Solids", **Impact Dynamics**, Zukas J. A. (Ed.), John Whiley and Sons, New York, 1982.

[11] Johnson W., **Impact Strength of Materials**, Edward Arnold, London, 1972.

[12] Zukas J.A., "Limitation of Elementary Wave Theory", **Impact Dynamics**, Zukas J. A. (Ed.), John Whiley and Sons, New York, 1982.

[13] Nicholas T., "Elastic-Plastic Stress Waves", **Impact Dynamics**, Zukas J. A. (Ed.), John Whiley and Sons, New York, 1982.

[14] Chou P. C., Hopkins A. K., "Dynamic response of Materials to Intense Impulsive Loading", **W. P. A. F. B.**, Dayton, OH, 1973.

[15] Liebowitz H., **Fracture**, Vol. I-VII, Academic Press, New York, 1968.

[16] van Vroonhoven J., **Dynamic Crack Propagation in Brittle Materials: Analysis Based on Fracture and Damage Mechanics**, Ph.D. Thesis, Eeindhoven University of Technology, 1996.

[17] Ashby M.J., Jones D.R.H., **Engineering Materials: An Introduction to their Properties and Application**, Vol. 1, Pergamon Press, Oxford, 1980.

[18] Brandon D. G., "Dynamic Loading and Fracture", **Materials At High Strain Rates**, Blazynski T.Z. (Ed.), Elsevier Applied Science, London, 1987, pp 1-45.

[19] Abrate S., "Impact of Laminated Composite Materials: A Review", **Applied Mechanical Review.,** Vol. 44, 1991, pp. 155-190.

[20] Elber W., "The Effects of Matrix and Fibre Properties on Impact Resistance", **Tough Composite Materials: Recent Developments**, Noyes N.J. (Ed.), 1985, pp. 89-110.

[21] Elber W., "Failure Mechanics in Low Velocity Impacts on Thin Composite Plates", **NASA TP-2152**, Langley, VA. 1983.

[22] Lagace P. A., Wolf E., "Impact Damage Resistance of Several Laminated Material Systems", **Proceedings of the 34th Annual AIAA/ ASME/ ASCE/ AHS/ ASC Structures, Structural Dynamics and Materials Conference, AIAA**, La Jolla, 1993, pp. 1863-1871.

[23] Backma M.E., Goldsmith W., "The Mechanics of Projectiles Into Targets", **Int. Jou. Eng. Sci.** Vol. 16,1978, pp. 1-99.

[24] Goldsmith W., **Impact**, Edwards Arnold Ltd, London, 1960

[25] Broutman L.J., Rotem A., "Impact Strength and Toughness of Fiber Composite Materials", **ASTM STP 568**, 1975, pp. 114-133.

[26] Roche, J. L., Kakarala, S. N., "Experimental Comparison of Several Impact Test Methods", **Instrumented Impact Testing of Plastics and Composite Materials**, ASTM STP 936, Kessler S. L., G. C. Adams, Driscoll S. B., Ireland D. R., American Society for Testing and Materials, Philadelphia, 1987, pp 144-162.

[27] Cantwell W. J., Morton J., "The Impact Resistance of Composite Materials – A Review", **Composites**, Vol. 22, 1991, pp. 347-361.

[28] Field J. E., Walley S. M., Bourne N. K., Huntley J. M., "Experimental Methods at High Rates of Strain", **Journal de Physique IV,** Vol. 4, 1994, pp. 3-22.

[29] Glathart J. L., Preston F. W., "The Behaviour of Glass Under Impact: Theoretical Considerations", **Glass Technology**, Vol. 9, 1968, pp. 89-100.

[30] Ball A., "The low Velocity Impact Behaviour of Glass-Polymer Laminated Plates" **Journal De Physique IV, 4**, 1994, pp. 783-788.

[31] Hertz H. R., **Hertz's Miscellaneous Papers**, Chs. 5 and 6, McMillan, London, 1896.

[32] Persson J., Breder K., Rowcliffe D. J., "Loading Rate Effects During Indentation and Impact On Glass With Small Spheres", **Journal of Material Science**, Vol. 28, 1993, pp. 6484-6489.

[33] Johnson K. L., O'connor J. J., Woodward A. C., **Proc. R. Soc. Lond.**, A. 334, 1973.

[34] Evans A. G., Wilshaw T. R., **Acta. Metall.**, Vol. 24, 1976.

[35] Auerbach F., Ann. Phys. Chem. 43,1891

[36] Ball A., "On the Bifurcation of Cone Cracks in Glass Plates", **A Philosophical Magazine**, Vol. 73, No. 4, 1996, pp. 1093-1103.

[37] GRC 930 I Instrumented Impact Test Data System Instruction Manual. Dynatup-General Research Corporation, Goleta, CA.

[38] Cheresh M. C., McMichael S., "Instrumented Impact Data Interpretation", **Instrumented Impact Testing of Plastics and Composite Materials**, ASTM STP 936, Kessler S. L., G. C. Adams, Driscoll S. B., Ireland D. R., American Society for Testing and Materials, Philadelphia, 1987, pp 144-162.

[39] Knakal C. W., Ireland D. R., "Instrumented Dart Impact Evaluation of Some Automotive Plastics and Composites", **Instrumented Impact Testing of Plastics and Composite Materials**, ASTM STP 936, Kessler S. L., Adams G. C., Driscoll S. B., Ireland D. R., American Society for Testing and Materials, Philadelphia, 1987, pp. 219-235.

[40] Driscoll S. B., "Variable Weight Impact Testing of Polymeric Materials: A Review", **Instrumented Impact Testing of Plastics and Composite Materials**, ASTM STP 936, Kessler S. L., G. C. Adams, Driscoll S. B., Ireland D. R., American Society for Testing and Materials, Philadelphia, 1987, pp 163-186.

[41] Server W. L., Henderson G. R., "The Measurement of Charpy Impact Energy Using A Vertical Drop Tower", **Journal of Testing and Evaluation**, Vol. 9, No. 3, 1981, pp. 210-213.

[42] Pearson G. C. **Projectile Penetration of Thin Aluminium Plates**, PhD Thesis, University of Cape Town, 1973.

[43] Rhodes M. D., Williams J. G., Starnes J. H., **Proceedings of the 34th Annual Technical Conference; Society of the Plastics Institute**, 1979.

[44] Joshi S. P., Sun C. T., "Impact Induced Fracture in a Laminated Composite", **Journal of Composite Materials**, Vol. 6, pp. 51-66.

Appendix A

Critical component drawings

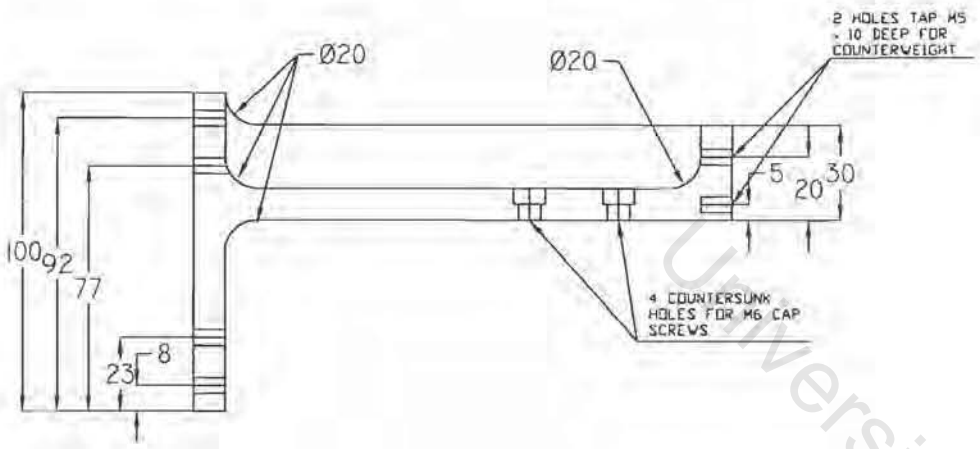

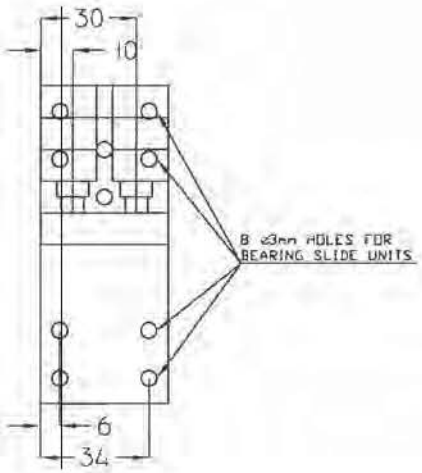

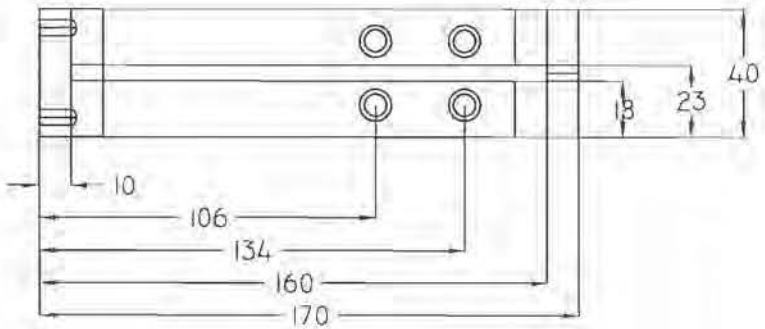

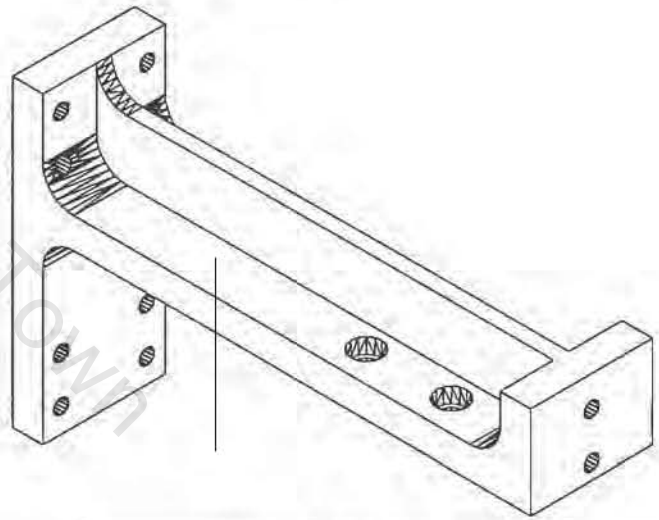

Dimensions are in mm
Overall tolerance is
0.1mm unless otherwise
stipulated

UNIVERSITY OF CAPE TOWN
DEPARTMENT OF MATERIALS ENGINEERING

CROSSHEAD

DRAWN BY: P. CARTMEL	DATE: 06/08/97
SCALE: DNS	MATERIAL: Alu Grade: 7075

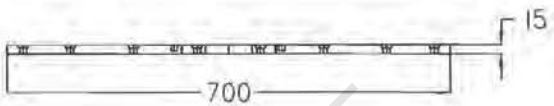

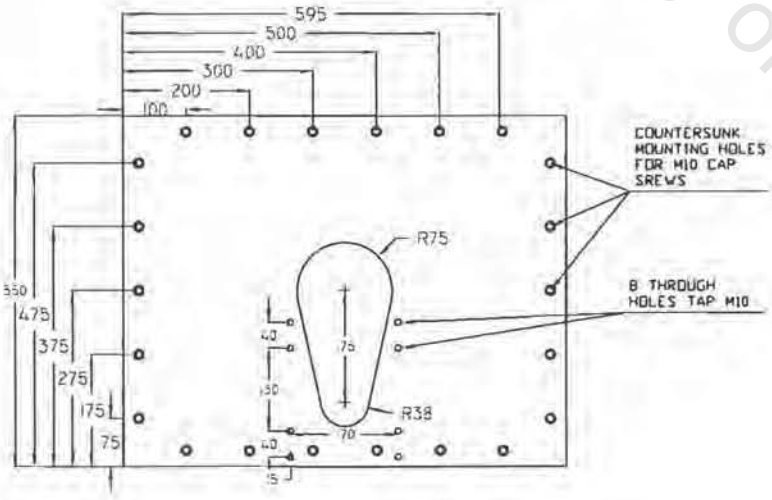

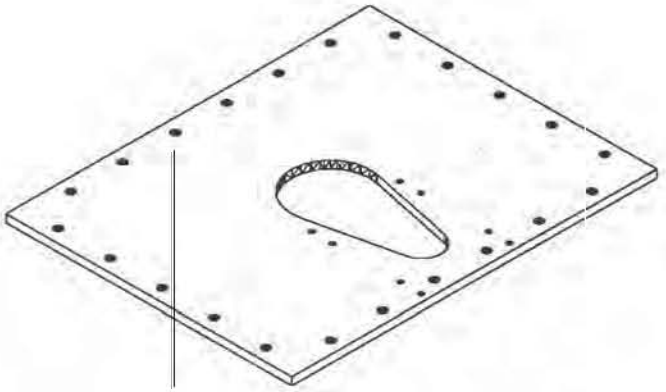

UNIVERSITY OF CAPE TOWN DEPARTMENT OF MATERIALS ENGINEERING	
BASE PLATE	
DRAWN BY: P. CARTMEL	DATE: 06/08/97
SCALE: DNS	MATERIAL: 3CR12

Dimensions are in mm
Overall tolerance is 0.1mm unless otherwise stipulated

NOTE: ALL TUBING 50mm x 50mm 4mm WALL THICKNESS

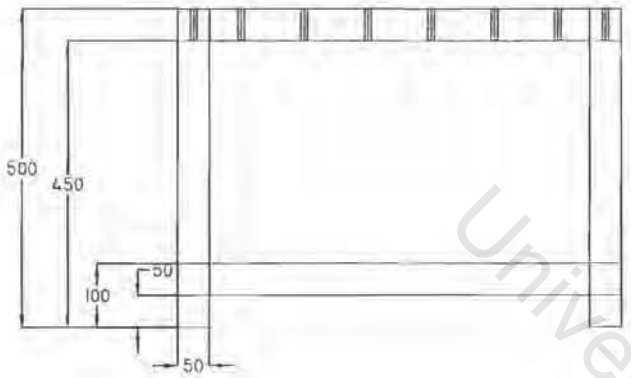

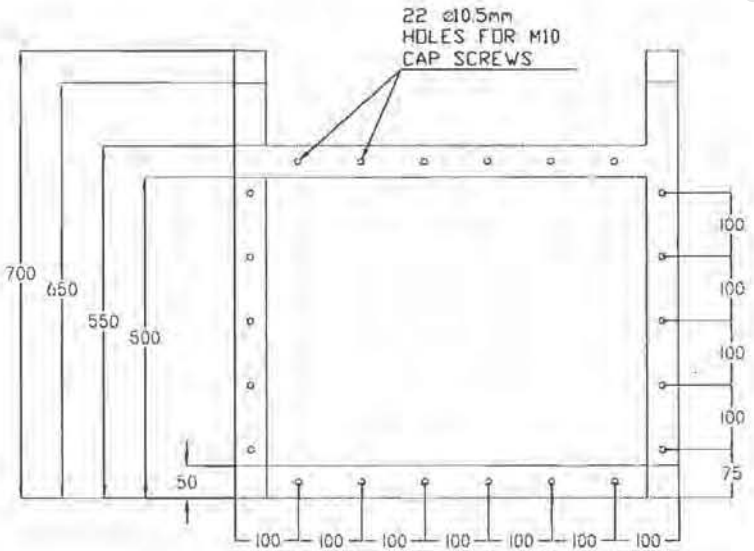

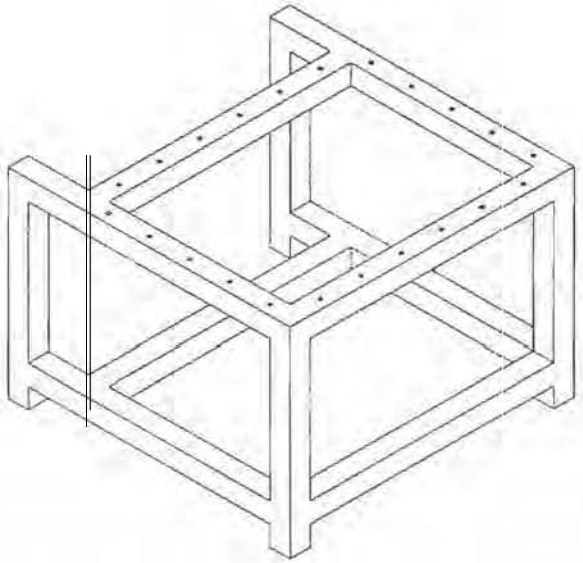

Dimensions are in mm
Overall tolerance is 0.1mm unless otherwise stipulated

UNIVERSITY OF CAPE TOWN
DEPARTMENT OF MATERIALS ENGINEERING

BASE FRAME

DRAWN BY: P. CARTMEL	DATE: 06/08/97
SCALE: DNS	MATERIAL: BS 070M20 MILD STEEL

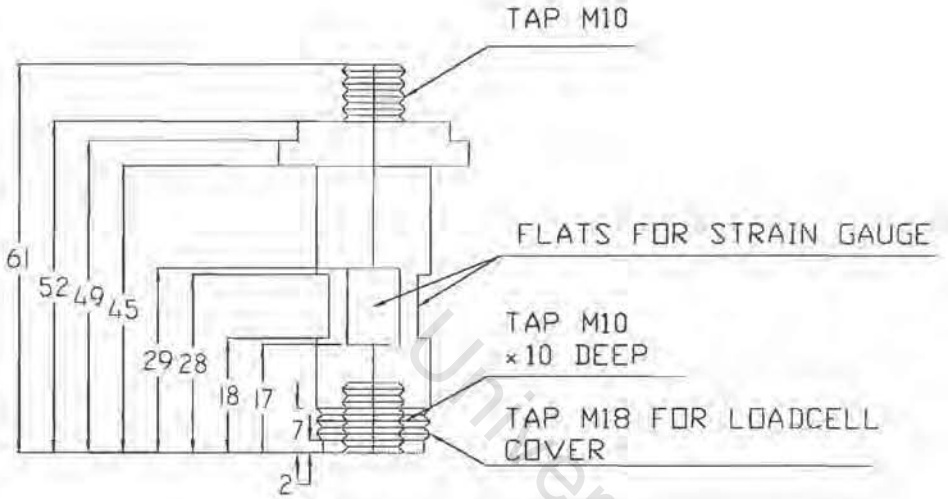

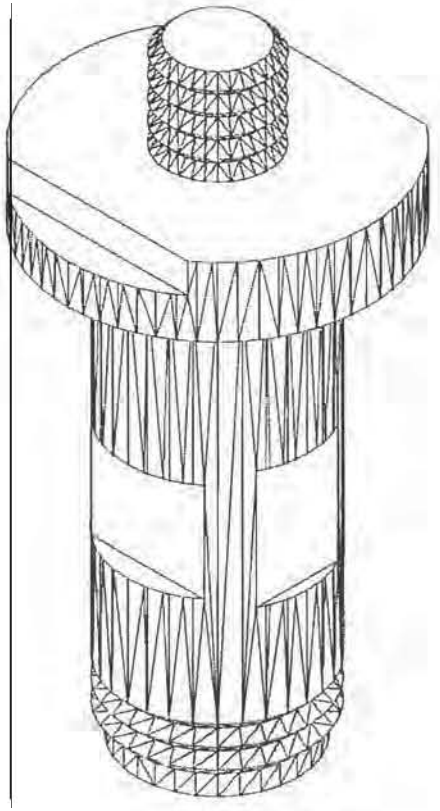

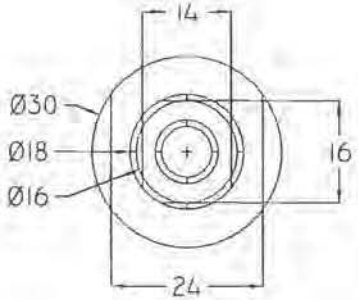

Dimensions are in mm
Overall tolerance is
0.1mm unless otherwise
stipulated

UNIVERSITY OF CAPE TOWN
DEPARTMENT OF MATERIALS ENGINEERING

LOAD CELL

DRAWN BY: P. CARTMEL	DATE: 06/08/97
SCALE: DNS	MATERIAL: AISI 316

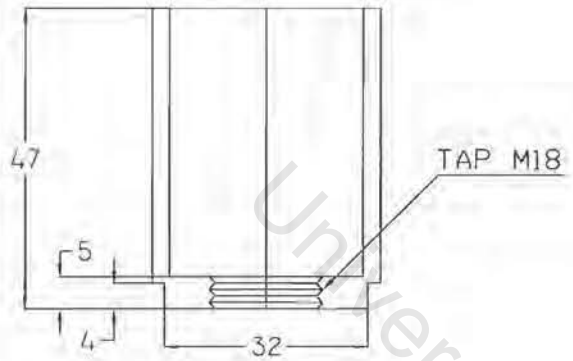

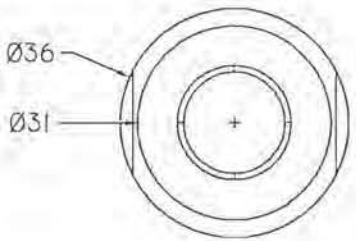

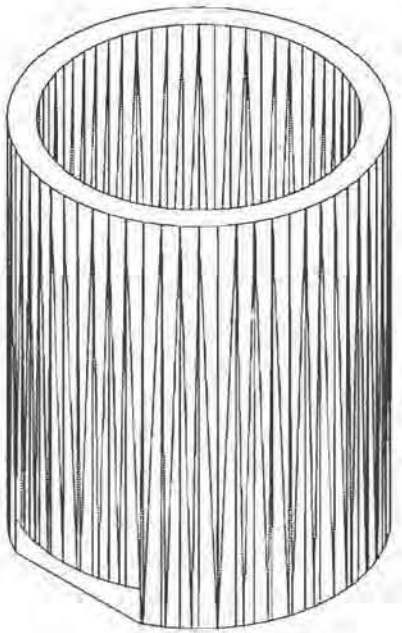

Dimensions are in mm
Overall tolerance is
0.1mm unless otherwise
stipulated

UNIVERSITY OF CAPE TOWN
DEPARTMENT OF MATERIALS ENGINEERING

LOAD CELL COVER

DRAWN BY: P. CARTMEL	DATE: 06/08/97
SCALE: DNS	MATERIAL: ALU GRADE 6261

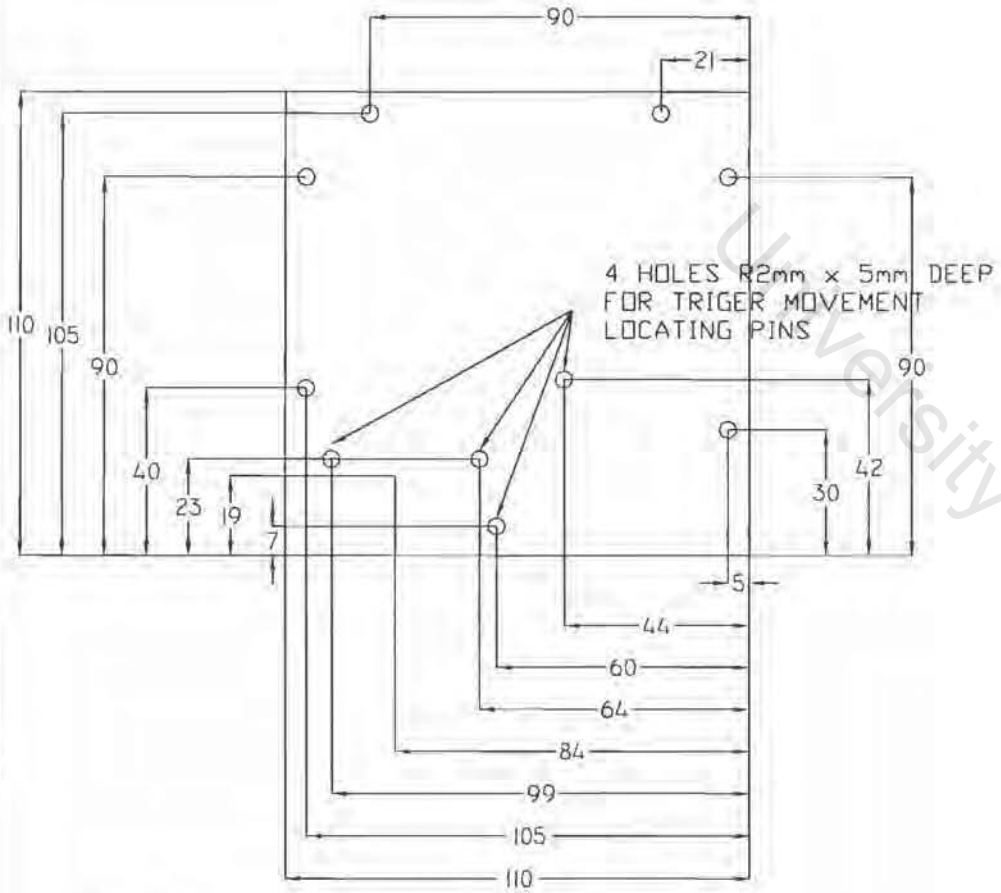

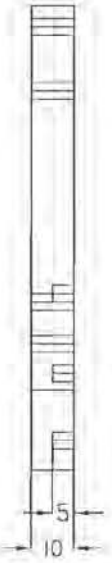

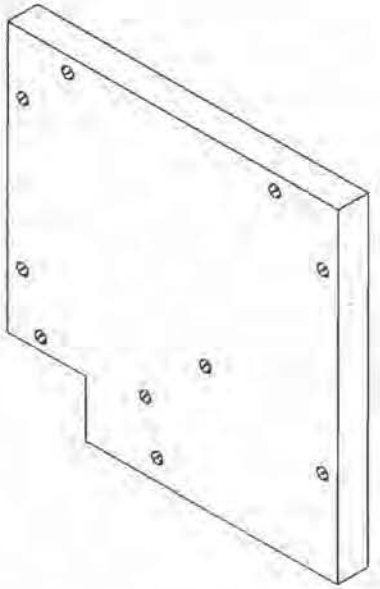

NOTE: HOLES ON PERIMETER ARE R2mm THROUGH HOLES

NOTE: 2 OFF, LEFT AND RIGHT FACE, MIRROR IMAGES

Dimensions are in mm
Overall tolerance is 0.1mm unless otherwise stipulated

UNIVERSITY OF CAPE TOWN
DEPARTMENT OF MATERIALS ENGINEERING

TRIGER SIDE FACES

DRAWN BY: P. CARTMEL	DATE: 06/08/97
SCALE: DNS	MATERIAL: ALU GRADE 6261

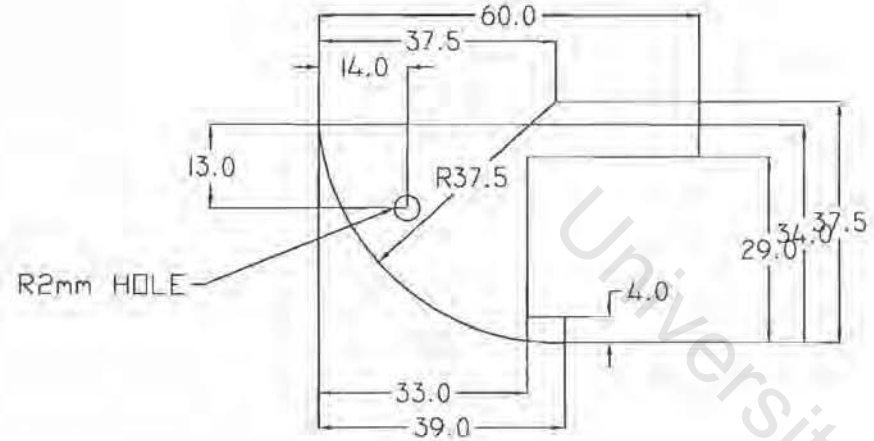

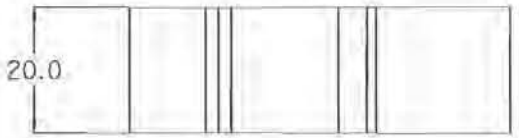

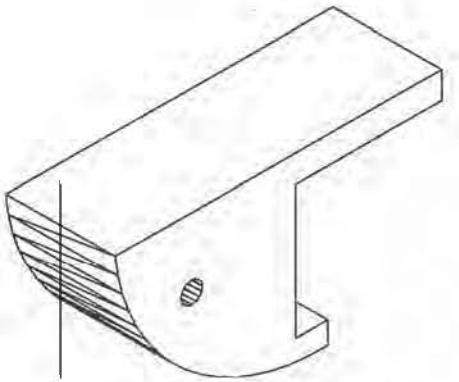

Dimensions are in mm
Overall tolerance is 0.1mm unless otherwise stipulated

UNIVERSITY OF CAPE TOWN
DEPARTMENT OF MATERIALS ENGINEERING

TRIGER MOVEMENT

DRAWN BY: P. CARTMEL	DATE: 06/08/97
SCALE: DNS	MATERIAL: 3CR12

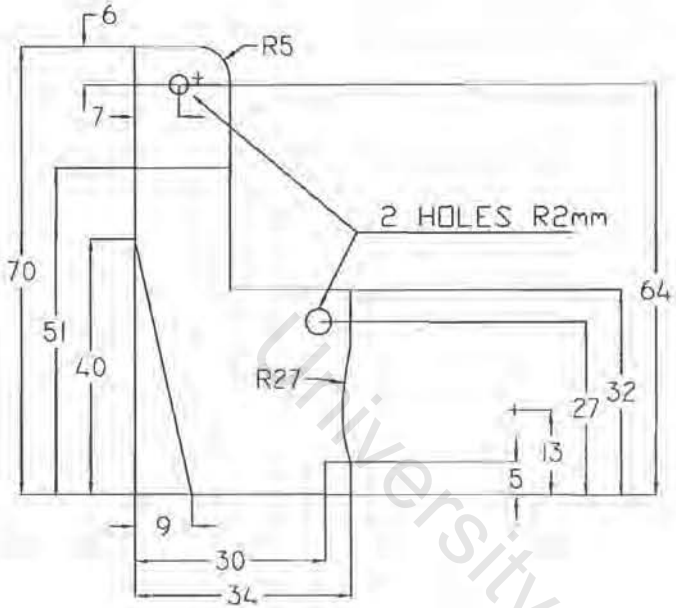

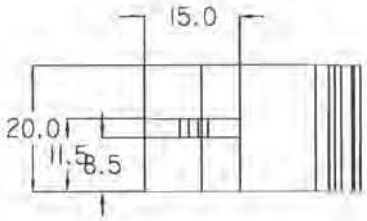

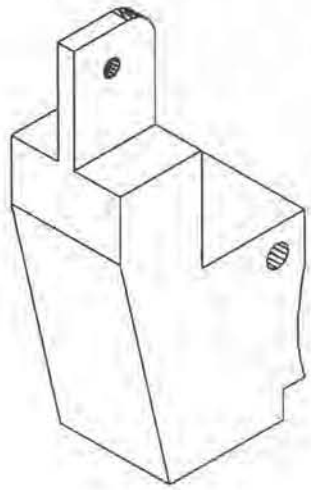

Dimensions are in mm
Overall tolerance is
0.1mm unless otherwise
stipulated

UNIVERSITY OF CAPE TOWN
DEPARTMENT OF MATERIALS ENGINEERING

TRIGER MOVEMENT

DRAWN BY: P. CARTMEL	DATE: 06/08/97
SCALE: DNS	MATERIAL: 3CR12

Appendix B

Critical bearing Selection Information

Structure and Features

IKO Linear Way L series is a compact linear motion rolling guide consisting of a slide unit and track rail. The two-row raceway design of Linear Way L series with stainless steel balls in four point contact with the raceways features high performance and durability against complex load and moment load occurring in many cases of actual service.

Since the casing, balls and track rail are made of special stainless steel, this series is superior in corrosion resistance and widely applicable for medical instruments, scanning or writing heads of memory storage devices such as hard disk drives, etc.

IKO Linear Way L series offers the following advantages.

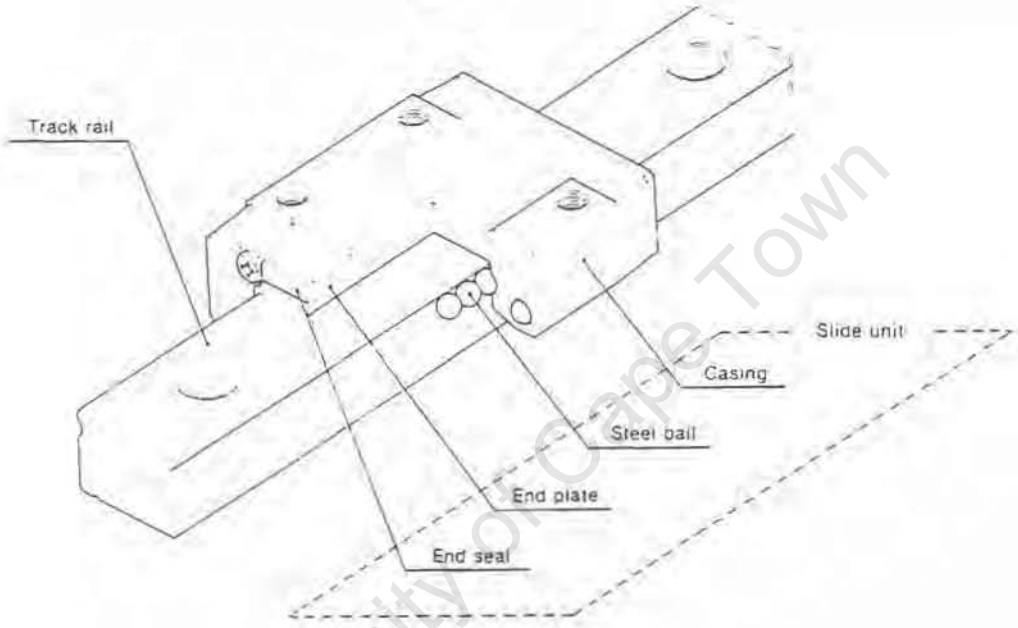

Fig. 1 Structure of Linear Way L

Note: This figure shows the structure of LWL type. The structure is subject to change without prior notice.

7 Features of Linear Way series

1. Large Load Capacity in Any Directions
2. Excellent Strength under Moment Load and Complex Load
3. High Accuracy with Simple Structure
4. High Rigidity and Good Absorption of Vibration
5. Long Life with High Reliability
6. Smooth Operation and Low Noise
7. Accurate and Simple Installation

Additional advantages of Linear Way L series are as follows:

❶ Superior corrosion resistance

The metallic parts of Linear Way L are made of special stainless steel, which is highly resistant to corrosion and therefore suitable for use in clean rooms.

❷ A small dimensional package

LWL is extremely small and light weight — suitable for high speed operation. LWLF is also small, although wider, making it suitable for use as a single track rail — eliminating the alignment requirements of two parallel rails.

<Main applications>

Semiconductor manufacturing equipments, OA system equipments, medical equipments, various disk readers, handling equipments, etc.

Accuracy

Accuracies for Linear Ways L series are shown in Table 4

Table 4 Accuracy

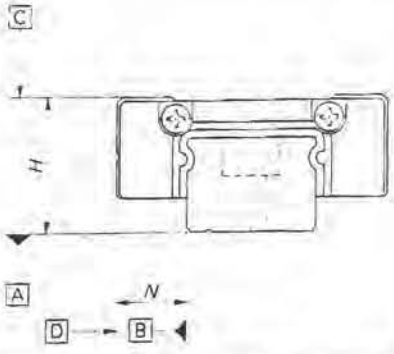

unit : mm

Item \ Classification (Symbol)	High (H)	Precision (P)
Dim. *H* tolerance	±0.020	±0.010
Dim. *N* tolerance [2]	±0.025	±0.015
Dim. variation of *H* [1]	0.015	0.007
Dim. variation of *N* [2] [3]	0.020	0.010
Parallelism in operation of C to A	See Fig. 2.	
Parallelism in operation of D to B	See Fig. 2.	

Note [1]: Dimensional variation of dimension *H* means the size variation between slide units mounted on the same track rail or on matched track rails
[2]: Dimensional variation of dimension *N* means the size variation between slide units mounted on the same track rail
[3]: These values also apply to Linear Way L series which have opposite reference surface arrangements.

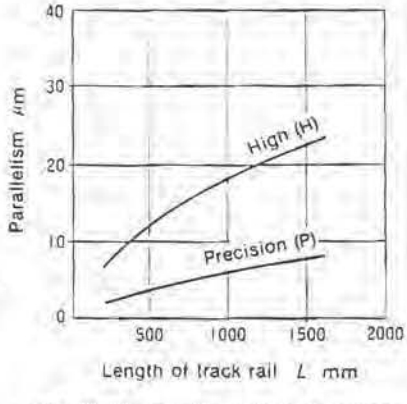

Fig. 2 Parallelism in operation

Preload

Average amount of preload for Linear Way L series are shown in Table 5.

Table 5 Preload amount

Item \ Preload class	Symbol	Preload amount (kgf)	Application
Clearance	To	0	•Extremely smooth motion
Standard preload	No symbol	0 -	•Smooth and precise motion
Light preload	T1	0.02C0	•Minimum vibration •Load is equally balanced.

Note : Zero or minimal amount of clearance
: Zero or minimal amount of preload
Remarks: Co means basic static load rating

Load Rating and Life

Load ratings by direction

The load ratings of designated Linear Way L series are changed by direction. The load ratings shown in the dimension tables are downward load ratings. Upward and lateral load ratings can be obtained by multiplying the load-directional factors shown in Table 6.

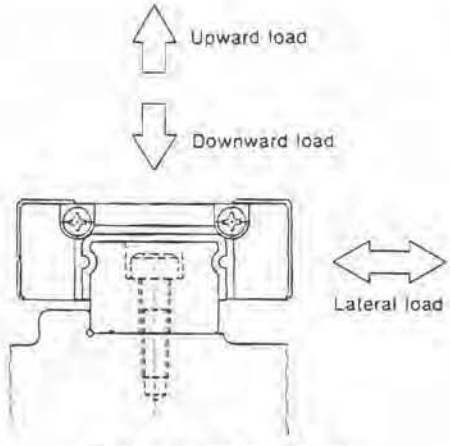

Fig. 3 Load direction

Table 6 Load direction and load ratings

Load direction \ Load rating	Basic dynamic load rating	Basic static load rating
Downward	C	Co
Upward	C	Co
Lateral	1.13C	1.19Co

Life

The rated life of Linear Way L series is obtained from the following formula.

$$L = 50\left(\frac{C}{fw\,Fc}\right)^3 \quad \cdots\cdots (1)$$

where, L : Rated life, 10^3m
C : Basic dynamic load rating, kgf
Fc : Theoretically calculated load, kgf
fw : Load factor (See Table 7.)

Therefore, if the stroke length and the number of strokes per minute are given, the life in hours can be obtained from following formula.

$$Lh = \frac{10^6 L}{2\,Sn_1 \times 60} \quad \cdots\cdots (2)$$

where, Lh : Rating life in hours, hours
S : Stroke length, mm
n_1 : Number of strokes per minute, cpm

The life can also be obtained from the nomograph shown in Fig. 2 on page 12.

Table 7 Load factor

Operating conditions	fw
Smooth operation free from vibration and/or shocks	1 ~ 1.2
Normal operation	1.2 ~ 1.5
Operation with vibration and/or shocks	1.5 ~ 3

Static safety factor

The static safety factor, fs, of Linear Way L series can be obtained from the following formula, and general values of this factor are shown in Table 8.

$$fs = \frac{Co}{Po} \quad \cdots\cdots (3)$$

where, fs : Static safety factor
Co : Basic static load rating, kgf
Po : Static load, kgf

Table 8 Static safety factor

Operating conditions	fs
Operation with vibration and/or shocks	3 ~ 5
High operating performance	2 ~ 4
Normal operation	1 ~ 3

Lubrication and dust protection

A quality No. 2 lithium-soap base grease containing extreme pressure additive is supplied in Linear Way L series. However, the quality of any grease will gradually deteriorate as operating time passes. Therefore, periodic relubrication is necessary. It is generally recommended that the grease is relubricated every six months under general usage and every three months for the daily operation consists of many cycles and long strokes. Use of lithium-soap base grease containing extreme pressure additive is recommended for general use. Relubrication is done by applying grease to the raceway surface of the track rail.
Lubricating oils, such as turbine oil and spindle oil, can be similarly applied to the raceways of the track rail.
IKO Linear Way L series are dust-protected with special rubber seals. However, when an excessive amount of contamination is present, it is recommended to provide protective covers or devices for the entire linear motion mechanism.

Linear Way L LWLF

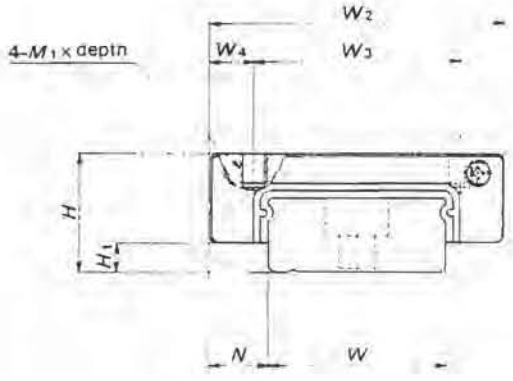

LWLF 14、LWLF 18、LWLF 24

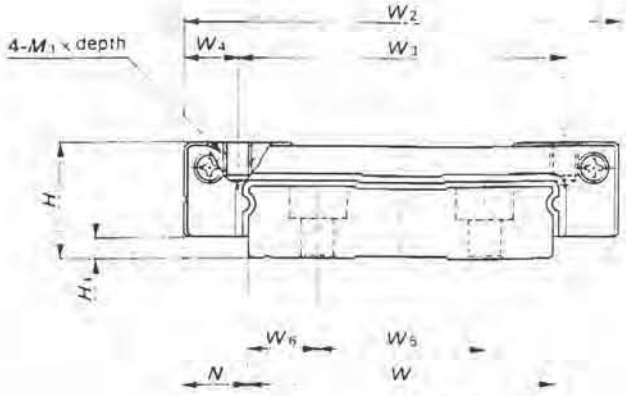

LWLF 42

Model number	Weight g		Dimensions of assembly mm			Dimensions of slide unit mm								
	Slide unit	Track rail (per 100 mm)	H	H1	N	W2	W3	W4	L1	L2	L3	M1×depth	W	H4
LWLF 14	23	53	9	1.7	5.5	25	19	3	31.5	10	21.9	M2.6×3 (M3×3)	14	5.2
LWLF 18	39	98	12	3	6	30	21	4.5	39	12	27.6	M2.6×3 (M3×3)	18	7.5
LWLF 24	74	150	14	3	8	40	28	6	44	15	31	M3×3	24	8.5
LWLF 42	140	300	16	3	9	60	45	7.5	55	20	39.5	M4×4.5	42	10

Note (1): Track rail length *L* is shown in Table 10 on page 99.
(2): Figures shown in "*To*" column and upper figures of all "*Tx*" and "*Ty*" of each model number apply to one slide unit as illustrated below. The values shown below the single case figures for "*Tx*" and "*Ty*" are for two slide units in close contact.
(3): Dimensions of "M3-thread specification" of female threads in slide units are put in parentheses. When ordering, add supplemental code "/M3" onto the identification number.

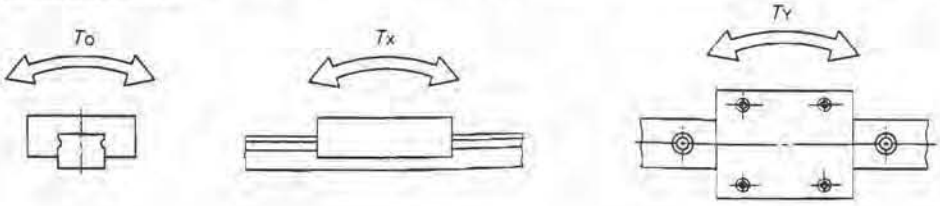

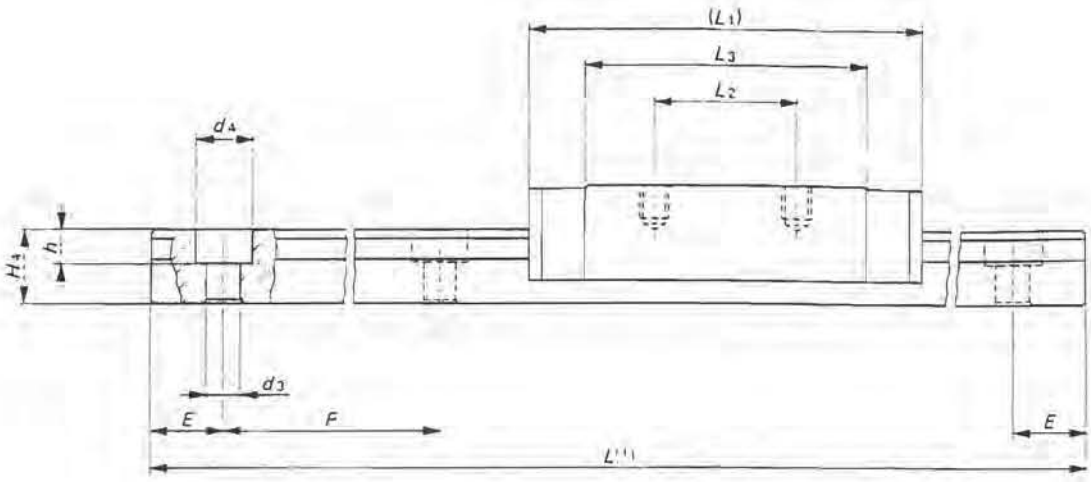

Dimensions of track rail mm							Mounting bolt for track rail	Basic dynamic load rating	Basic static load rating	Static rated moment (2)			Model number
W_5	W_6	d_3	d_4	h	E	F	mm Bolt size × length	C kgf	C_0 kgf	T_0 kgf•m	T_X kgf•m	T_Y kgf•m	
		3.5	6	3.2	15	30	M3× 6	140	250	1.9	0.89	1.1	LWLF 14
											4.9	5.8	
		3.5	6.5	4.5	15	30	M3× 8	250	420	4.0	1.9	2.2	LWLF 18
											10.0	11.9	
		4.5	8	4.5	20	40	M4×10	360	560	7.1	2.7	3.2	LWLF 24
											15.3	18.2	
23	9.5	4.5	8	4.5	20	40	M4×12	590	900	19.7	5.5	6.6	LWLF 42
											30.8	36.7	

Appendix C

A typical load cell calibration curve used in this study

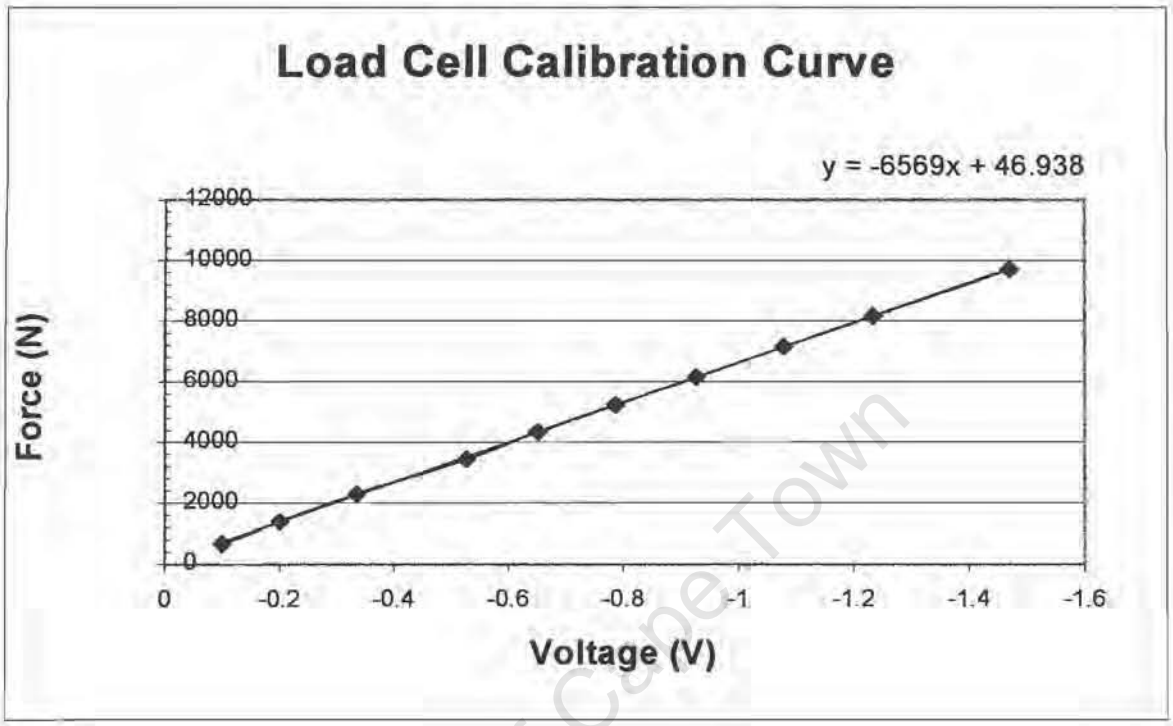

Appendix D

Source code for the data acquisition software package

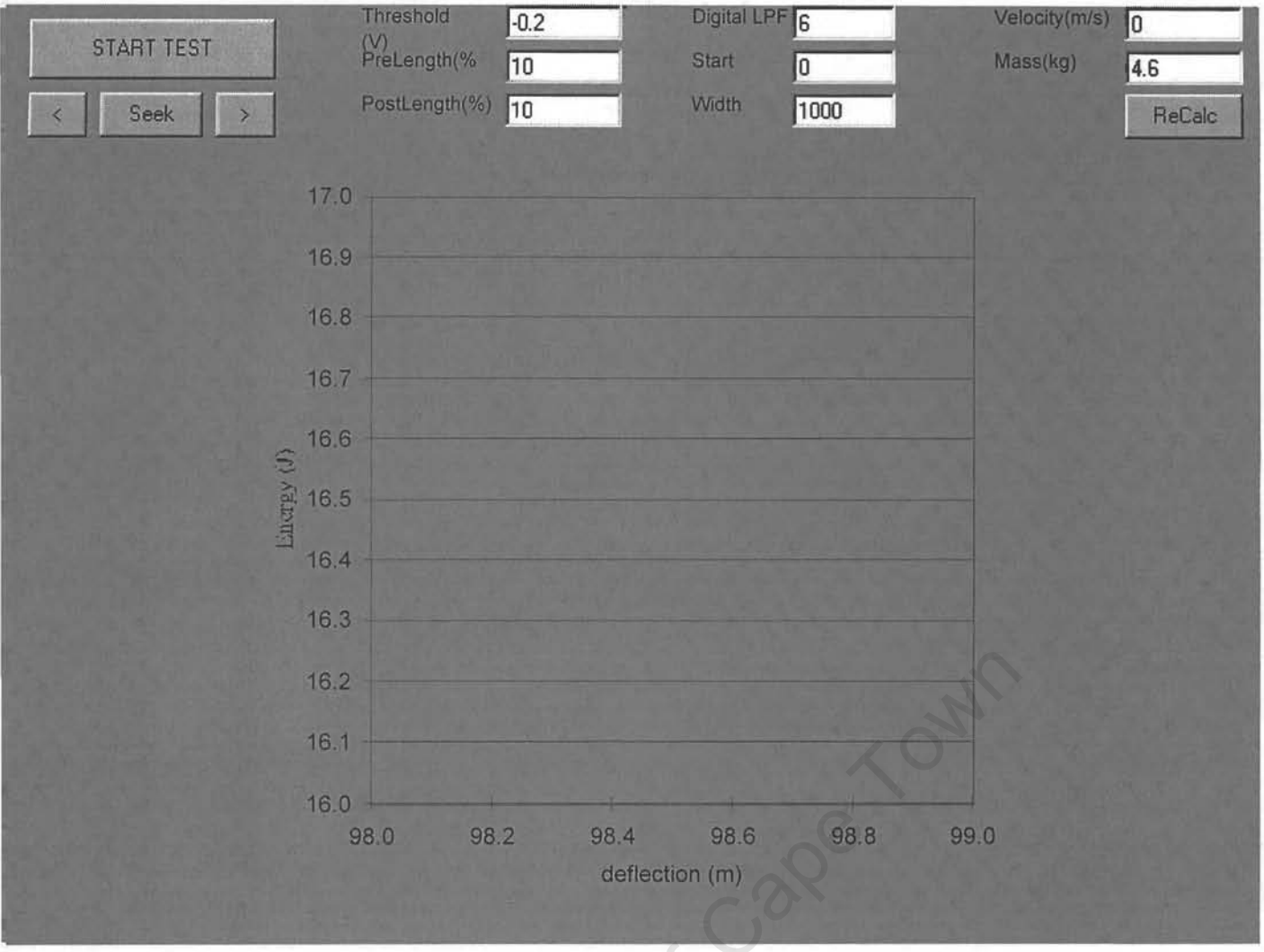

```
DropMain - 1


Private Sub Command1_Click()
Sampler.Show
End Sub

Private Sub cmdEditGrTitle_Click()
frmGraphTitle.Show
End Sub

Private Sub Command4_Click()
Sampler.Show
End Sub

Private Sub CpyGr_Click()

MSChart1.EditCopy
MSChart2.EditCopy
MSChart3.EditCopy
MSChart4.EditCopy

End Sub

Private Sub Form_Load()
    Dim er As Long

    bh = 1 ' must be same as Board Number in Control Panel
    ' Makes sure there is no voltage on the Solenoid Relay
    er = EDR_DAOutVoltage(bh, 1, 0)
     er = EDR_DAOutVoltage(bh, 0, 0)
    If er = Not EDR_OK Then
     MsgBox "Edr DAOutVoltage error: reboot computer"
     Exit Sub
    End If

    er = EDR_SetADTransferMode(bh, EDR_STREAM) 'Hardcoded as 5 for EDR_STREAM
    If er = Not EDR_OK Then
     MsgBox "Edr SetADTransferMode error: reboot computer"
     Exit Sub
    End If
    er = EDR_SetADClockmilliHz(bh, 100000000)  ' Should be set to 100kHz
    If er = Not EDR_OK Then
     MsgBox "Edr SetADClockmilliHz error: reboot computer"
     Exit Sub
    End If
    er = EDR_SetADChanListLen(bh, 0)
    If er = Not EDR_OK Then
     MsgBox "Edr SetADChanListLen error: reboot computer"
     Exit Sub
    End If
    er = EDR_AddToADChanList(bh, 2)
    If er = Not EDR_OK Then
     MsgBox "Edr AddToADChanList error: reboot computer"
     Exit Sub
    End If

End Sub



Private Sub MassBox_Change()
 change title text
Dim m, v, NewTitle As String
m = MassBox.Text
v = txtVelo.Text
NewTitle = "Mass: " + m + " [kg]; Velocity: " + v + " [m/s]"
```

```
)ropMain - 2

'If mnuFd.Checked = True Then
 MSChart1.TitleText = NewTitle
End If
If mnuEd.Checked = True Then
 MSChart2.TitleText = NewTitle
End If
If mnuFT.Checked = True Then
 MSChart3.TitleText = NewTitle
End If
If mnuVT.Checked = True Then
 MSChart4.TitleText = NewTitle
End If
End Sub



' fills force and accel
Private Sub SmoothNow()
Dim i As Long, startvl As Long, n As Long, nsmooth As Long
Dim volt As Double, Mass As Double, grav As Double, k1 As Double, k0 As Double, mg As Double,
 sum As Double

    nsmooth = Smoothing.Text
    startvl = SampleStart.Text
    n = SampleWidth.Text
    k0 = Sampler.k0box.Text
    k1 = Sampler.k1box.Text
    offsetuvolts = k1 * 1000000
    Mass = DropMain.MassBox.Text
    grav = 9.81
    mg = Mass * grav

    If nsmooth < 2 Then 'no smoothing
     For i = 0 To n - 1
      volt = (uvolts(i + startvl)) / 1000000
      force(i) = mg - (k0 * (volt - k1))
      accel(i) = force(i) / Mass
     Next i
    Else 'smoothing
     sum = 0
     For i = 0 To nsmooth - 1
      sum = sum + (uvolts(i + startvl)) / 1000000
     Next i
     For i = 0 To n - 1
      volt = sum / nsmooth
      force(i) = mg - (k0 * (volt - k1))
      accel(i) = force(i) / Mass
      sum = sum + (-uvolts(i + startvl) + uvolts(i + startvl + nsmooth)) / 1000000
     Next i

    End If
End Sub



Private Sub ReCalculate_Click()
Dim grav As Double, mg As Double, Mass As Double, vImpact As Double, dtime As Double, sofar A
s Double, volt As Double
Dim startvl As Long, i As Long, n As Long

    Mass = DropMain.MassBox.Text
    vImpact = DropMain.txtVelo
    startvl = SampleStart.Text
    grav = 9.81
    mg = Mass * grav
```

```
DropMain - 3

    n = SampleWidth.Text

   SmoothNow

'integrates v=int(ac)+v0
'simpsons rule
 dtime = 1 / 100000
 sofar = 0
 For i = 2 To n - 1
   sofar = sofar + dtime * (accel(i - 2) + 4 * accel(i - 1) + accel(i)) / 6
   veloc(i) = sofar + vImpact
 Next i
 veloc(0) = vImpact
 veloc(1) = vImpact
 sofar = 0
 For i = 2 To n - 1
   sofar = sofar + dtime * (veloc(i - 2) + 4 * veloc(i - 1) + veloc(i)) / 6
   displ(i) = sofar
 Next i
 displ(0) = 0
 displ(1) = 0
'Energy calc

 For i = 0 To n - 1
 energy(i) = Mass / 2 * (vImpact * vImpact - veloc(i) * veloc(i)) + (mg * displ(i))
 Next i

  DropMain.MSChart1.Plot.UniformAxis = False
  DropMain.MSChart2.Plot.UniformAxis = False
  DropMain.MSChart3.Plot.UniformAxis = False
  DropMain.MSChart4.Plot.UniformAxis = False

    With DropMain.MSChart1
    .ChartType = VtChChartType2dXY
        .ColumnCount = 2
        .RowCount = n
        .Column = 1
        For i = 1 To n 'X axis
         .Row = i
         .Data = displ(i - 1)
        Next i
        .Column = 2
        For i = 1 To n ' Y Axis
                .Row = i
                .Data = -force(i - 1)
        Next i
    End With

    With DropMain.MSChart2
    .ChartType = VtChChartType2dXY
        .ColumnCount = 2
        .RowCount = n
        .Column = 1
        For i = 1 To n 'X axis
         .Row = i
         .Data = displ(i - 1)
        Next i
        .Column = 2
        For i = 1 To n ' Y Axis
                .Row = i
                .Data = energy(i - 1)
        Next i
    End With

    With DropMain.MSChart3
```

```
DropMain - 4

    .ChartType = VtChChartType2dXY
        .ColumnCount = 2
        .RowCount = n
        .Column = 1
        volt = 0
        For i = 1 To n 'X axis
         .Row = i
          .Data = volt
         volt = volt + 1 / 100000
        Next i
        .RowCount = n
        .Column = 2
        For i = 1 To n 'Y axis
         .Row = i
         .Data = -force(i - 1)
        Next i
    End With
    With DropMain.MSChart4
    .ChartType = VtChChartType2dXY
        .ColumnCount = 2
        .RowCount = n
        .Column = 1
        volt = 0
        For i = 1 To n 'X axis
         .Row = i
          .Data = volt
         volt = volt + 1 / 100000
        Next i
        .RowCount = n
        .Column = 2
        For i = 1 To n 'Y axis
         .Row = i
         .Data = (uvolts(i - 1 + startvl)) / 1000000 'force(i - 1)
        Next i
    End With
End Sub

Public Sub Seek_Click()
Dim Peak As Long, i As Long, startvl As Long, endvl As Long, impact As Long, thresh As Long,
1 As Long
Dim postdtmp As Double, predtmp As Double, dthresh As Double, k1 As Double

   k1 = Sampler.k1box.Text
   dthresh = Threshold.Text 'uvolts
   predtmp = PreLength.Text
   postdtmp = PostLength.Text

   thresh = (dthresh + k1) * 1000000
   Peak = 1000000
   impact = 0
   i = preimpact - 50
   If i < 0 Then
     i = 0
   End If

   While i < MaxNum
         If uvolts(i) < Peak Then
           Peak = uvolts(i)
           impact = i
         End If
         i = i + 1
   Wend

 If Peak > thresh Then
  MsgBox ("Failed to find bump: change threshold ")
```

```
)ropMain - 5

 End If
 'find start
 i = impact
 While i > 0
  If uvolts(i) > thresh Then
   startvl = i
   i = 0
  End If
  i = i - 1
 Wend
 i = impact
 While i < MaxNum
  If uvolts(i) > thresh Then
   endvl = i + endvl
   i = MaxNum
  End If
  i = i + 1
 Wend

 n = endvl - startvl 'for now
 predtmp = (n * predtmp) / 100
 postdtmp = (n * postdtmp) / 100
 startvl = startvl - predtmp
 endvl = endvl + postdtmp
 If startvl < 0 Then
    startvl = 0
 End If

 If endvl > MaxNum Then
    endvl = MaxNum
 End If
 n = endvl - startvl - 1
 If n < 2 Then
  n = 2
 End If
 If n > 10000 Then
  If (MsgBox("Warning: dislay elements >10000; press cancel to abort", 1) = vbCancel) Then
   Exit Sub
  End If
 End If

 SampleStart.Text = startvl
 SampleWidth.Text = n

 ReCalculate_Click
End Sub

)rivate Sub SeekBack_Click()
)im tmp As Long, i As Long, n As Long, Peak As Long, startvl As Long, endvl As Long, impact A
s Long, thresh As Long
)im dthresh As Double, k1 As Double, wdtmp As Double

   k1 = Sampler.k1box.Text
   impact = SampleStart.Text
   n = SampleWidth.Text
   dthresh = Threshold.Text 'uvolts
   wdtmp = PreLength.Text
   wdtmp = (n * wdtmp) / 100
   startvl = wdtmp

   wdtmp = PostLength.Text
   wdtmp = (n * wdtmp) / 100
   endvl = wdtmp

   thresh = (dthresh + k1) * 1000000
```

```
)ropMain - 6


   tmp = 0
   i = impact
 While i > 0
  If uvolts(i) < thresh Then
   endvl = i + endvl
   tmp = i
   i = 0
  End If
  i = i - 1
 Wend

 If tmp < 1 Or tmp >= impact Then
  MsgBox ("Could not find another peak; lower threshold")
   Exit Sub
 End If

   i = tmp
 While i > 0
  If uvolts(i) > thresh Then
   startvl = i - startvl
   i = 0
  End If
  i = i - 1
 Wend

  If startvl < 0 Then
  startvl = 0
  End If

  n = endvl - startvl - 1
 If n < 2 Then
  n = 2
 End If
 If n > 10000 Then
  If (MsgBox("Warning: dislay elements >10000; press cancel to abort", 1) = vbCancel) Then
   Exit Sub
  End If
 End If

 SampleStart.Text = startvl
 SampleWidth.Text = n

 ReCalculate_Click
End Sub

)rivate Sub SeekOn_Click()
)im Peak As Long, i As Long, n As Long, startvl As Long, endvl As Long, impact As Long, thres
1 As Long, tmp As Long
)im wdtmp As Double, dthresh As Double, k1 As Double


   k1 = Sampler.k1box.Text
   impact = SampleStart.Text
   n = SampleWidth.Text
   dthresh = Threshold.Text 'uvolts

   wdtmp = PreLength.Text
   wdtmp = (n * wdtmp) / 100
   startvl = wdtmp

   wdtmp = PostLength.Text
   wdtmp = (n * wdtmp) / 100
   endvl = wdtmp
```

```
DropMain - 7

   tmp = 0

   thresh = (dthresh + k1) * 1000000
   i = impact + n
 While i < MaxNum
  If uvolts(i) < thresh Then
   startvl = i - startvl
   tmp = i
   i = MaxNum
  End If
  i = i + 1
 Wend

 If tmp < impact + n Or tmp > MaxNum - 1 Then
  MsgBox ("Could not find another peak; lower threshold")
   Exit Sub
 End If

   i = tmp + 50
 While i < MaxNum
  If uvolts(i) > thresh Then
   endvl = i + endvl
   i = MaxNum
  End If
  i = i + 1
 Wend

  If startvl < 0 Then
  startvl = 0
  End If

  n = endvl - startvl - 1
 If n < 2 Then
  n = 2
 End If
 If n > 10000 Then
  If (MsgBox("Warning: dislay elements >10000; press cancel to abort", 1) = vbCancel) Then
   Exit Sub
  End If
 End If

 SampleStart.Text = startvl
 SampleWidth.Text = n

 ReCalculate_Click
End Sub

Private Sub txtVelo_Change()
MassBox_Change
End Sub

Private Sub mnuAbout_Click()
About1.Show
End Sub

Private Sub mnuEd_Click()
MSChart1.Visible = False
MSChart2.Visible = True
MSChart3.Visible = False
MSChart4.Visible = False
mnuFd.Checked = False
mnuEd.Checked = True
mnuFT.Checked = False
mnuVT.Checked = False
End Sub
```

```
DropMain - 8

Private Sub mnuFd_Click()
MSChart1.Visible = True
MSChart2.Visible = False
MSChart3.Visible = False
MSChart4.Visible = False
mnuFd.Checked = True
mnuEd.Checked = False
mnuFT.Checked = False
mnuVT.Checked = False
End Sub

Private Sub mnuFT_Click()
MSChart1.Visible = False
MSChart2.Visible = False
MSChart3.Visible = True
MSChart4.Visible = True
mnuFd.Checked = False
mnuEd.Checked = False
mnuFT.Checked = True
mnuVT.Checked = False
End Sub

Private Sub mnuVT_Click()
MSChart1.Visible = False
MSChart2.Visible = False
MSChart3.Visible = False
MSChart4.Visible = True
mnuFd.Checked = False
mnuEd.Checked = False
mnuFT.Checked = False
mnuVT.Checked = True
End Sub

Private Sub mnuPrint_Click()
PrintForm
'If mnuFd.Checked = True Then
' MSChart1.PrintForm
'End If
'If mnuEd.Checked = True Then
' MSChart2.PrintForm
'End If
'If mnuFT.Checked = True Then
  MSChart3.PrintForm
'End If
End Sub

Private Sub mnutesbrdset_Click()
 Sampler.Show
End Sub
```

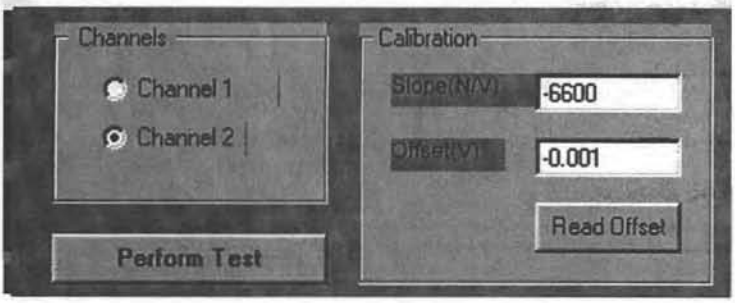

```
Sampler - 1

Private Sub btnAbout_Click()
    About1.Show
End Sub

Private Sub Option1_Click()
    Dim er As Long
    er = EDR_StopBackgroundADIn(bh)
    er = EDR_SetADChanListLen(bh, 0)
    If er = Not EDR_OK Then
     MsgBox "Edr SetADChanListLen error: reboot computer"
     Exit Sub
    End If
    er = EDR_AddToADChanList(bh, 1)
    If er = Not EDR_OK Then
     MsgBox "Edr AddToADChanList error: reboot computer"
     Exit Sub
    End If
End Sub

Private Sub Option2_Click()
    Dim er As Long
    er = EDR_StopBackgroundADIn(bh)
    er = EDR_SetADChanListLen(bh, 0)
    If er = Not EDR_OK Then
     MsgBox "Edr SetADChanListLen error: reboot computer"
     Exit Sub
    End If
    er = EDR_AddToADChanList(bh, 2)
    If er = Not EDR_OK Then
     MsgBox "Edr AddToADChanList error: reboot computer"
     Exit Sub
    End If
End Sub

Private Sub ReadVolt_Click()
 Dim tmp As Double

    CalibrateNow
    tmp = offsetuvolts / 1000000
    klbox.Text = tmp
End Sub

Private Sub CalibrateNow() ' calculates offset
   Dim er As Long, sofar As Long

    ' Start sampling - Sample in bg
    er = EDR_ADInBinBackground(bh, 50000, bin(0))
    If er = Not EDR_OK Then
     MsgBox "Edr ADInBinBackground error: reboot computer"
     Exit Sub
    End If
    sofar = 0
    While sofar >= 0 And sofar < 50000 'wait till finished
     sofar = EDR_BackgroundADInStatus(bh)
    Wend
    EDR_StopBackgroundADIn (bh)
    If er = Not EDR_OK Then
     MsgBox "Edr StopBackgroundADIn error: reboot computer"
     Exit Sub
    End If

    er = EDR_ADInBinToVoltageBlock(bh, uvolts(0), bin(0), 50000, 0)
    If er = Not EDR_OK Then
     MsgBox "Edr ADInBinToVoltageBlock error: reboot computer"
```

```
     Exit Sub
    End If
    offsetuvolts = 0
    For sofar = 0 To 49999
     offsetuvolts = offsetuvolts + uvolts(sofar)
    Next sofar
    offsetuvolts = offsetuvolts / 50000
End Sub


Private Sub PerformTest_Click()
   Dim er As Long, i As Long, impact As Long, Peak As Long, n As Long, startvl As Long
   Dim Dio As Long, D1  As Long, D2 As Long, D3 As Long, D4 As Long, D5 As Long, D6 As Long,
D7 As Long, D8 As Long, D9 As Long, D10 As Long, D11 As Long, D12 As Long
   Dim Speed As Integer, DecimalTotal As Integer, lasttotal As Integer
   Dim dtime As Double, sofar As Double, Mass As Double, k0 As Double, mg As Double, grav As
Double, vImpact As Double

     If (MsgBox("Commencing test, keep clear of crosshead", vbOKCancel, "WARNING") = vbCancel
) Then
     Exit Sub
     End If

'//////////////////////CALIBRATE
    ReadVolt_Click
'//////////////////////CLEAR COUNTER
    dtime = Timer + 0.1
    Do While Timer < dtime
     er = EDR_DAOutVoltage(bh, 1, 5000000)  ' 5V out
    Loop
    er = EDR_DAOutVoltage(bh, 1, 0) ' 0V out !
    If er = Not EDR_OK Then
     MsgBox "Edr DAOutVoltage error: reboot computer"
     Exit Sub
    End If

'//////////////////////START SAMPLING
    er = EDR_ADInBinBackground(bh, MaxNum, bin(0))
    If er = Not EDR_OK Then
     MsgBox "Edr ADInBinBackground error: reboot computer"
     Exit Sub
    End If
    i = 0
    ' MAKE sure Sampling has started
    While i < 1
        i = EDR_BackgroundADInStatus(bh)
        If i < 0 Then
        MsgBox ("error")
        End If
    Wend

    er = EDR_DAOutVoltage(bh, 0, 5000000)  ' 5V out release
    If er = Not EDR_OK Then
     MsgBox "Edr DAOutVoltage error: reboot computer"
     Exit Sub
    End If

    i = 0
    lasttotal = 0
    preimpact = 0 'passed thru flipflop
    Speed = 0
    While i >= 0 And i < MaxNum 'wait till finished

    ' Converter for opto velocity trigger
    Dio = EDR_DIOLineInput(bh, 0, 0, D1)
```

```
Sampler - 3

    Dio = EDR_DIOLineInput(bh, 0, 1, D2)
    Dio = EDR_DIOLineInput(bh, 0, 2, D3)
    Dio = EDR_DIOLineInput(bh, 0, 3, D4)
    Dio = EDR_DIOLineInput(bh, 0, 4, D5)
    Dio = EDR_DIOLineInput(bh, 0, 5, D6)
    Dio = EDR_DIOLineInput(bh, 0, 6, D7)
    Dio = EDR_DIOLineInput(bh, 0, 7, D8)
    Dio = EDR_DIOLineInput(bh, 2, 4, D9)
    Dio = EDR_DIOLineInput(bh, 2, 5, D10)
    Dio = EDR_DIOLineInput(bh, 2, 6, D11)
    Dio = EDR_DIOLineInput(bh, 2, 7, D12)
    DecimalTotal = (1 * D1 + 2 * D2 + 4 * D3 + 8 * D4 + 16 * D5 + 32 * D6 + 64 * D7 + 128 * D
3 + 256 * D9 + 512 * D10 + 1024 * D11 + 2048 * D11 + 4096 * D12)

    i = EDR_BackgroundADInStatus(bh)
    If preimpact = 0 And DecimalTotal > 0 And DecimalTotal = lasttotal Then
     preimpact = i
     Speed = DecimalTotal
    End If
    lasttotal = DecimalTotal
    Wend
    er = EDR_StopBackgroundADIn(bh)

    If er = Not EDR_OK Then
     MsgBox "Edr StopBackgroundADIn error: reboot computer"
     Exit Sub
    End If

    er = EDR_DAOutVoltage(bh, 0, 0)  ' 0V out
    If er = Not EDR_OK Then
     MsgBox "Edr DAOutVoltage error: reboot computer"
     Exit Sub
    End If

    If Speed = 0 Then
     vImpact = 0
     MsgBox ("Failed to determine speed, enter velocity and press ReCalculate")
    Else
    vImpact = (0.01 / (Speed / 100000))
    vImpact = vImpact * 1000
    er = vImpact
    vImpact = er / 1000
    End If

    ' Converts the data to microvolts.
    er = EDR_ADInBinToVoltageBlock(bh, uvolts(0), bin(0), MaxNum, 0)
    If er = Not EDR_OK Then
     MsgBox "Edr ADInBinToVoltageBlock error: reboot computer"
     Exit Sub
    End If
 DropMain.txtVelo = vImpact
 '////////////////////////////GOT speed and Samples
 DropMain.Seek_Click
End Sub
```

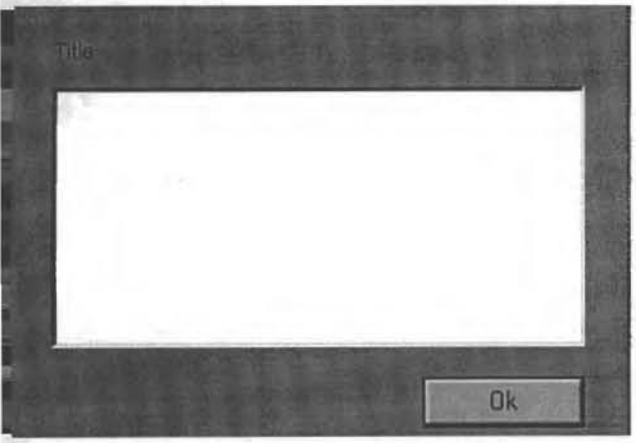

```
frmGraphTitle - 1

Private Sub cmdOk_Click()
 If DropMain.mnuFd.Checked = True Then
  DropMain.MSChart1.TitleText = NewTitle.Text
 End If
 If DropMain.mnuEd.Checked = True Then
  DropMain.MSChart2.TitleText = NewTitle.Text
 End If
 If DropMain.mnuFT.Checked = True Then
  DropMain.MSChart3.TitleText = NewTitle.Text
 End If
 If DropMain.mnuVT.Checked = True Then
  DropMain.MSChart4.TitleText = NewTitle.Text
 End If
 Unload frmGraphTitle
End Sub

Private Sub Form_Load()
 If DropMain.mnuFd.Checked = True Then
  NewTitle.Text = DropMain.MSChart1.TitleText
 End If
 If DropMain.mnuEd.Checked = True Then
  NewTitle.Text = DropMain.MSChart2.TitleText
 End If
 If DropMain.mnuFT.Checked = True Then
  NewTitle.Text = DropMain.MSChart3.TitleText
 End If
 If DropMain.mnuVT.Checked = True Then
  NewTitle.Text = DropMain.MSChart4.TitleText
 End If
End Sub
```

```
Saveglobals - 1

Option Explicit

Global bh As Long      ' Our board handle

  Buffers for holding raw data and microvolts
Global Const MaxNum = 200000
Global bin(MaxNum) As Integer     ' for bin data
Global uvolts(MaxNum) As Long ' for uv data
Global offsetuvolts As Double ' for uv data
Global smoothvolts(MaxNum) As Double ' for uv data
Global force(MaxNum) As Double ' for uv data
Global accel(MaxNum) As Double ' for uv data
Global veloc(MaxNum) As Double ' for uv data
Global displ(MaxNum) As Double ' for uv data
Global energy(MaxNum) As Double ' for uv data
Global lastspeed As Double
Global preimpact As Long
```

A thesis submitted to the faculty of Engineering at the University of Cape Town in fulfilment of the requirements for the degree of Masters of Science in Engineering

By
Paul Cartmel
Department of Material Engineering
June 1999